THESIS

DESIGN AND FABRICATION OF A FLOW CHAMBER FOR THE STUDY OF CELL ADHESION AND HEMOCOMPATIBILTY IN DYNAMIC CONDITIONS

Submitted by

Kevin Migita

The Graduate Degree Program in Bioengineering

In partial fulfillment of the requirements

For the Degree of Master of Science

Colorado State University

Fort Collins, Colorado

Summer 2011

Master's Committee:

Advisor: Ketul Popat
Co-Advisor: Lakshmi Prasad Dasi

Ashok Prasad

ABSTRACT

DESIGN AND FABRICATION OF A FLOW CHAMBER FOR THE STUDY OF CELL ADHESION AND HEMOCOMPATIBILTY IN DYNAMIC CONDITIONS

Cell adhesion is a well characterized condition of both biomaterial and tissue engineering research. It plays a role in biocompatibility and the proliferation, differentiation and viability of seeded cells. With respect to hemocompatibility, platelet adhesion and subsequent activation is a driving factor in the failure of blood contacting medical devices. Platelets aggregates are vital components in the wound healing and foreign body responses and display various forms of adhesion based on blood flow. However, the study of platelet adhesion on implantable tissue engineering scaffolds under dynamic conditions is very limited, particularly with directional flow.

A flow chamber which incorporates a tissue engineering scaffold or functionalized biomaterial was designed and fabricated for investigation of flow patterns and cellular adhesion in response to dynamic conditions on these surfaces. The device utilizes a combination of aspects from both tissue engineering bioreactors and microfluidics platforms to result in a flow chamber which provides the directional flow of a perfused flow bioreactor with the advantages of controlling chamber shape and real time monitoring presented by Polydimethylsiloxane microfluidics chambers.

Results of fluid flow study in the chamber modeled for laminar and shear gradient simulated flow demonstrate the ability of the device to manipulate flow patterns. Dynamic and static studies of platelet adhesion to poly-(ε-caprolactone) flat and electrospun nanofiber surfaces

utilizing the flow chamber provide insight into the hemocompatibility of tissue engineering scaffolds in a dynamic flow setting.

TABLE OF CONTENTS

LIST OF TABLES

LIST OF FIGURES

INTRODUCTION

As the number of patients in need of tissue and organ repair continues to rise, a focus of the biomedical community has been the increasing development of porous, biodegradable, three dimensional scaffolds seeded with cells for the growth of new tissue.[1] There is a growing need to understand and develop implantable medical devices and scaffolds that balance mechanical strength with biofactor delivery providing a sequential transition of cellular integration. [2-4] Threats of biomaterial rejection and foreign body reactions remain a problem eliciting the need for increased attention to material tissue interactions such as protein adsorption, cellular adhesion and inflammatory response.

The biocompatibility of a number of biomaterials intended for tissue engineering scaffolds have been studied with respect to their ability to promote cell adhesion and proliferation[5-7], cell phenotypic behavior[8-9], protein folding and interactions[11-12] and the material biodegradability[12-14] and cytotoxic effects[15-16]. In addition, modifying the surface of scaffold materials with bioactive surface coatings, facilitating the release of growth factors[17-18] and micro- and nanoscale topologies has shown increases of cell adhesion, proliferation and phenotypic behavior.[19-21]

Hemocompatibility is defined as the "ability of a material to perform with an appropriate host response in a specific application" and relates to the thrombotic response induced by an implanted material. Implantable materials are non-toxic and often biocompatible, but occasionally stimulate foreign body responses. These reactions are directly correlated with cells in the blood presenting themselves in the form of inflammation, fibrosis capsule development and thrombosis following injury in vascular tissue.[22] Thrombosis associated with implanted biomaterials is the result of

complex system of pathways and reactions.[23-25] However, immediate responses to implanted materials include adsorption of plasma proteins to the material surface, coagulation reactions and platelet activation. While tissue factor expression, complement activation and inflammatory cells such as leukocytes all play additional, important roles in thrombus formation[23], preventing coagulation and the activation of platelets remain key focuses in testing the hemocompatibility of biomaterials.[26-30] There are a very limited number of studies reporting the hemocompatibility of these scaffold materials particularly in dynamic settings comparable to conditions in the body.

Microfluidic flow chambers are medical devices used to directly study the effects of fluid flow. They are based off capillaries often with lateral dimensions of 10-1000μm[31-32] though the development of nanoscale channels have been described[33-34] and are applied in medical analysis, microchemistry, environmental monitoring. There is growing interest in the cultivation of cells, [31,35-37] and creation of tissue engineering scaffolds in micro fluid channels and formation of microfluidics networks in tissue engineering scaffolds[38-40]. One of the most actively developed materials for the creation of microfluidic devices is polydimethylsiloxane (PDMS) this polymer is easily fabricated, has visual clarity and is nontoxic and biologically inert[41-43]. Use of PDMS microfluidics for research of fluids and biological processes allow for the use of live imaging through a number of forms of microscopy and the advantage of smaller sample sizes. A number of studies have documented the use of these microfluidics devices for the in vitro study of the properties of blood[44-45]. However, due to the scale of these devices integration of biomaterials and scaffolds from sources external to the device are rarely documented.

Bioreactors are generally defined as a device in which a biological or biochemical processes develop with reproducibility and control being the main advantages of such devices[46]. Application of bioreactors to tissue engineering commonly involves improving the in vitro culture of a three dimensional cell-scaffold. Key processes in the ex vivo engineering of tissues which bioreactors assist include cell seeding of porous scaffolds, supply of nutrients and mechanical

stimulation of developing tissues[47-48]. Testing biochemical processes related to tissue engineering such as cell adhesion, biodegradation and toxicity response in fluid flow qualify as valid bioreactor use. However, typical tissue engineering approaches to bioreactors cater to extended studies of improving tissue culture methods[50-51]. In addition bioreactors are often larger devices and lack the capacity to provide real time and detailed observation of flow and the samples without disrupting the experiment thus rely on kinetics and modeling to predict the patterns of flow and cell growth[46,52].

This work presents a detailed account of the design, fabrication and experimental validation of a device that incorporates a three dimensional tissue engineering scaffold or functionalized biomaterial for characterization and analysis of flow patterns and cell adhesion in response to dynamic conditions. The device utilizes a combination of aspects from both tissue engineering bioreactors and microfluidics platforms to result in a flow chamber which provides the directional flow of a perfused flow bioreactor with the advantages of controlling chamber shape and real time monitoring presented by PDMS microfluidics chambers.

The flow chamber validation is based on its ability to run flow patterns in accordance with chamber conformation and dynamic platelet adhesion studies. Particle image velocimetry (PIV) is used to visualize the creation of homogeneous, laminar flow at a target area within the chamber and the creation of shear gradients and transitional flow. The interior shape was modeled to achieve the desired flow pattern in each experiment. Dynamic and static studies of platelet adhesion to poly-(ε-caprolactone) flat and electrospun nanofiber surfaces follow in detail and serve to expand on findings from the PIV, research hemocompatability of PCL nanoscale surfaces and as proof of concept for platelet adhesion and aggregation based on shear gradients.

While validation of the chamber is based on the ability to create flow patterns and flow plasma across a surface modified biomaterial for tissue engineering application, the device is not limited

to the study of blood contacting materials. The flexibility of this device is unique with adjustable operational and design variables which include: interior shape, total interior volume, cell type, fluid type, flow rate, immobilized scaffold or biomaterial and the mechanism of study (cell adhesion, cell proliferation, material degradation, etc). The final goal is a flow device which is robust and flexible, applicable to the study of a biological process in any fluid dynamic environment within limitations of scale.

MATERIALS AND METHODS

Flow Chamber Design and Fabrication

Sheets of Cavex dental wax (Ted Pella 109) were cut by hand using an X-Acto© knife into 35mmx 95mm sections to make the body of the flow chamber. Two identical cut sections were bound together by clear silicone (G.E.) to promote a water tight seal between the two layers. The height of these combined sections is 3.5mm. Sandwiched between the two sections are 100mm long, 1/32 inch inner diameter Teflon tubing (McMaster-Carr) for the inlet and outlet flows, fastened to the chamber by silicone. Following fabrication the completed samples were left to cure for 24 hours before use.

The interior of each wax piece was cut by hand utilizing a template with the maximum diameter being 22.5mm at the inlet and outlet with the smallest interior diameter being 10mm. Length of all interior chambers was set to 55mm. Interior shape was designed to promote laminar flow through the 10 mm diameter of the chamber. The target area for laminar flow is 10mm wide and 10mm in length positioned 35mm from the inlet of the flow chamber and is designed to immobilize a tissue engineering scaffold for exposure to a dynamic setting. (Figure 1a) As an additional safeguard for promoting laminar flow wax sections 5mm in length are left intact at the 5mm and 15mm points in the chamber. To allow flow to pass through these walls the 1/32 inch inner diameter Teflon tubing is utilized to imprint 3 holes in each section. (Figure 1b)

Chambers designed to study the flow of a stent were cut with a 6mm maximum diameter and 2mm interior diameter with a template. The patterning of the stent chamber was made by initially cutting a 2mm wide, 55 mm long channel. Alternating 2mm by 2mm squares are cut for the

entire length of the chamber on both sides of the channel resulting in a zipper-like conformation. After silicone sealing the chamber was trimmed of loose wax and uneven squares. (Figure 1c)

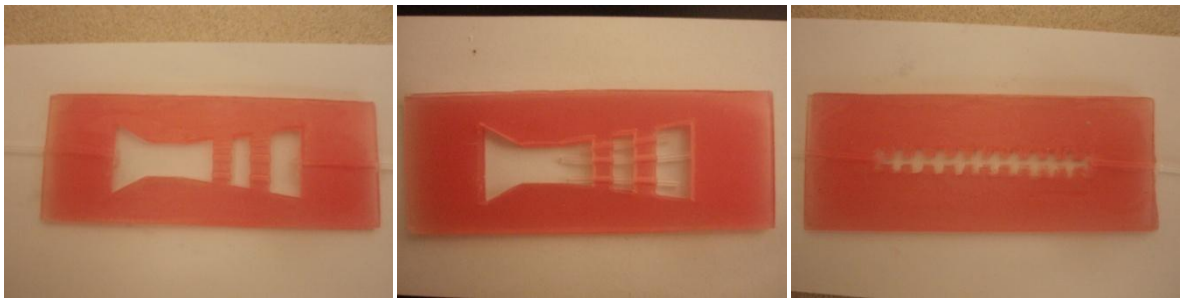

(a) (b) (c)

Figure 1– (a) Wax chamber with 10mm x 10mm target area. (b) Wax chamber demonstrating tube imprinting. (c) Wax chamber with 2mm square indents.

Operating the Flow Chamber and Visualization

Characterization of the flow in both chambers is based on imaging and observation of fluid flow patterns. To run the flow the chambers were sealed with a layer of 1/32 inch thick silicone membrane (McMaster-Carr) cut to 75mm x 30mm dimensions and a microscope slide on both open ends. These were clamped by small binder clips (Acco) to create pressure for the seal. The fluid utilized for the analysis is an emulsion consisting of 0.25 g of 20 µm diameter polyamide seeding particles (PSP) (Dantec) and 50 mL of distilled water, this solution is designed to be conditioned for particle image velocimetry (PIV) analysis. The particle seeded water was pushed through the chamber by a syringe pump (Pump 11 Harvard Apparatus) at a flow rate of 10mL/minute. A 50mL syringe (BD) was fixed on the pump to which the PSP emulsion was inserted, a 17 gauge needle (BD) was set into the inlet tube of the clamped chamber and fastened to the syringe. The chamber was placed into a compound microscope (Olympus) with a high speed camera (pco.) attached with the outlet flowing into a petri dish catch. The syringe was refilled repeatedly with PSP solution and the chamber was opened and cleared after 3 runs to remove interference from settled particles. Images of the flow in the chamber were taken and controlled using Camware software (pco) to adjust frame rate and contrast. Imaging was optimized at 800 frames per second for the laminar flow chamber and 400 frames per second for

the stent flow chamber. Videos were recorded at 10x, 16x and 32x magnification with focal point in the center of the implantable material target area for the laminar flow chamber and in the center of the protruding boxes for the stent chamber. For each recorded run 100 images were saved and later compiled into a video for analysis.

To further characterize flow in the chamber with the use of bio fluids the fluid of interest was rotated to human plasma in excess of 60 days old. The expired plasma was donated by the Poudre Valley Hospital in 200mL bags obtained every 2 weeks. Changing to expired plasma reduced the size of the suspended particles being tracked to 3-4 μm in diameter and simulated an environment similar to that of blood contacting. Additional preparation for the experiments involving expired plasma included adding plastic wrap to the microscope base and recording video in three planes for each set position due to the smaller particles. Particle image velocimetry (PIV) and video editing were then conducted with DaVis 7.2 software (LAVision). (Figure 2) Qualitative analysis of both flow chambers were studied through imaging and observation of the resultant patterns and flow was characterized by calculation of Reynolds number and shear stress.

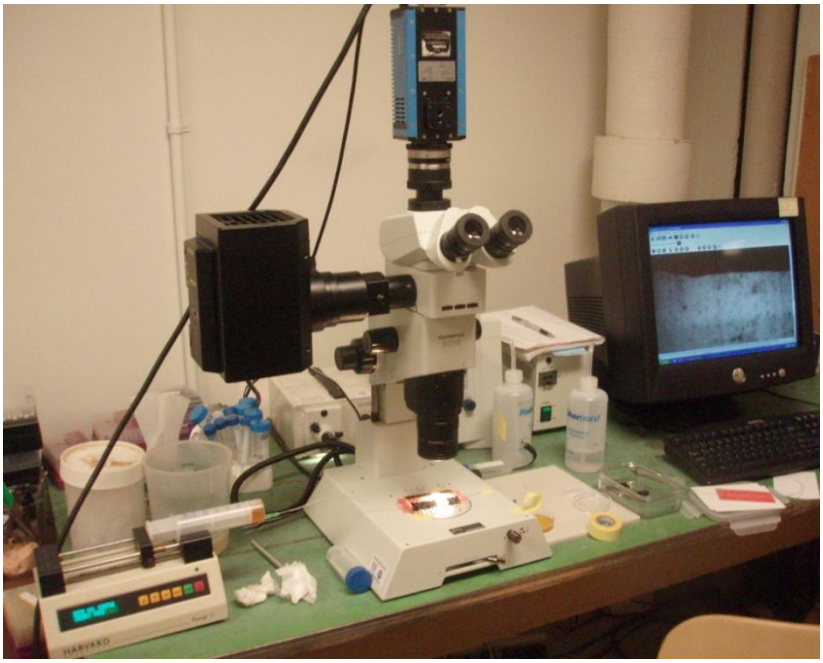

Figure 2 – Flow set up with microscope and camera for recording PSP and plasma flow in the chambers.

PCL Nanofiber Scaffold Fabrication

PCL nanofiber scaffolds were fabricated using an electrospinning technique. The electrospinning apparatus consisted of a syringe pump (Pump 11 Harvard Apparatus), a glass syringe (Hamilton, model 1010), Teflon fluidic tubing (Hamilton, model 86510), a 20-gauge blunt-tip catheter (Hamilton, model 7746-04), and a male luer lock adapter (Hamilton, model 86511). A high-voltage power source (Gamma High Voltage Research, model ES30P-10W/DAM) was connected to the catheter tip with a standard binder clip. The collector consisted of an aluminum foil fastened onto a 0.5 in. thick copper plate (McMaster Carr) with electrical tape and positioned horizontally below the catheter. Polymer solution was prepared by dissolving oleic acid sodium salt (OLA) (Sigma) in methanol. PCL pellets (Mw = 80,000, Sigma) were dissolved in chloroform and the polymer solution was mixed with OLA in methanol on a magnetic stir plate to produce a homogeneous mixture with a 4:1 chloroform:methanol volume ratio. The final solution was 12% solid w/w and the PCL:OLA ratio of the solid weight was 97:3. The volumetric flow rate was 2.8 ml/hr, applied voltage 21 kV and tip-to-collector distance 10 cm. The PCL on the collector was cut into 1cm by 2cm rectangles for immobilization and in the flow chamber. Smooth PCL (control) samples were constructed by sintering PCL powder (Mw = 50,000, CAPA) sandwiched between two glass plates. The resulting flat sheet was allowed to air cool before being removed from the glass surfaces and cropped into 1cm by 2cm rectangles. (Figure 3)

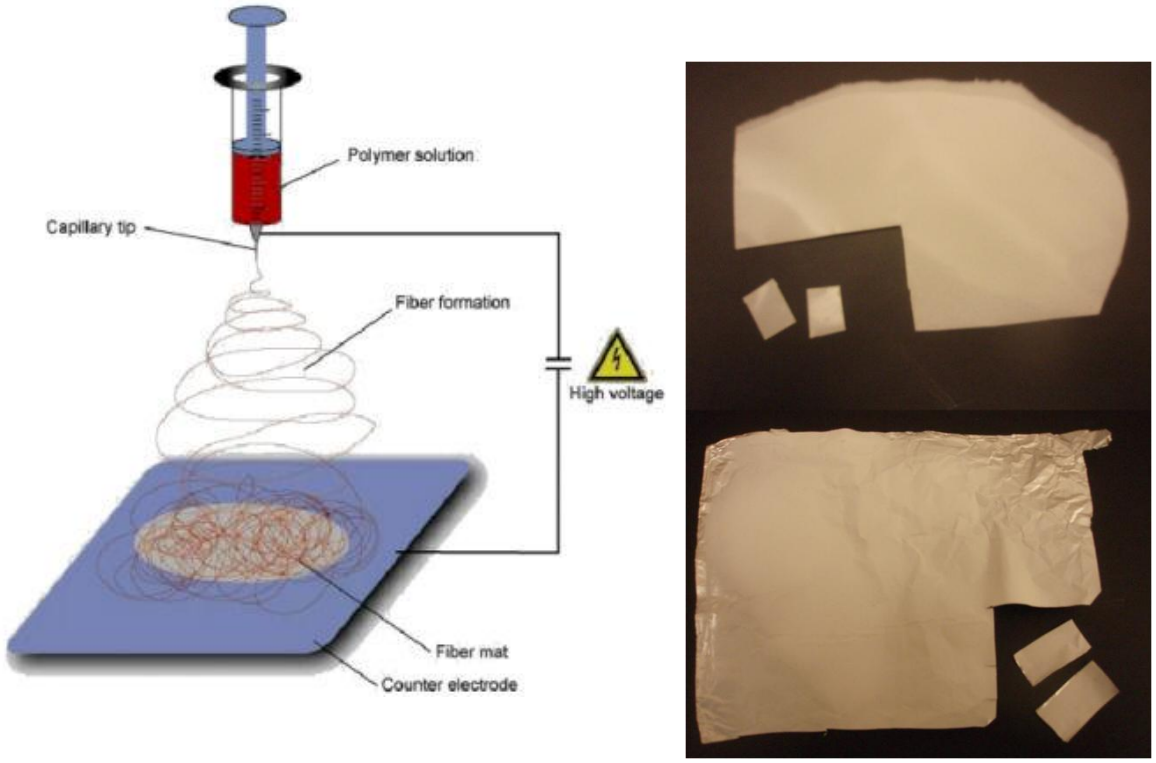

Figure 3 – (left) Polymer electrospinning set up diagram by Dreiner/Wendorf. (right-top) Flat PCL with sample cut outs. (right-bottom) Electrospun PCL nanofibers with sample cut outs.

Platelet Adhesion and Activation Studies

Whole blood from a sample size of three healthy individuals, acquired through venopuncture, was drawn into standard vacuum tubes coated with the anti-coagulant, ethylenediaminetetraaceticacid (EDTA) (Fisher Scientific). The EDTA tubes were centrifuged at 150g for 15 min to separate the plasma and buffy coat from the hematocrit. The plasma and buffy coat layer from these tubes were pooled into a single centrifuge tube. (Figure 4) To visualize possible platelet activation the stent flow chamber was run and visualized using the isolated plasma following the same procedure as the experiments in which expired plasma was used. Video of the flow in the stent chamber was recorded at 500 frames per second at 16, 20, 25, 32 and 40 times magnification and the flow rate was set at 10 ml/min.

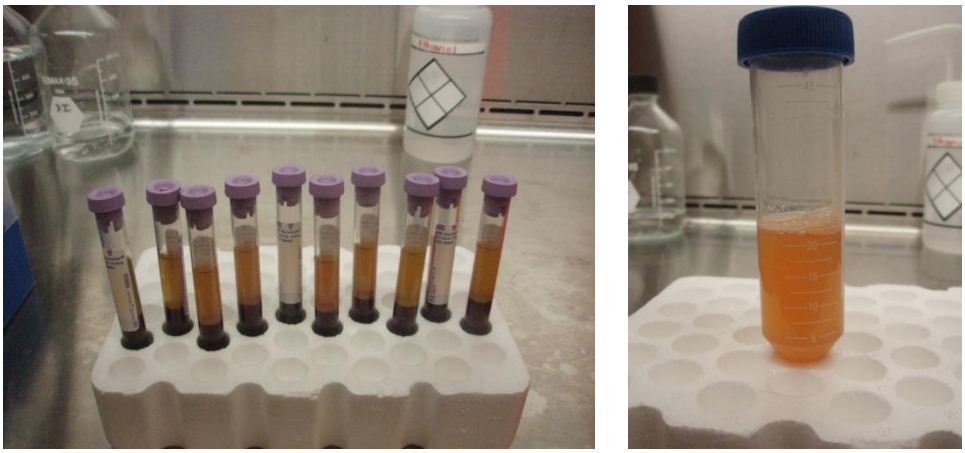

(a) (b)

Figure 4 – (a) Blood samples after centrifugation in EDTA coated tubes. (b) Pooled Plasma from 60 mL of whole blood.

PCL samples (control and nanofibers) were sterilized by washing three times for five minutes in 70% ethanol, rinsing twice with sterile phosphate buffer saline (PBS) for 5 minutes and then exposed to ultraviolet light for 30 minutes. The chamber was sterilized by wiping down the wax body, microscope slides and silicone membrane with 70% ethanol then assembling the full chamber with binder clips and washing the interior twice with sterile PBS injected through a 10mL syringe (BD). The chamber was then deconstructed, the individual components were dried and exposed to ultraviolet light for 30 minutes.

Samples of flat PCL and nanofiber PCL scaffold were positioned at the 10mm diameter section of the chamber and compressed by the silicone membrane and microscope slides before being clamped by binder clips to form a seal. (Figure 5) Two chambers were prepared with the samples, one as a control for static exposure to the extracted plasma the other for dynamic conditions. The flow setup was repeated in a sterile hood without the use of the microscope or camera. (Figure 6) The control chamber was manually injected with plasma with a 10mL syringe and left to incubate the samples for 30 minutes. The other chamber was attached to the flow setup and extracted plasma was run through the chamber at 10ml/min. When the syringe was near empty the pump was halted so that the chamber would not drain, and the syringe was refilled with plasma from the outlet catch and the syringe and pump were reset. This process as repeated

until the chamber had experienced 30 minutes of continuous flow. After rinsing with sterile PBS the PCL samples were fixed for field emission scanning electron microscopy (SEM, JOEL JSM-6300) imaging to observe differences in platelet adhesion and activation according to material and flow conditions. The fixative solution consists of 3% glutaraldehyde (Sigma), 0.1M sodium cacodylate (Polysciences), and 0.1M sucrose (Sigma) and the PCL samples were incubated for 45 minutes. The samples were then transferred to a buffer containing 0.1M sodium cacodylate and 0.1M sucrose for 10 minutes. The platelets were dehydrated by soaking the substrates in increasing concentrations of ethanol (35%, 50%, 70%, and 100%) for 10 minutes each. Further dehydration was achieved by soaking the substrates in hexamethyldisilazane (HMDS, Sigma) for 10 min. Samples were dried for another 10 minutes in a fume hood. Before imaging the samples were cut to 1cm diameter circles using a biopsy punch (Acuderm) and coated with a 10nm layer of gold. Imaging was performed at 15 kV. The SEM images were used to determine the population density and activation characteristics of the platelets that had adhered on each type of surface with the consideration of flow.

This process was repeated for the stent chambers with some modifications. Due to the maximum width of the stent chambers being 6mm the PCL rectangles were placed vertically on the wax chamber before sealing and exposing to flow. In addition samples were placed near the inlet and outlet of the flow adding another variable based on exposure to an increasing number of shear gradients and the flow travels through the chamber. SEM images were used to analyze platelet activation and adhesion not only based on flow and surface characteristics but also on the basis of location in the chamber.

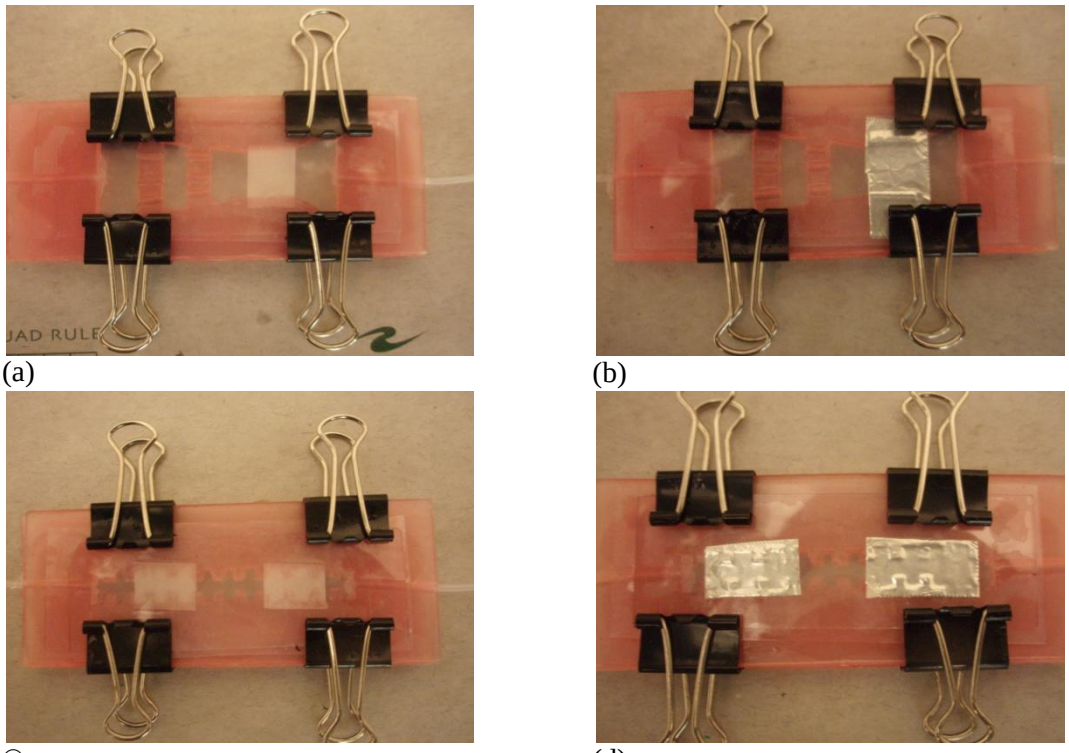

Figure 5 – Flow chambers with immobilized PCL samples. (a) Flat PCL sample in laminar flow chamber. (b) PCL nanofiber sample in laminar flow chamber. (c) Flat PCL samples in stent flow chamber. (d) PCL nanofiber samples in stent flow chamber.

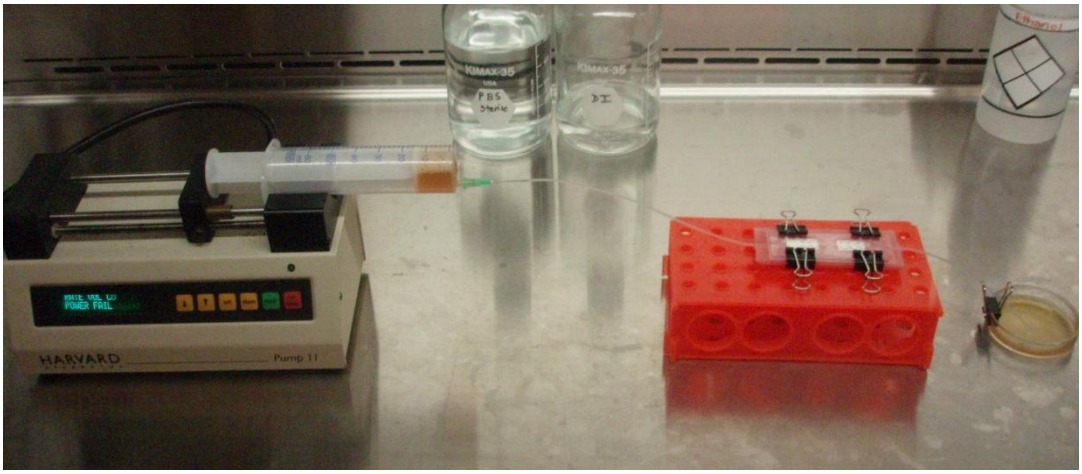

Figure 6 – Platelet adhesion study set up in sterile hood.

Live staining and fluorescence microscopy

The procedures established for exposing PCL samples to flowing plasma for SEM fixing were repeated in a sterile hood. Once both flat PCL and electrospun nanofiber samples had been exposed to plasma for 30 minutes and rinsed with sterile PBS they were placed in individual 6-

well plates, face up. The lights were turned off and to each well containing sample was added 2mL of 2µM calcein-AM (invitrogen) suspended in sterile PBS. The substrates were incubated for 30 minutes in the calcein stain followed by two rinses for 5 minutes in sterile PBS. The samples were imaged with a fluorescence microscope (ziess) using FITC MF101 Green filters.

RESULTS AND DISCUSSION

Flow Chamber Design

In this work we have designed and fabricated a perfused flow chamber that combines the benefits both microfluidics devices and bioreactors, notably the ease of fabrication, ability to immobilize samples such as tissue engineering scaffolds in fluid flow and use of microscopy for live imaging. Dental modeling wax used for the body of the chamber provides a bio inert and highly moldable substrate and is similar to PDMS in this respect. Visual clarity is maintained the use of microscope slides while a silicone membrane bound to the chamber contacting surfaces of the slides upkeeps the bio inert internal environment. The design allows for samples to be loaded and removed quickly, without damage to the flow chamber. Chamber design has also proved resistance to leaking at pressures initiated by fluid flow rates in excess of 25 ml/min for a period of 30 minutes and 60 ml/min for a short exposure.

Figure 7A displays the chamber designed to study the effect of laminar flow on a tissue engineered scaffold or medical device. The 10mm by 10mm area designated (A) represents the target area in which a sample would be immobilized. The inlet flow is modeled after a parallel plate flow chamber and separates the inlet stream making a uniform flow. Blood flow in most areas of the body is laminar except in areas of the aorta or when stenosis occurs within blood vessels, thus most implanted materials or scaffolds would be subject to this type of flow.

Figure 7B displays the flow chamber designed to portrait the shear gradients and stagnation zones formed by stents in the plane parallel to flow. The point marked (A) is where the chamber widens creating a 2mm x 2mm box in which we'd expect slower flow while point (B) is in the center of the stent chamber with a diameter of 2mm where'd we would expect the fastest flow.

The scale in comparison to an implantable stent is exaggerated due to limitations of the fabrication technique, accuracy was achieved with cuts of 2mm or larger. The maximum length of both interior chamber designs is 55mm to accommodate the length of a microscope slide.

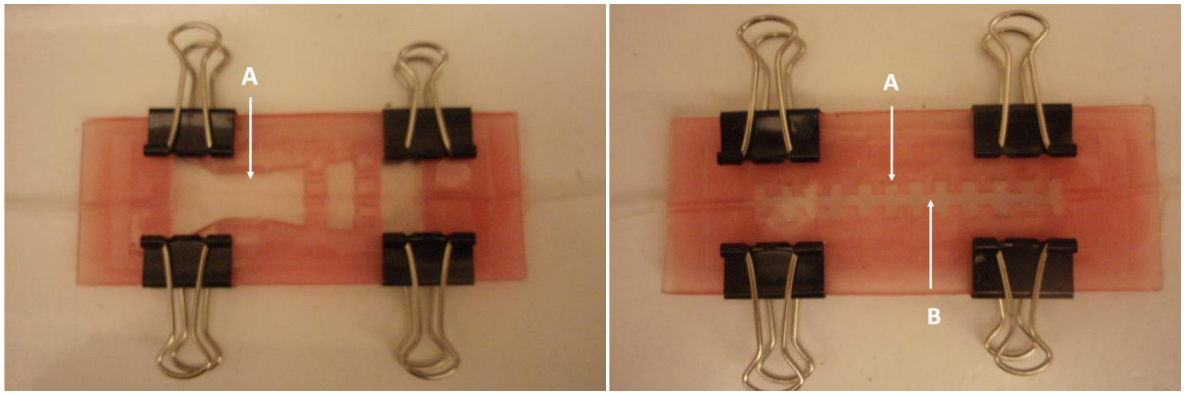

A B

Figure 7 – (A) Chamber set up designed for laminar flow. (B) Chamber set up designed to model stent conformation and creation of shear gradients in the flow.

Stents are wire tubes supported by struts used to add mechanical strength to arteries during angioplasty. Experimental models have shown strut width to be on the order of 10^{-1}mm and protrusion into the flow domain on the order of 10^{-2}mm with spacing from 2-4 mm apart.[53-54] The most common cause of long term stent failure is the reduction in lumen size or, restenosis initially caused by thombus formation following implantation. Stent implantation alters the geometry of the flow and studies have found that strut protrusion into the flow stream and strut spacing are critical to stent design and the rate of restenosis. A flow visualization study has observed vortices created in an implanted stent, the size of these flow disturbances were larger than the stent struts and were followed by zones of stagnation dependant on strut spacing[55]. Changes in shear at flow disturbances such as these vortices are precursors to platelet activation and the formation of discoid platelet aggregates leading to thrombi[56-60]. The stent flow chamber model seeks to replicate the results with the creation of flow patterns at a larger scale.

Fluid Flow and Particle Image Velocimetry

Figures 10-18 depict processed videos from fluid flow in the designed chambers. Each figure includes snapshots from (A) the compiled raw, (B) a layered image of all 100 frames which allows us to follow the path of tracking particles, (C) a color inverted video with background reduction and (D) a vector field created through PIV analysis of the video from (C). In the vector field arrows represent the distance a particle at the vector's starting point would move relative to the next frame, distance can be extrapolated using the legend in the upper left corner which consists of an arrow depicting a 5 pixel shift. All images are oriented so that the inlet of the chamber is on the left with outlet on the right.

The laminar flow chamber provides flow which is largely homogenous across the focal plane of the target there is some directional flow that enters the first third of the target area (Figures 8, 11 and 14). The stent flow chamber creates two different flow patterns, a homogenous high velocity linear channel in the center of the chamber and cyclical areas with back flow. These stagnation zones are ideal for the creation of shear gradients along the border where these flow patterns meet (Figures 9, 10, 12,13,15 and 16). Magnification at 10x and 16x appear to be too weak to visualize platelets for PIV analysis (Figures 12, 14 and 15).

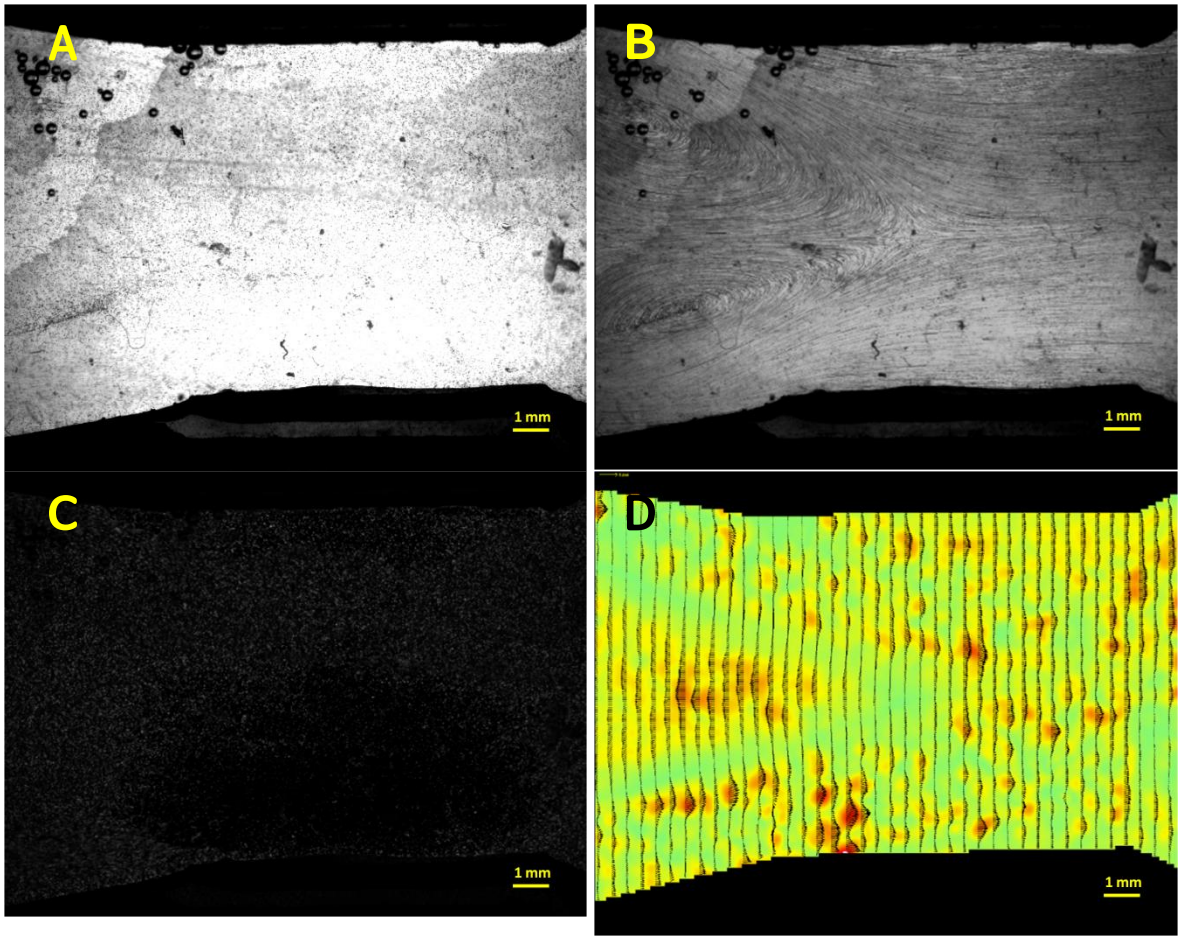

Figure 8 – Laminar flow chamber. Polyamide seeding particles suspended in water, flow at 10ml/min with magnification at 10x. Layered image (B) shows the path of the fluid while vector field (D) shows observable back flow near the inlet and homogenous flow through most of the chamber.

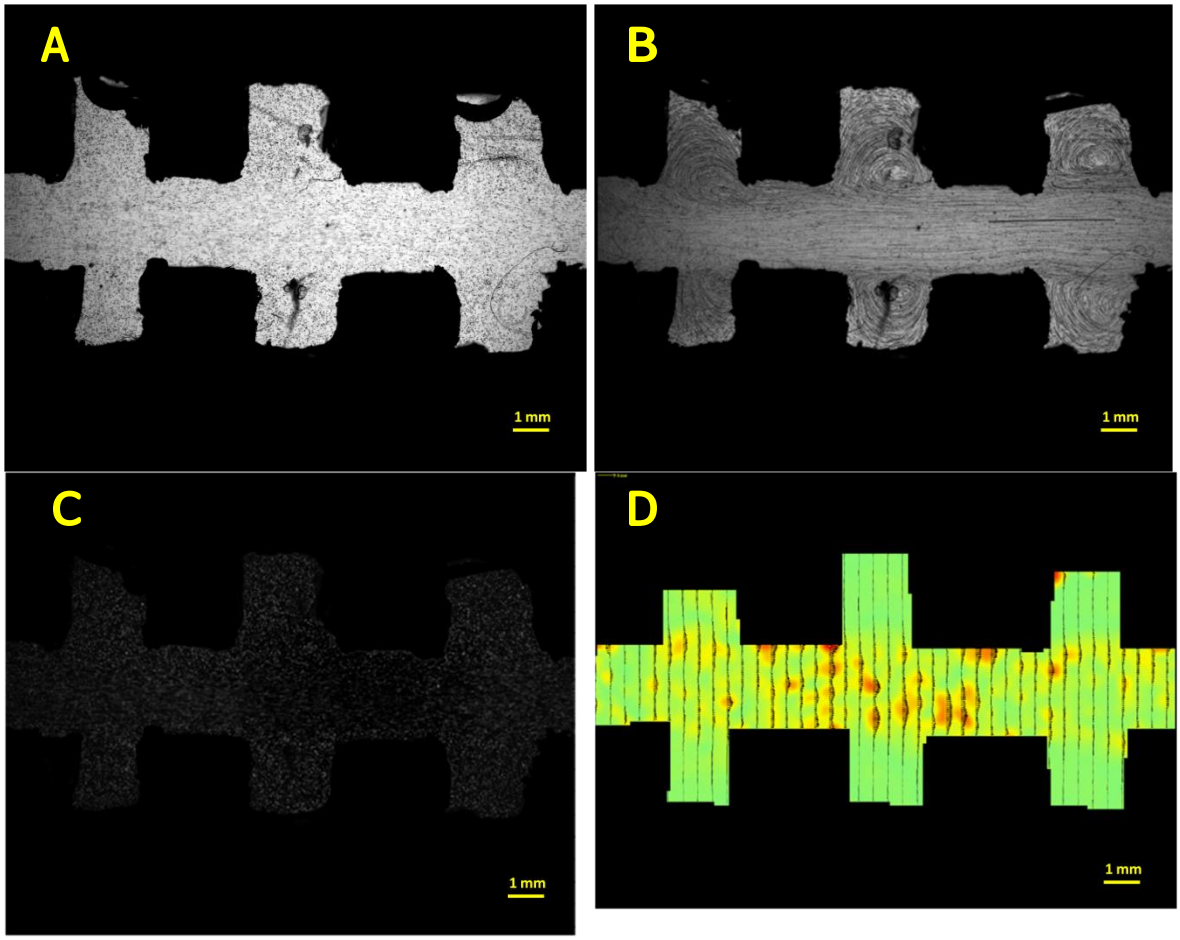

Figure 9 – Stent flow chamber. Polyamide seeding particles suspended in water, flow at 10ml/min with magnification at 10x. Layered image (B) follows the path of the fluid, there are observable stagnation vortices in each inlet while flow in the central channel appears to be homogenous. Vector field (D) shows us the speed of the flow in the central channel.

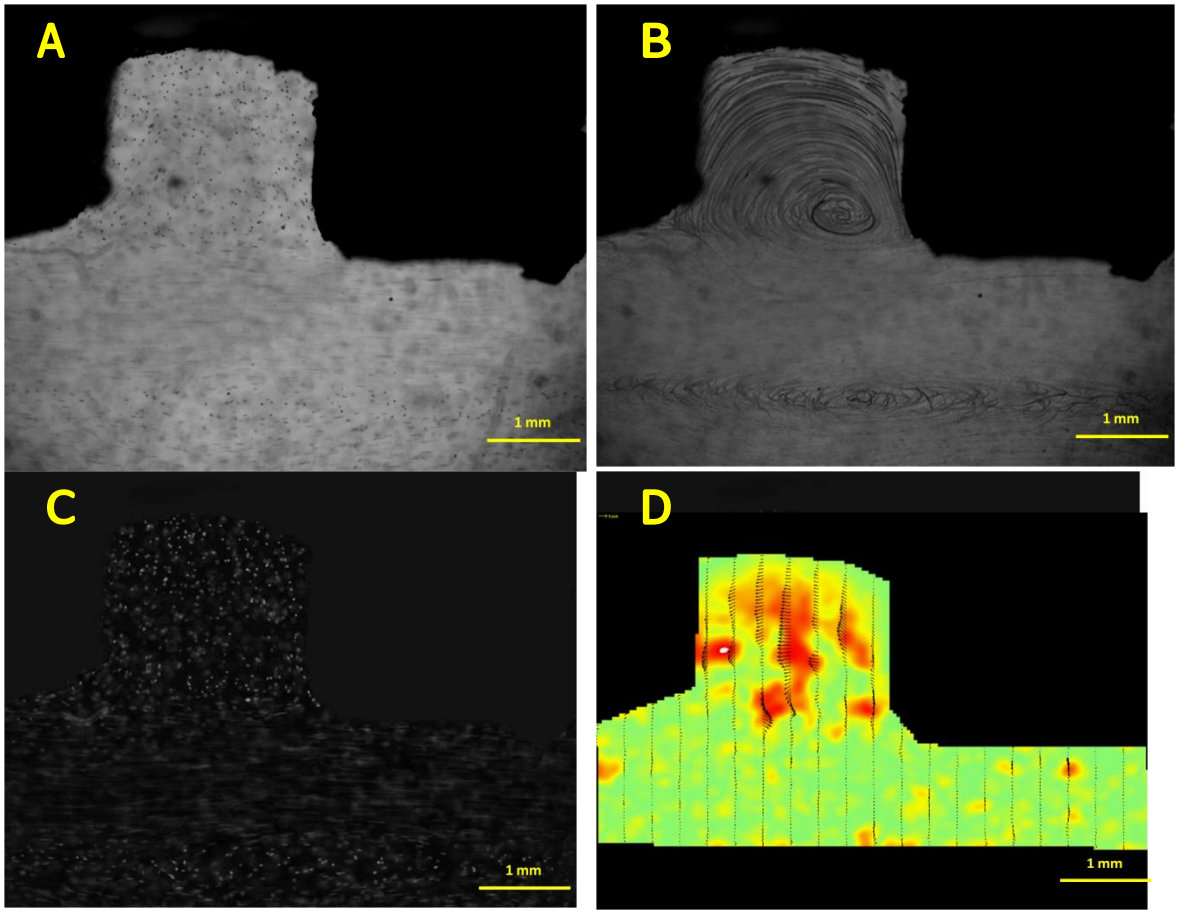

Figure 10 – Stent flow chamber. Polyamide seeding particles suspended in water, flow at 10ml/min with magnification at 32x. Layered image (B) shows the path of the fluid highlighting the stagnation zone in the indent. Vector field (D) highlights the velocity of back flow in the indent.

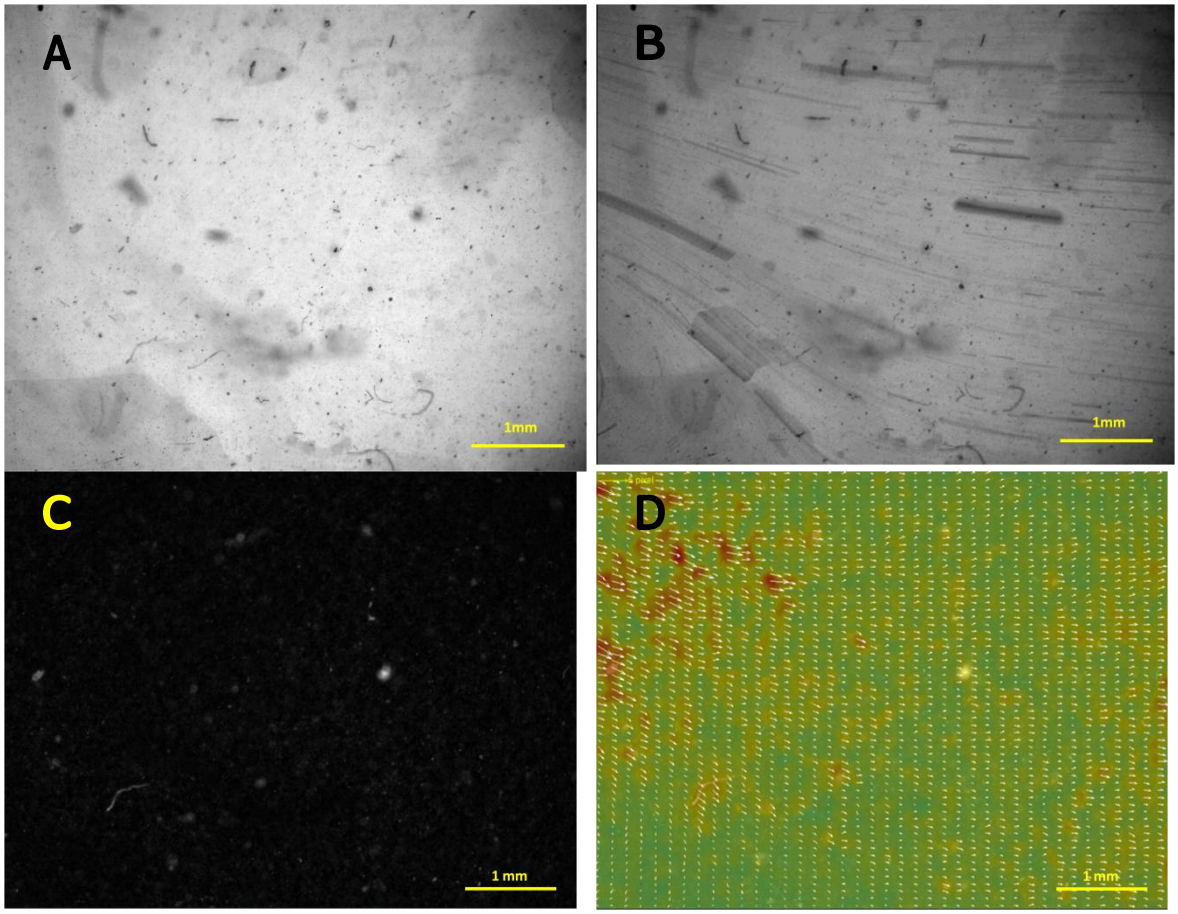

Figure 11 – Laminar flow chamber. Fluid is expired plasma, flow at 10ml/min with magnification at 32x. Layered image (B) shows the path of the fluid coming from the inlet, the vector field (D) shows that flow becomes homogenous. Higher magnification necessary to track platelets that have a diameter a fifth the size of a PSP.

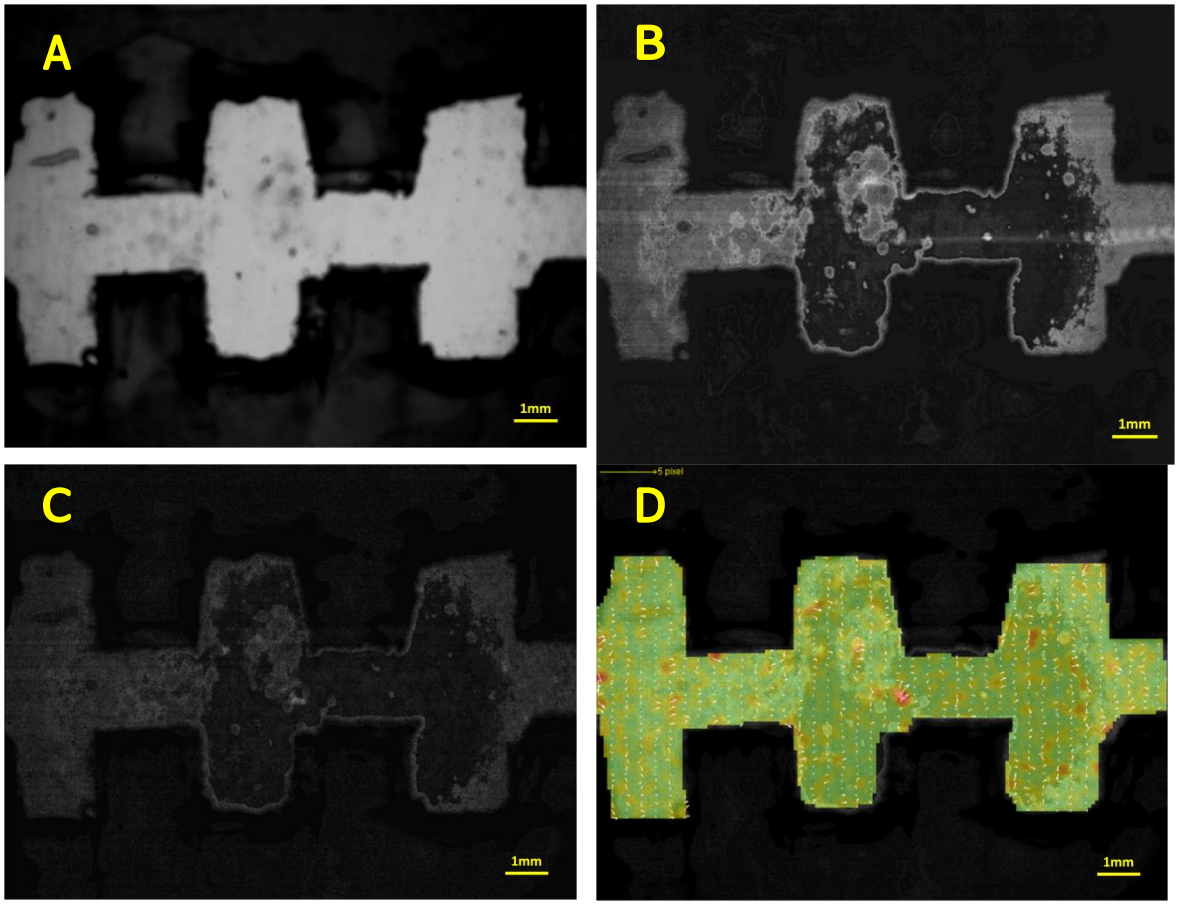

Figure 12 – Stent flow chamber. Fluid is expired plasma, flow at 10ml/min with magnification at 10x. Layered image (B) shows the path of fluid though there are only a couple of large particles to track, vector field (D) is sporadic, software may not be suited to tracking platelets at this magnification.

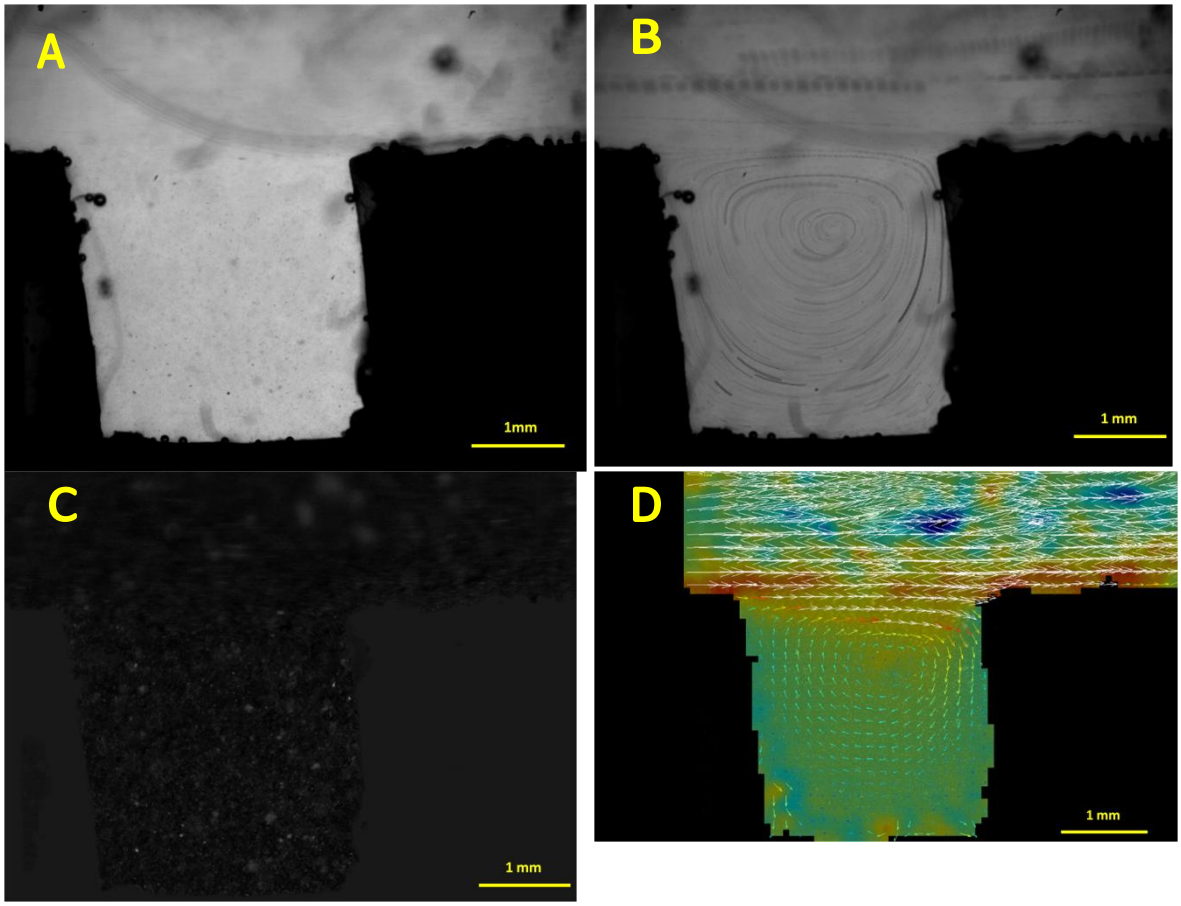

Figure 13 – Stent flow chamber. Fluid is expired plasma, flow at 10ml/min with magnification at 32x. Layered image (B) shows the path of fluid both back flow in the stagnation zone and central flow are observable. Vector field (D) highlights the linear velocity of the fluid turbulence near the walls of the chamber.

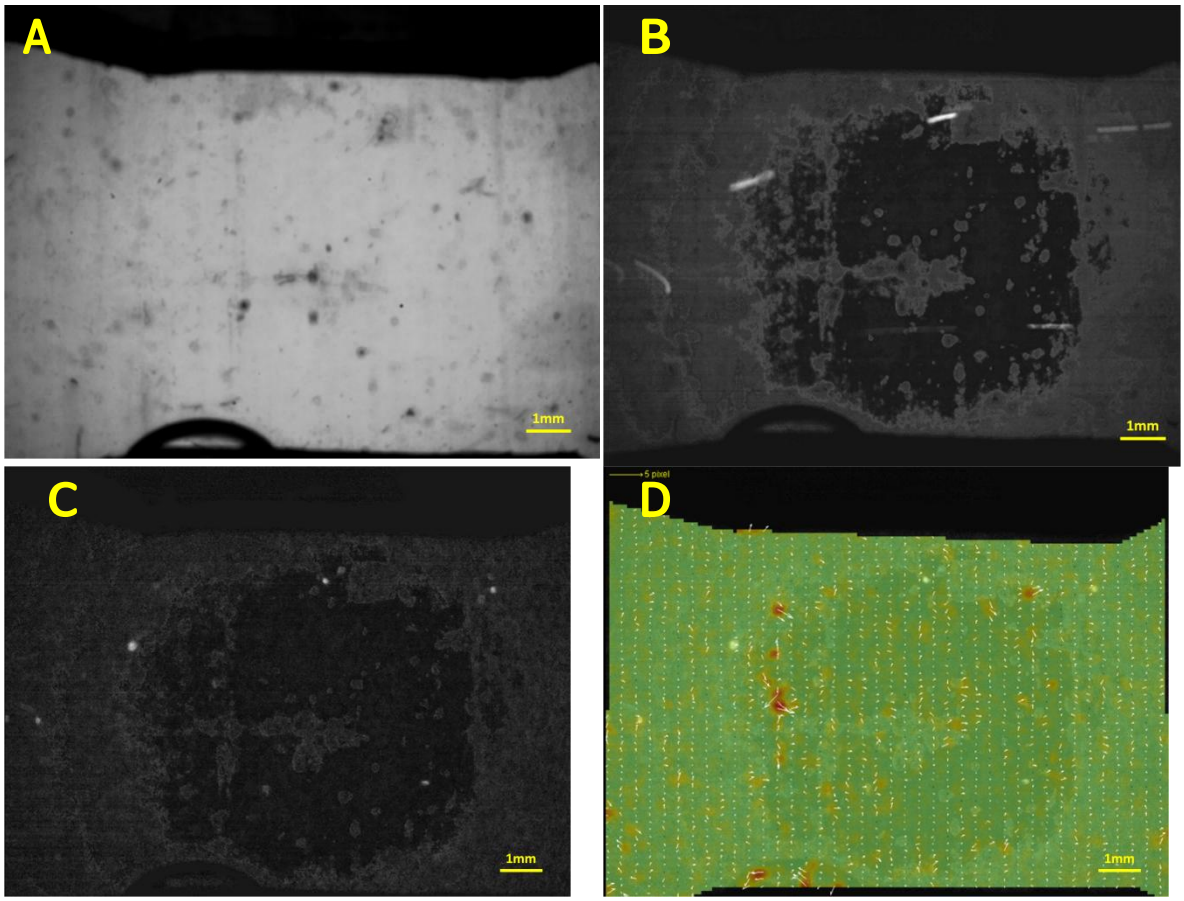

Figure 14 – Laminar flow chamber. Fluid is human plasma extracted from whole blood, magnification at 10x. Layered image (B) is unable to track more than a couple of large particles. Vector field (D) is also very sporadic and unable to confirm uniform flow or platelet tracking at this magnification.

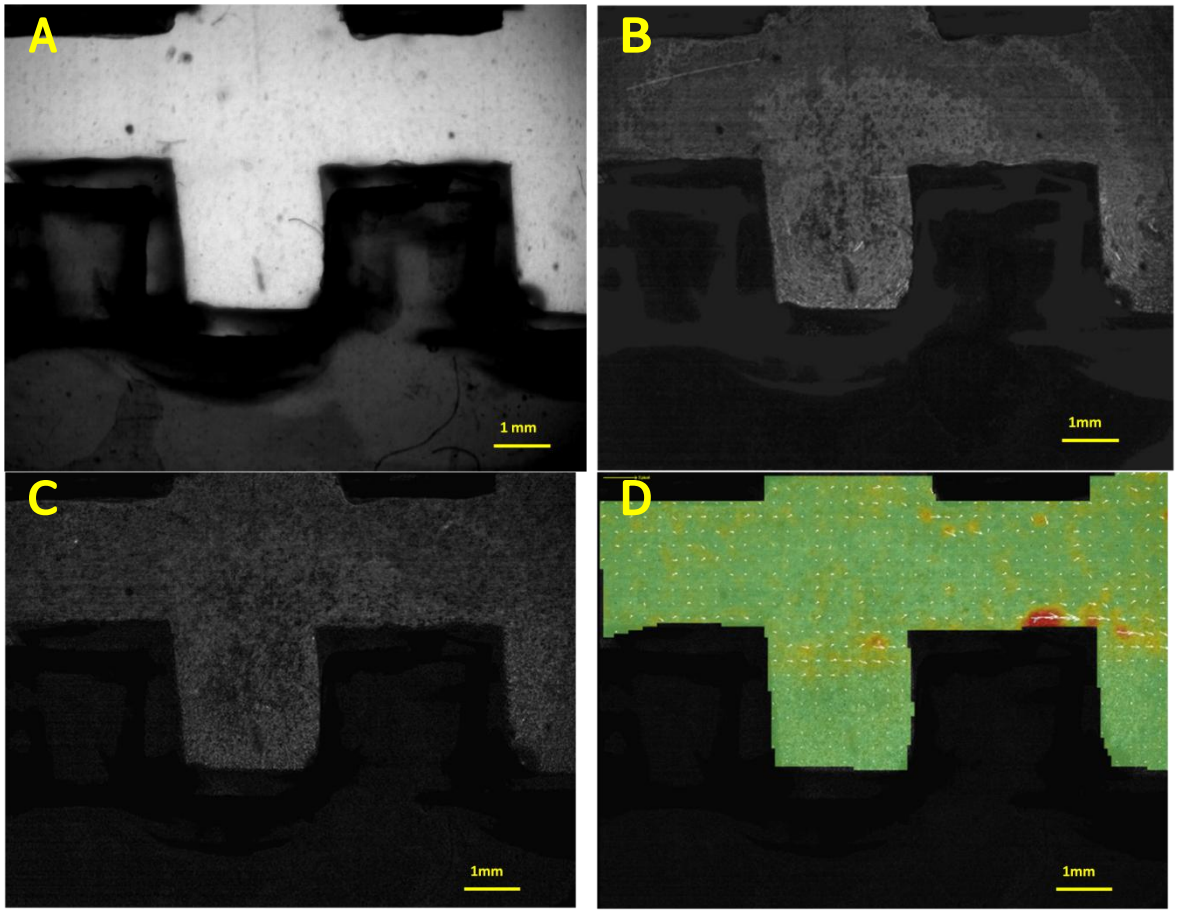

Figure 15 – Stent flow chamber. Fluid is human plasma extracted from whole blood, magnification at 16x. Layered image (B) is able to track some particles but there are not enough targets to show fluid path. Vector field (D) is able to track flow in the main flow channel and the entrance to a stagnation zone.

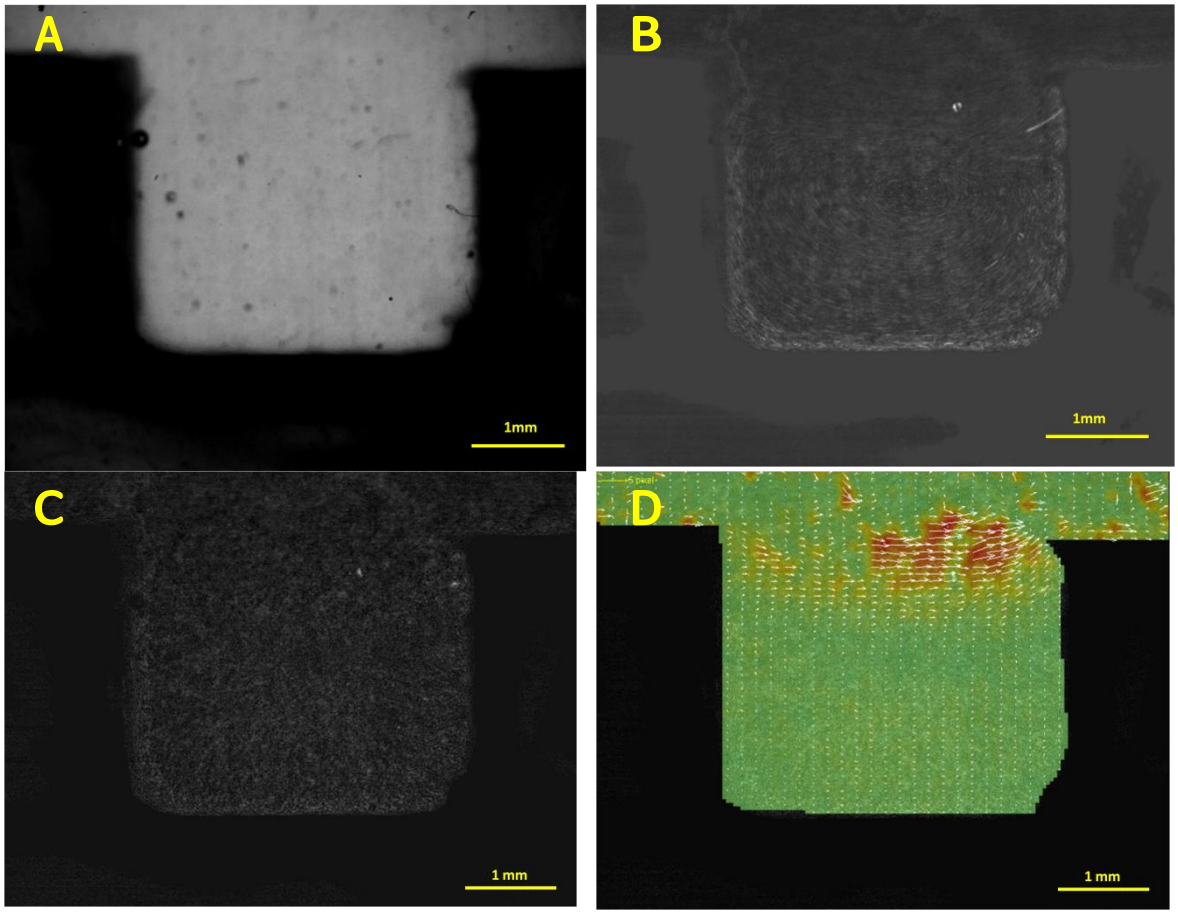

Figure 16 – Stent flow chamber. Fluid is human plasma extracted from whole blood, magnification at 32x. Layered image (B) is able to track particles and cyclical flow in the stagnation zone. Vector field (D) is able to track flow in the main flow channel and the entrance to a stagnation zone while velocity doesn't appear cyclical though there is observable turbulence.

The velocity of extracted plasma traveling through both flow chambers were calculated through use of retention time and extrapolated with the PIV vector fields. Focal point is centered over the section of the chamber with the smallest diameter thus vector analysis will be designated in the same space. Average experimental velocity from the laminar flow chamber was obtained by recording the vector length at 9 evenly distributed nodes(3x3) across the 10mm by 10mm target area for sample immobilization and computing the average of those vectors before extrapolating with the vector legend and the scale bar. (Figure 17A) Average experimental velocity for the stent chamber was calculated in a like manner with two distributions of nodes being issued both the center of the 2mm x 2mm stagnation zone and in the center of the flow. (Figure 17B) For simplicity we assume the distribution of flow in the stagnation areas is uniform though cyclical,

in addition the combined area of the stagnation zones are equivalent to the area of central flow. The average velocity in the stent chamber was calculated by the mean of all the vector lengths recorded. Maximum velocity of the fluid is calculated from the average of longest vectors measured in 5 different frames within the focal area. Average and maximum speed calculated in this manner are used to find the fluid dynamic parameters of Reynold's Number and shear stress. (Table 1)

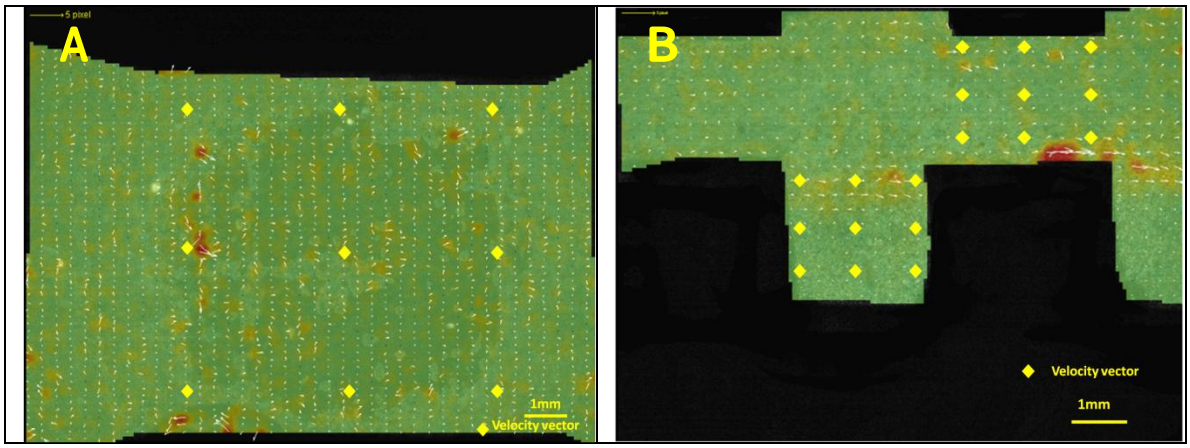

Figure 17 – (A) Laminar flow chamber, extracted whole blood plasma, 10x zoom with nodes at which vectors were calculated from. (B) Stent flow chamber, extracted whole blood plasma, 10x zoom with nodes in the stagnation and flow zones at which vectors were calculated from.

Table 1 – Calculated velocity of plasma extracted from whole blood based of retention time and PIV imaging. Flow rate (Q) = 10mL/min. Volume and cross-sectional area of laminar flow chamber: 2275mm^3 and 35mm^2 respectively. Volume and cross-sectional area of stent flow chamber: 385mm^3 and 7mm^2 respectively.

	Hydraulic Diameter (d_h)	Retention Time	Calculated fluid velocity (v)	Experimental average velocity	Experimental maximum velocity
Laminar Flow Chamber	5.185 mm	13.65 s	4.762 mm/s	3.15 mm/s	11.3 mm/s
Stent Flow Chamber	2.545 mm	2.31 s	23.81 mm/s	25.943 mm/s	44.27 mm/s

Reynolds number is a dimensionless fluid parameter used to describe the nature of flow. It is defined as the ratio of dynamic forces to viscous forces and is also an important application of dynamic symmetry in modeling. The Reynolds number is defined as :

$$Re = \frac{\rho V d}{\mu}$$

Where V= fluid velocity, d represents characteristic length (hydraulic diameter for rectangular ducts) and μ is the dynamic viscosity[61]. The critical Reynolds number is 2300, below this number flow is laminar and occurs in layers with no mixing of adjacent fluid. Flow is considered transitional if 4000 > Re > 2300 and turbulent when Re > 4000. Reynolds number was calculated for both flow chambers using maximum experimental velocity and calculated velocity. (Table 2) All results return Reynolds numbers that are well below 2300 defining laminar flow.

Table 2 – Calculated Reynolds numbers for both types of fluid chambers, $\rho = 1.025\ kg/m^3$ and dynamic viscosity $\mu = 1.6*10^{-3}\ N*s/m^2$.

	Re (calculated fluid velocity)	Re (experimental average fluid velocity)
Laminar Flow Chamber	0.01582	0.01046
Stent Flow Chamber	0.03883	0.04230

Shear stress is a well defined factor in platelet aggregation and thrombi formation as well as a determining factor in the aspects which drive the formation of platelet aggregates. Application of constant flow through the chambers allows us to assume parabolic plasma velocity profiles similar to steady Poiseuille flow[62]. Use of the hydraulic diameter of each chamber reduces expression of shear stress to the Hagen-Poiseuille equation modified for rectangular ducts:

$$\tau = \mu \frac{4Q}{\mathrm{Ad_h}}$$

Where A is the cross sectional area of the rectangular duct, d_h is the hydraulic radius, Q is volumetric flow rate and μ is dynamic viscosity. Table 3 shows the shear stress in both the laminar and stent chambers calculated in this manner, both are well below the $1000s^{-1}$ shear mark required to change the characteristics of platelet adhesion. Activation and the presence of platelet proteins such as fibrinogen drive aggregate formation in both flow chambers. (Table 3)

Table 3 – Average shear stress in flow chambers using assumption of constant parabolic velocity profiles.

	Average Shear Stress
Laminar Flow Chamber	5.877 s^{-1}
Stent Flow Chamber	48.648 s^{-1}

Platelet adhesion study on PCL scaffold material

Poly(ε-caprolactone) (PCL) is a homo polymer with a semi-crystalline structure that has a slow biodegradation rate and low melting temperature[63]. PCL is degraded by hydrolysis of ester linkages in physiological conditions and resulting degradation products are easily bioresorbed by the body[64]. Extensive research on PCL biocompatibility and efficacy have been performed in vivo and in vitro and it has garnered US Food and Drug Administration approval as an implantable biomaterial for medical devices[65-68]. Historically PCL has had extensive clinical use in biomedical applications such as drug delivery and sutures. Capitalizing on its slow degradation rate and low melting temperature, PCL structures such as nano particles and membranes can be fabricated and impregnated with bioactive molecules for extended delivery to the body[69-70]. PCL is able to be processed and combined with a number of existing micro- and nanoscale fabrication technologies such as electrospinning and nanowire extrusion [64,71,]. These qualities make it an ideal material for three dimensional scaffolds of both hard (bone) [64, 72] and soft (vascular) tissues[73]. Platelets are small cells (3-4 microns in diameter) derived from megakaryocytes found in the blood that play a primary role in hemostasis through activation and the formation of a platelet plug and later a fibrin clot to support vascular wall integrity and assist in further platelet recruitment. Platelet adhesion to biomaterial surfaces are often the result of platelet activation. Activating factors include plasma proteins such as thrombin and firbrinogen, vascular wall products such as collagen, activation of integrin αIIbβ3 by fibrinogen and soluble agonists secreted from activated platelets: von Willebrand Factor(vWF), adenosine diphosphate(ADP) and thromboxane A2.[23,74] Platelet activation is characterized by a drastic shape change from a discoid to amorphous form, exocytosis of granules containing ADP, thrombin and activating

factors and adhesion to bioactive surfaces like collagen and other platelets resulting in an aggregate.

In contrast to scaffold biomaterials the hemocompatibility of common blood contacting medical devices such as heart valves, stents, vascular grafts, catheters and fluid pumps are well studied.[53-54, 75-82] An additional factor for analysis of hemocomapibility with these medical devices is the addition of flow. Fluid dynamics control the growth of thrombi and deposition of fibrin based on shear gradients within the flow. The delivery of cells and proteins to a wound site is an additional consideration. Extra considerations are taken in the design criteria of blood contacting devices to assure that zones of stagnation and recirculation are avoided, these patterns in flow are susceptible to thrombus growth. In addition platelet aggregation is controlled by differing mechanisms at varying shear rates.[56-60]

Studies have shown that shear microgradients occurring in vivo as a result of thrombus formation or vessel stenosis can lead to the development of stable discoid platelet aggregates without functional agonist responses of cytosolic calcium increase, shape change or alpha granule secretion. [59,48] Shear accelerating zones in which platelets experience shear rates in excess of $1000s^{-1}$ trigger the development of membrane tethers on the platelets and platelet recruitment. Exposure to a shear deceleration zone allows for the stabilization and reconfiguration of these membrane tethers resulting in a platelet aggregate forming in the downstream shear expansion zone.[56, 59, 60, 84] The arrival of soluble agonists such as vWF and fibronectin coupled with activated integrin αIIbβ3 on platelet surfaces can then activate platelets and stabilize the aggregate promoting thrombus growth.[23,84] These studies show that fluid forces can directly drive initial platelet aggregation independent of biochemical cues. In contrast, observation of platelet aggregate formation in laminar flow (typically shear rates < $1000s^{-1}$) reveals similarities to static adhesion dependant on soluble agonists and activation of integrin αIIbβ3 to facilitate platelet

aggregation and stabilization.[56, 59, 60, 84] Figure 18 [60] Contrasts the flow rates and illustrates the effect of increased shear on discoid platelet aggregation. Figure 19[58] highlights given characteristics of platelet adhesion for rising shear rates.

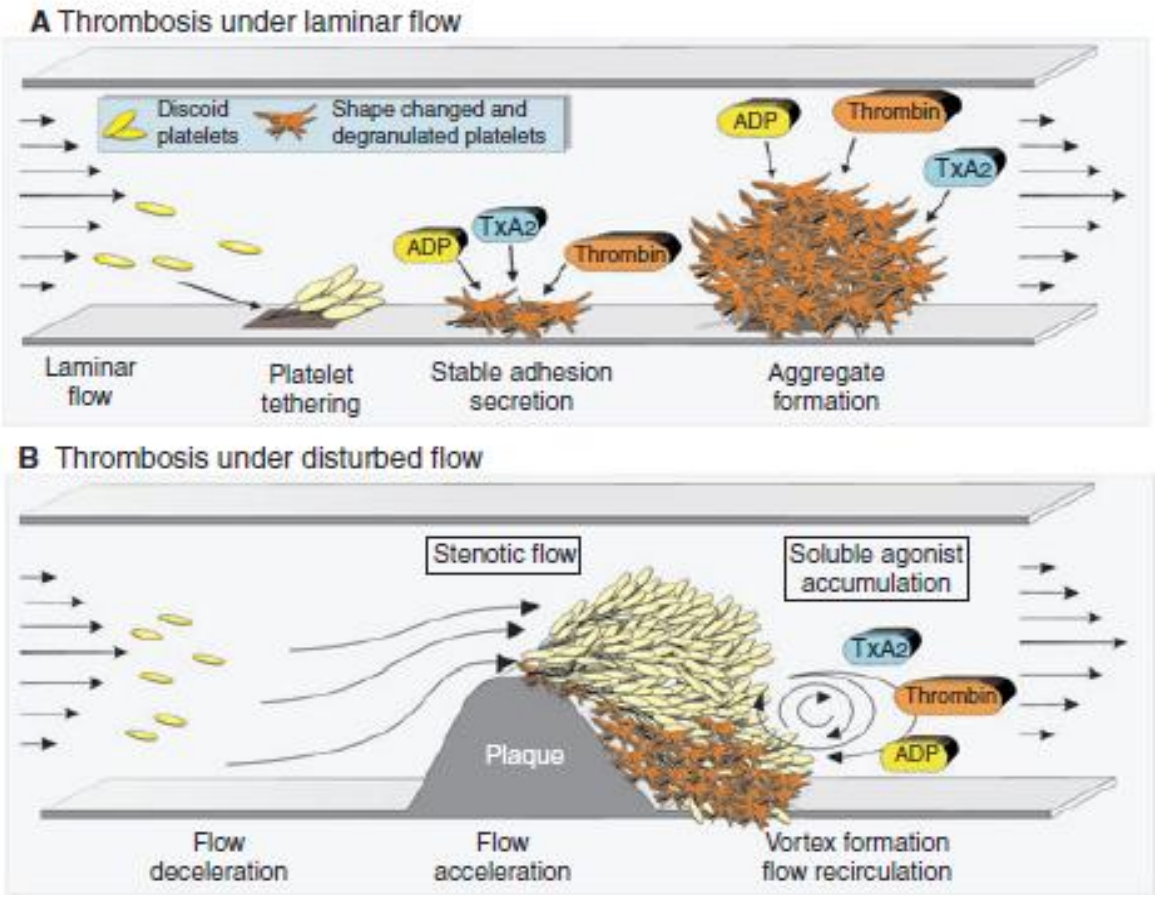

*Figure 18 – Illustation of a shear micrograd*ient on cell aggregation.

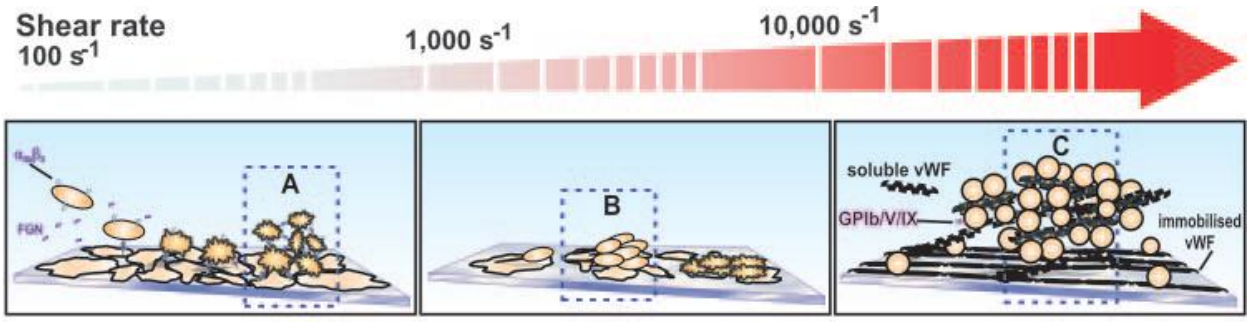

Characteristic features			
Adhesion Receptor	αIIbβ3	αIIbβ3, GPIb/V/IX	GPIb/V/IX
Activation Dependent	yes	yes	no
Tether Formation	no	yes	yes
Ligand	Fibrinogen	vWF, Fibrinogen	vWF
Platelet Morphology	Sphere + Filopodia	Discoid	Smooth Spherical

Figure 19 – Characteristic features of platelet adhesion and activation with rising shear rate.

Platelet adhesion and subsequent activation is a on the surface of a biomaterial is a strong indicator of hemocompatibility. In this study, platelets isolated from human whole blood and their adhesion and activation was explored in both static and dynamic settings. Dynamic studies included the use of both the laminar and stent flow chambers to test the affect of different flow patterns on platelet adhesion and activation. Platelet activation after 30 minutes of contact time to PCL nanofiber and flat surfaces under static and flow conditions were investigated by SEM imaging.

Scanning electron microscopy

Low magnification SEM images show significantly higher platelet adhesion on PCL nanofibers as compared to flat PCL surfaces. Comparisons are made with similar studies that share all non test variables. (Figures 20 vs.23, 26 vs. 29, 32 vs. 35, 38 vs. 44 and 41 vs. 47) Comparison of higher magnification SEM images comparing flat PCL surfaces to nanofibers in similar studies we observe that while platelets on both substrates are able to show platelet activation in the form of dendritic fiber elongation and adhesion to the surfaces (Figures 22, 25, 28 and 37). PCL

nanofiber surfaces however, show more evidence of clustering and platelet to platelet adhesion. (Figures 25 and 37).

Comparison of platelet activation and adhesion comparing static to dynamic flow settings with low magnification shows that platelet adhesion and concentration is much higher on the PCL surfaces with exposure to static surfaces. (Figures 20 vs. 26, 23 vs. 29, 32 vs. 38 and 41 and 35 vs. 44 and 47.) Comparison of static to dynamic flow at high magnification reveals that on flat surfaces observation of activated platelets with dendritic fibers is much more prevalent on surfaces exposed to flow. (Figures 27, 28 and 34 vs. 40 and 43) However PCL nanofibers did not show this trend and we observe either equivalent activation from both static and dynamic tests (Figure 36 vs 45 and 48) or in some cases, more activation from platelets under static conditions (Figure 24 vs. 30). This can be explained due to the dense platelet concentrations found on nanofibers in static settings, platelets secrete activating factors such as thrombin, vWF and ADP. While flow can serve to deliver these soluble agonists to platelets and activate them, platelet activation occurs within minutes during a wound healing response and high concentrations of these factors can be secreted by platelets and carried through the fluid by simple diffusion. The lack of flow prevents activating factors from diffusing into the fluid initiating activation in a large percentage of observable platelets.

Comparison of platelet activation and adhesion comparing the laminar flow chamber to the stent flow chamber with SEM at low magnification show very little to no difference in platelet density on flat PCL surfaces for both static and flow parameters. Comparison of PCL nanofibers in dynamic flow yielded less platelets in the center flow of the stent chamber while all other nanofibers comparisons were similar. (Figure 29 vs. 44) At higher magnification comparison of the two flow chambers show no major differenced either in increased adhesion or activation of platelets except in the case mentioned earlier. (Figures 21 vs. 31, 24 vs. 36, 27 vs. 39 and 42 and 30 vs. 45 and 48.)

In the stent flow chamber two areas of focus were compared during the study of the dynamic fluid flow to study the effect of platelet adhesion and activation within the chamber. The area of high flow rate is designated where the chamber narrows and the stagnation zone where the chamber flares out. Comparison of these areas in the stent chamber returns that while platelet deposition and density are higher in the zone of stagnation (Figures 38 vs. 41 and 44 vs. 47) there is no evidence of differences in platelet activation. Platelets in both areas show considerable amounts of activation particularly on flat PCL. (Figures 39, 40, 42 and

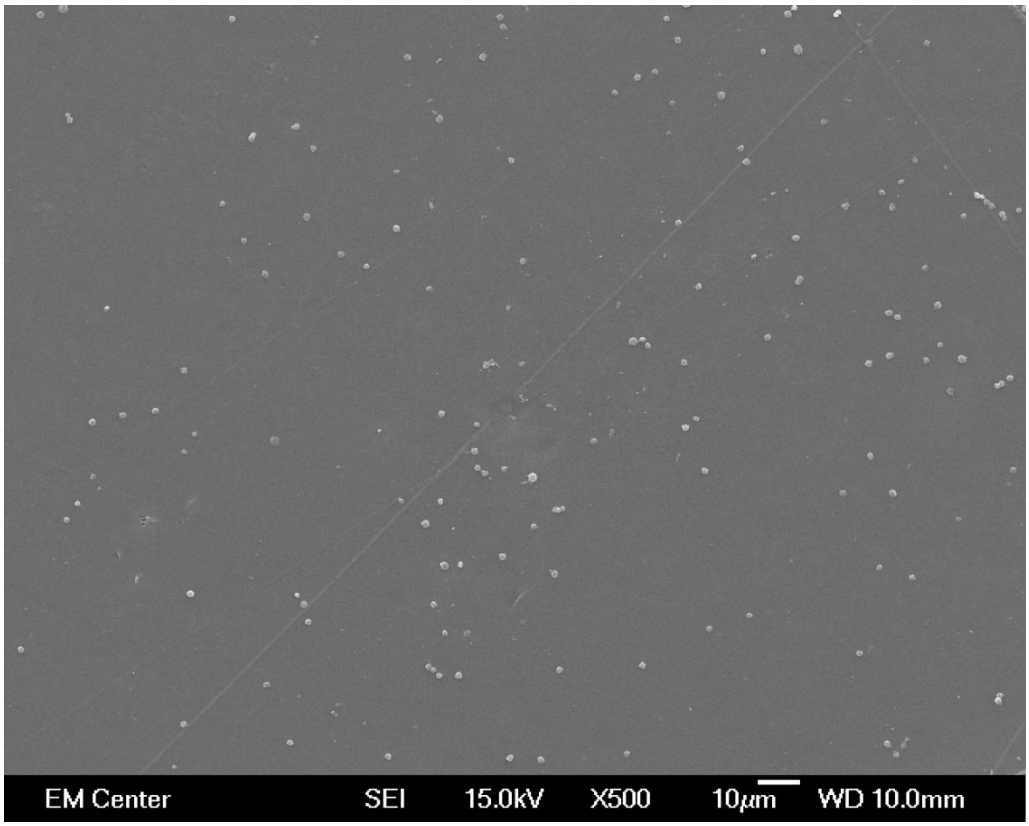

Figure 20 – Laminar flow chamber, static plasma exposure, flat PCL, 500x.

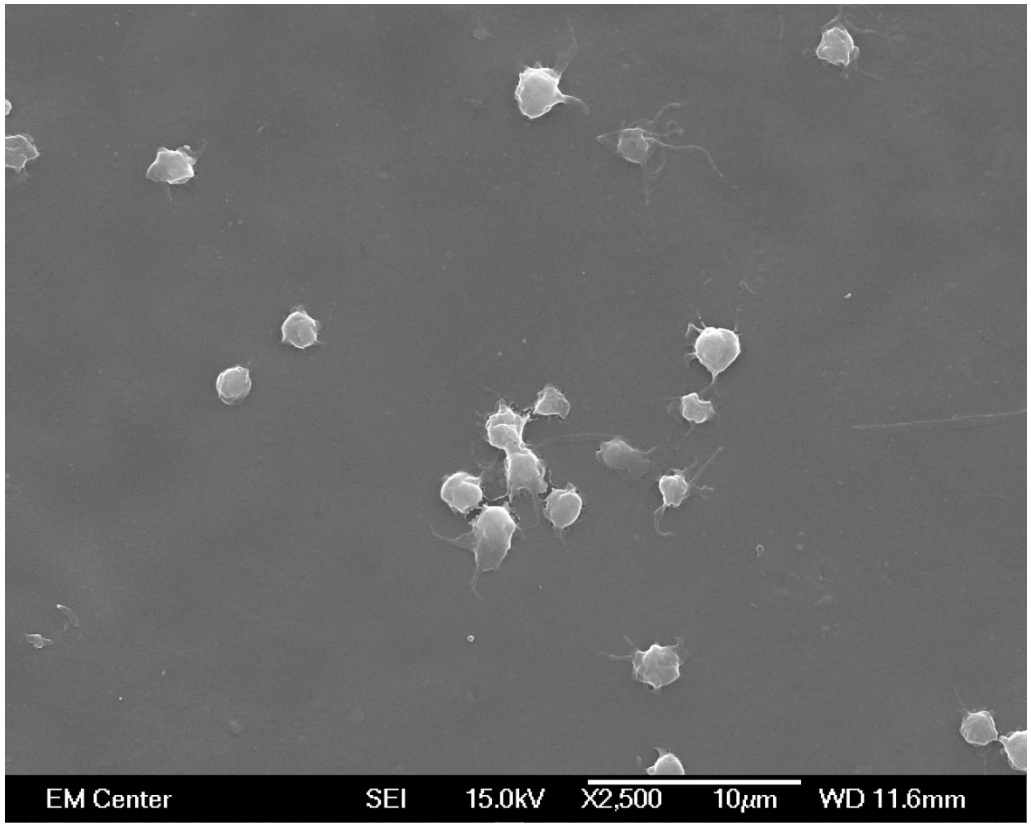

Figure 21 – Laminar flow chamber, static plasma exposure, flat PCL, 2500x.

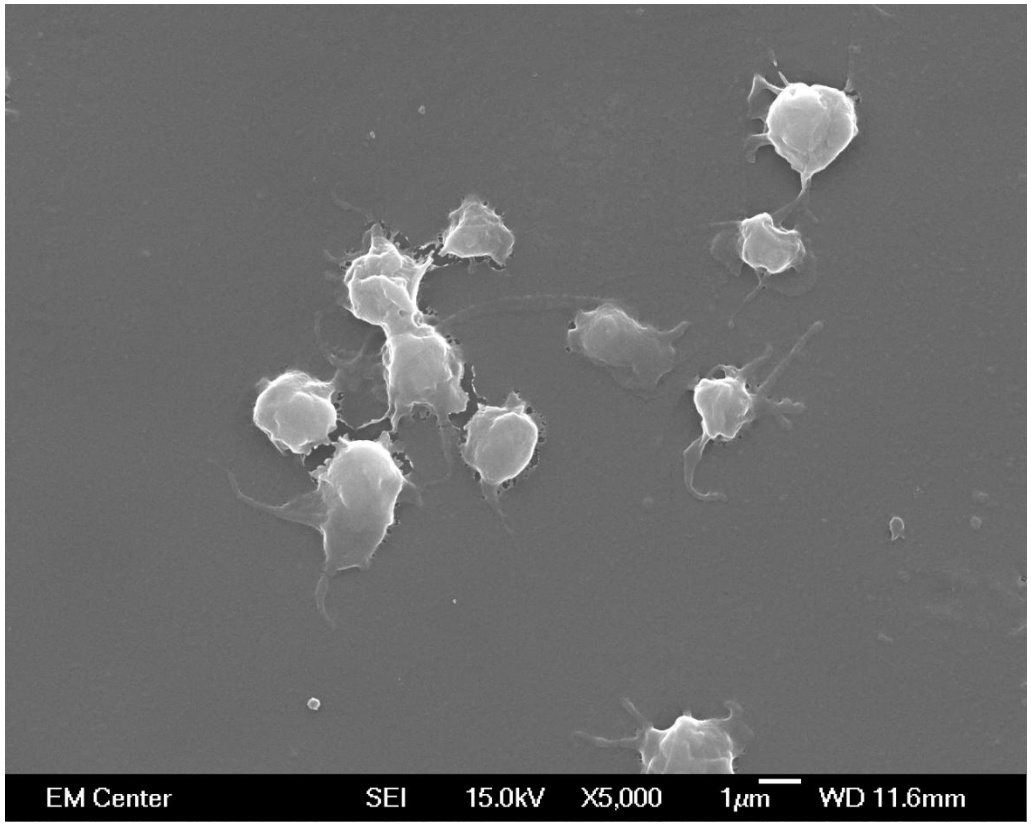

Figure 22 – Laminar flow chamber, static plasma exposure, flat PCL, 5000x.

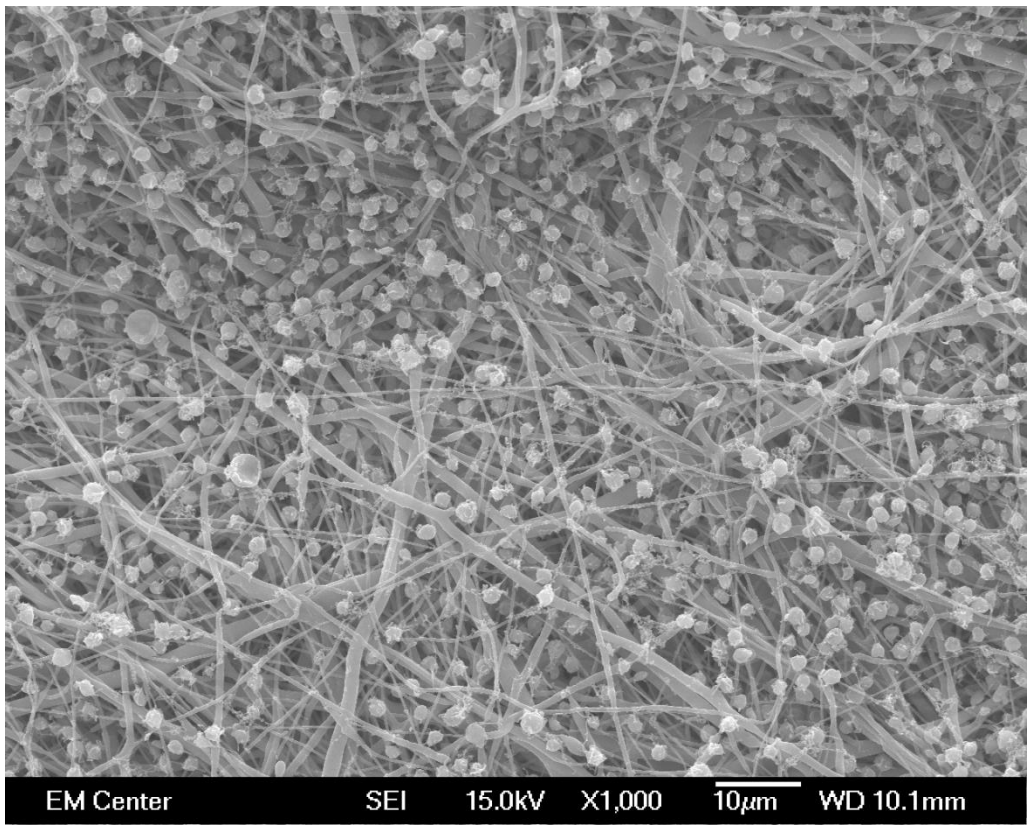

Figure 23 – Laminar flow chamber, static plasma exposure, PCL fibers, 1000x.

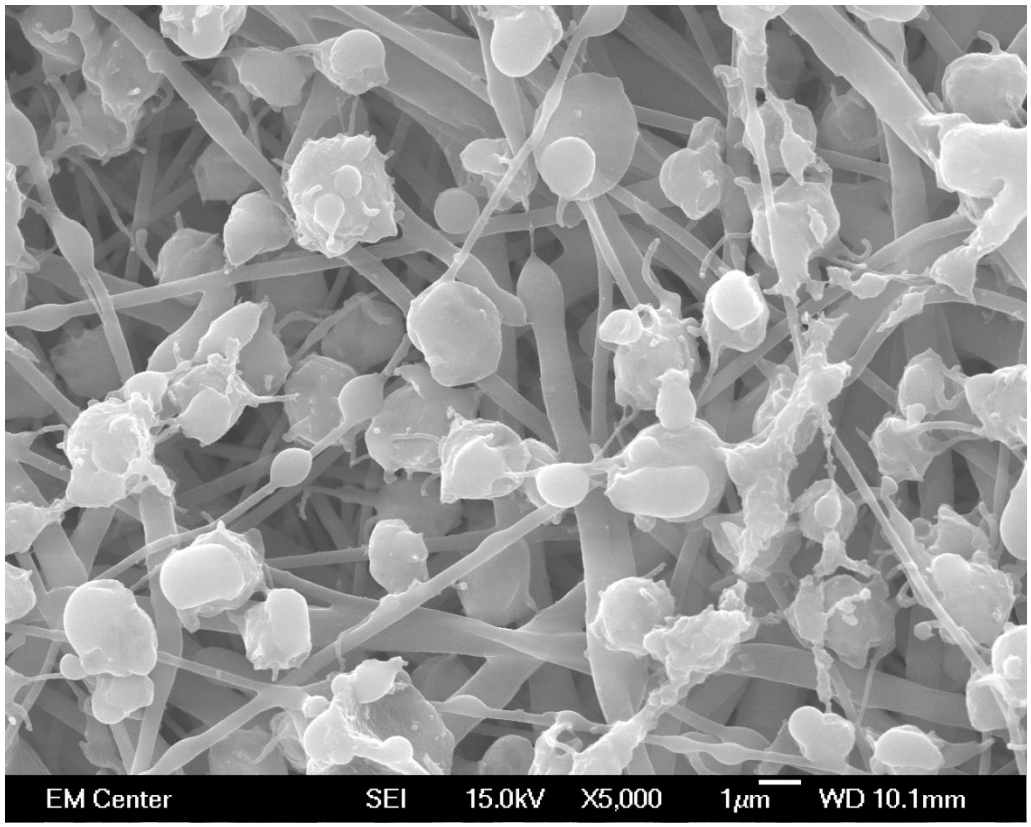

Figure 24 – Laminar flow chamber, static plasma exposure, PCL fibers, 5000x.

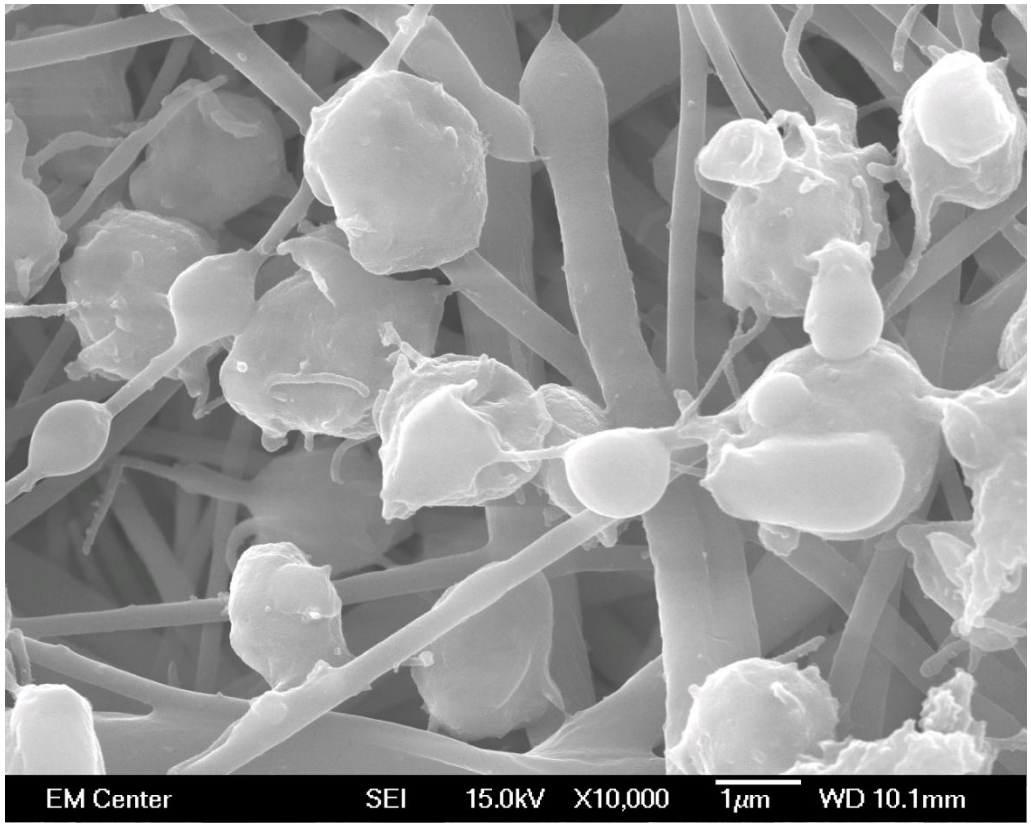

Figure 25 – Laminar flow chamber, static plasma exposure, PCL fibers, 10000x.

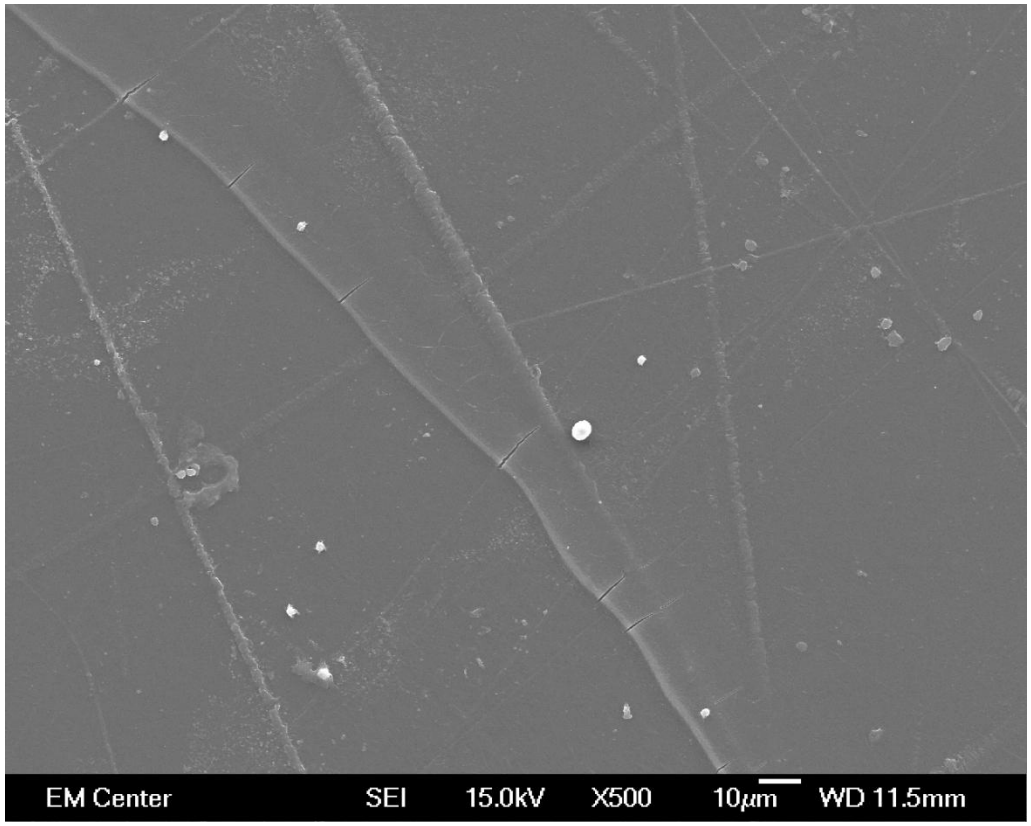

Figure 26 - Laminar flow chamber, dynamic plasma exposure, flat PCL, 500x.

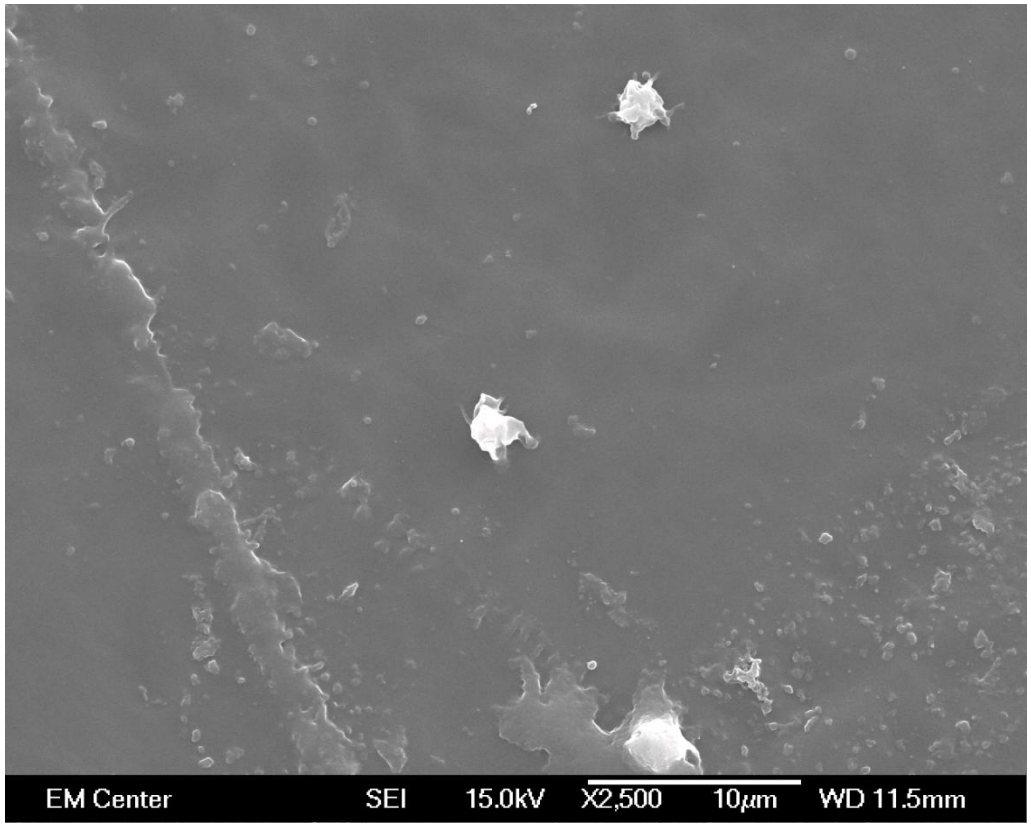

Figure 17 – Laminar flow chamber, dynamic plasma exposure, flat PCL, 2500x.

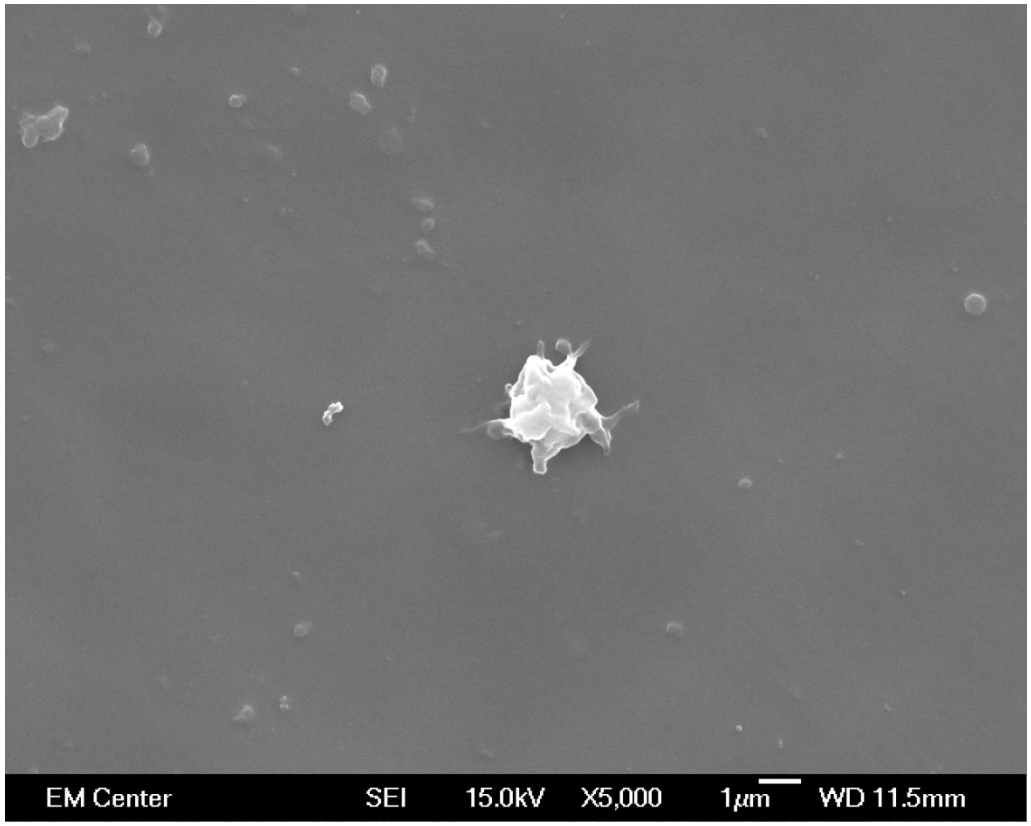

Figure 28 – Laminar flow chamber, dynamic plasma exposure, flat PCL, 5000x.

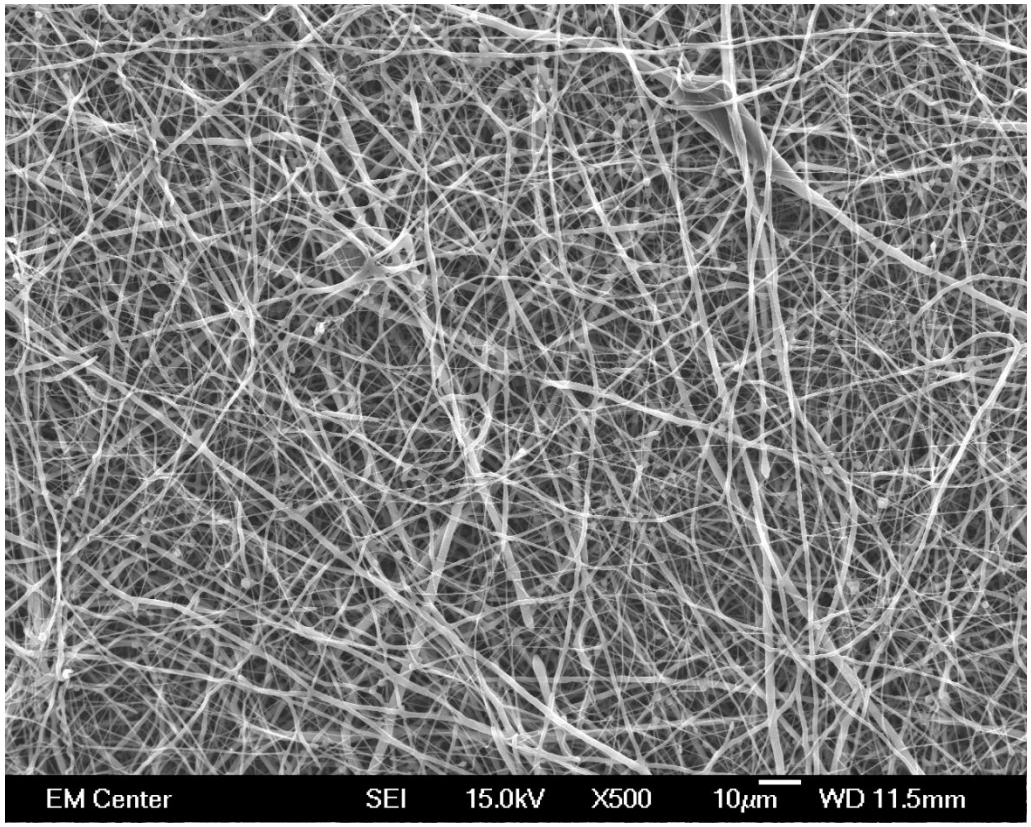

Figure 39 – Laminar flow chamber, dynamic plasma exposure, PCL fibers, 500x.

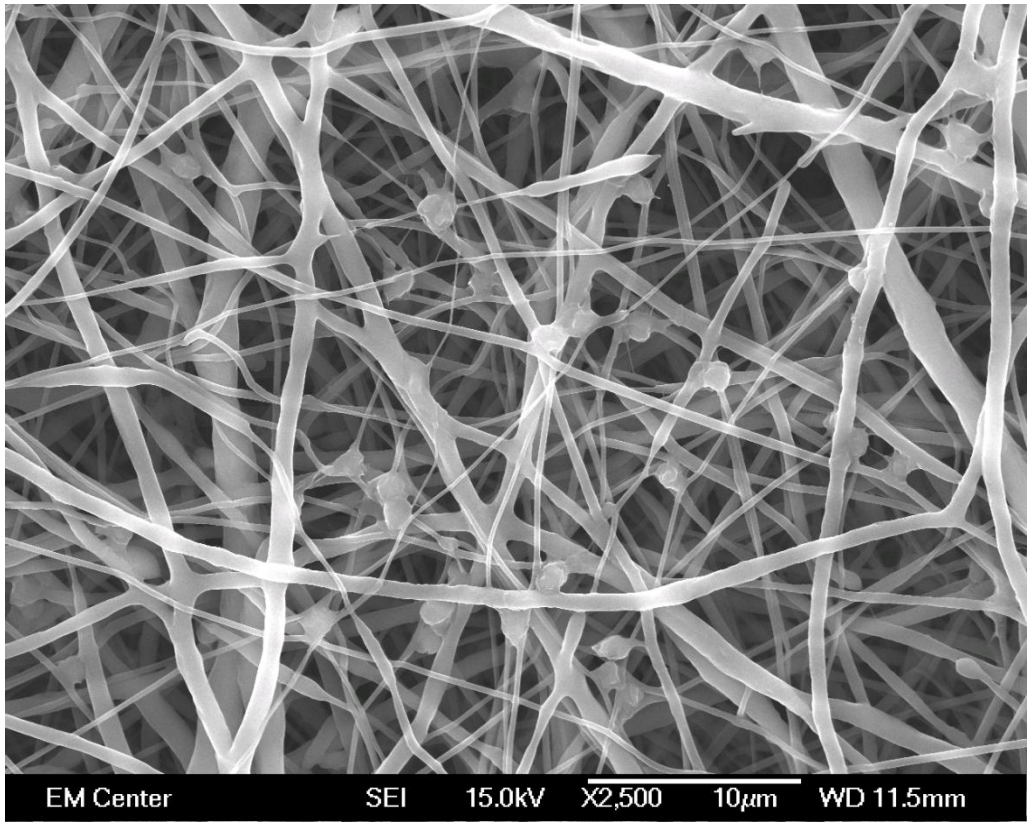

Figure 30 – Laminar flow chamber, dynamic plasma exposure, PCL fibers, 2500x.

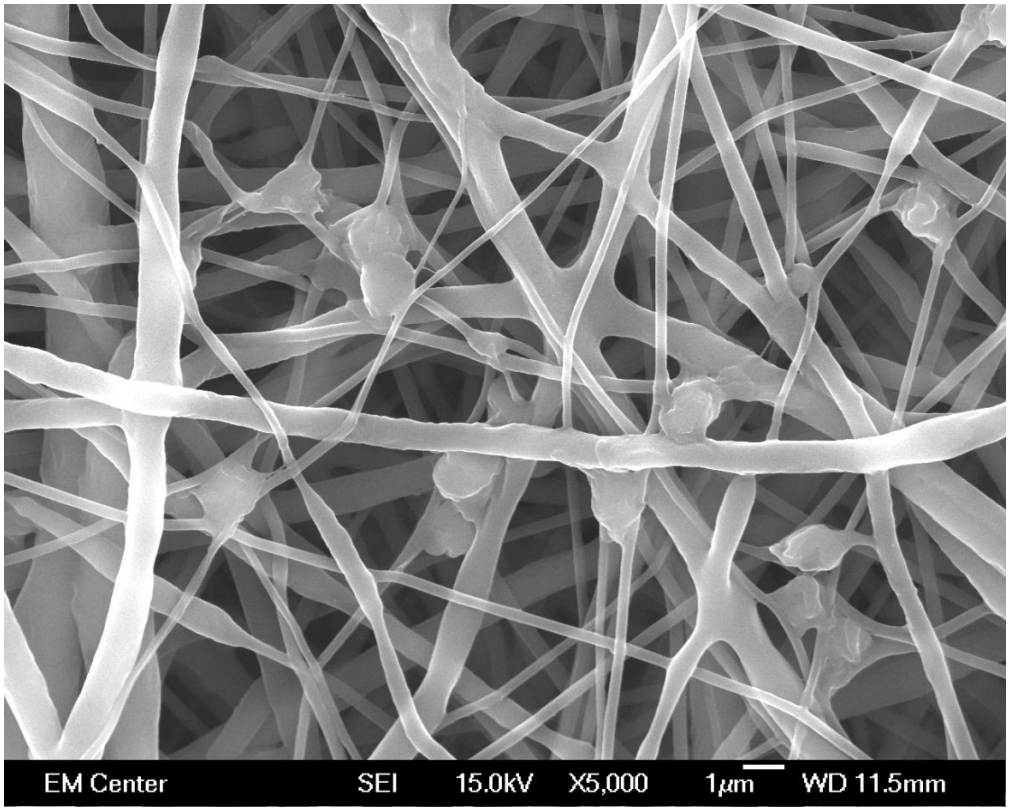

Figure 31 – Laminar flow chamber, dynamic plasma exposure, PCL fibers, 5000x.

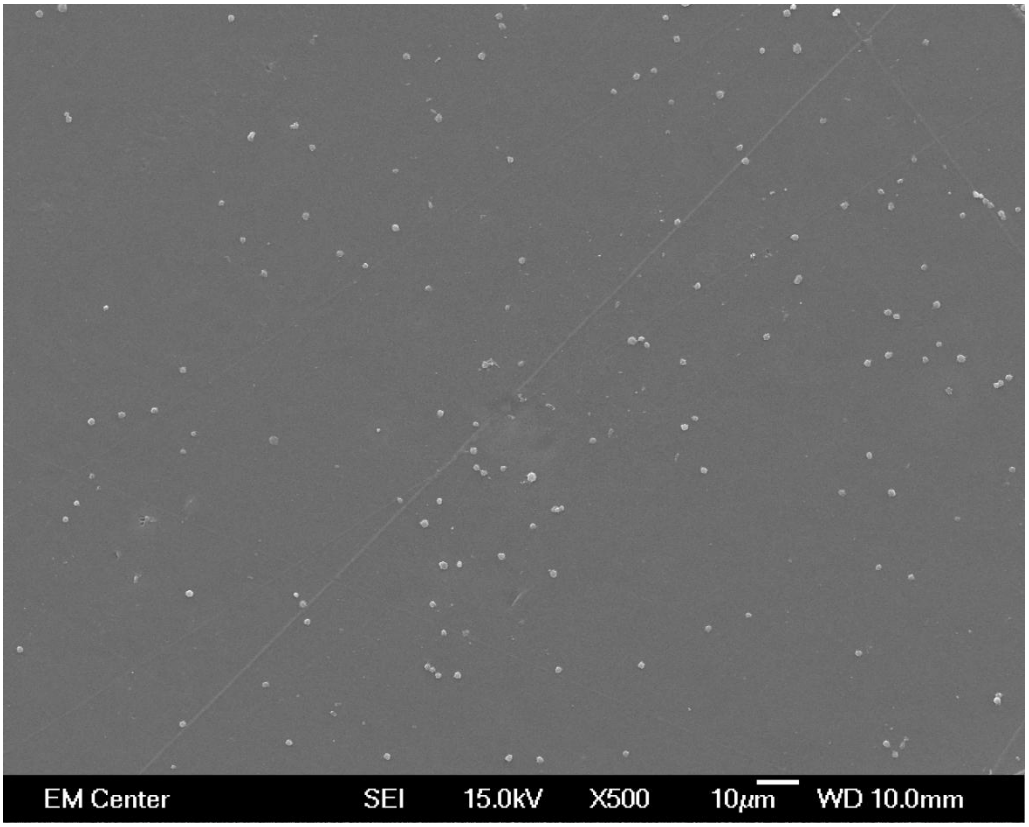

Figure 32 – Stent flow chamber, static plasma exposure, flat PCL, 500x.

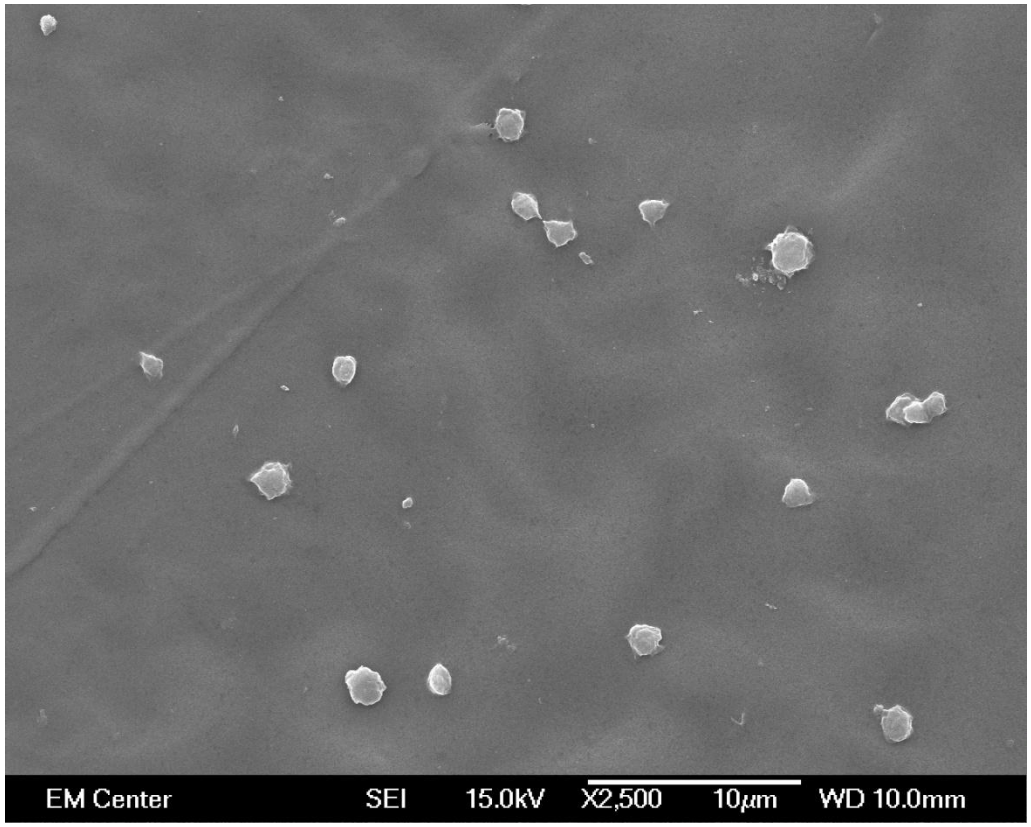

Figure 33 – Stent flow chamber, static plasma exposure, flat PCL, 2500x

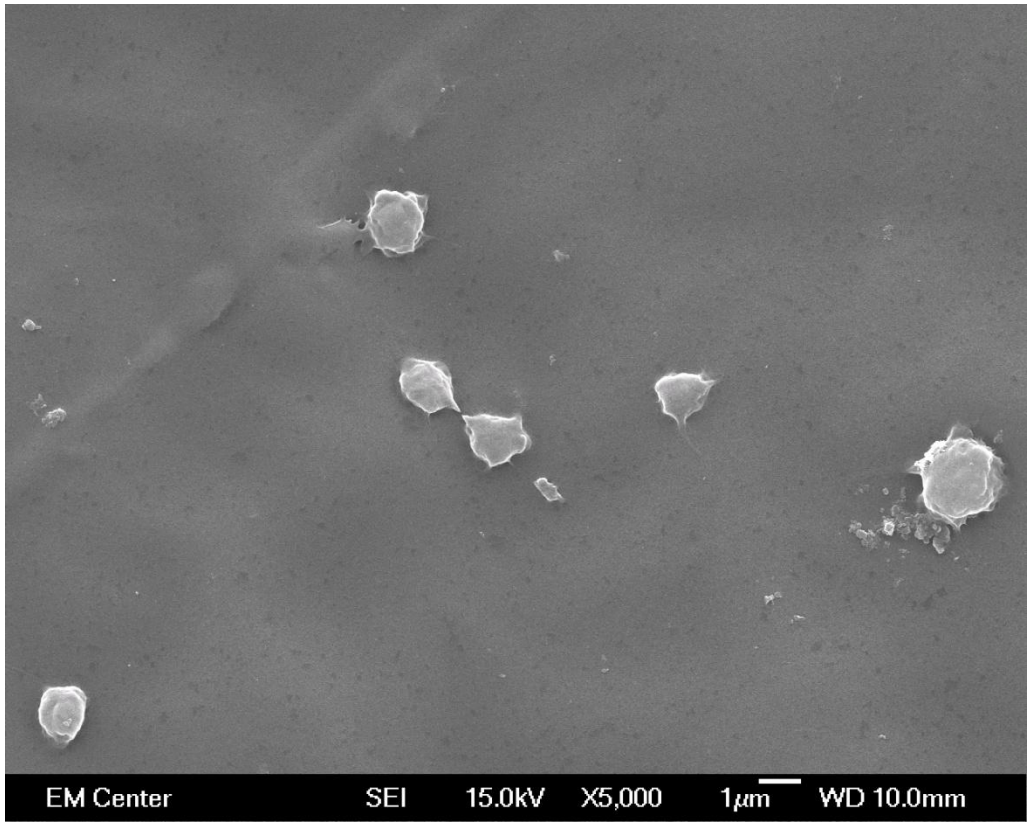

Figure 34 – Stent flow chamber, static plasma exposure, flat PCL, 5000x

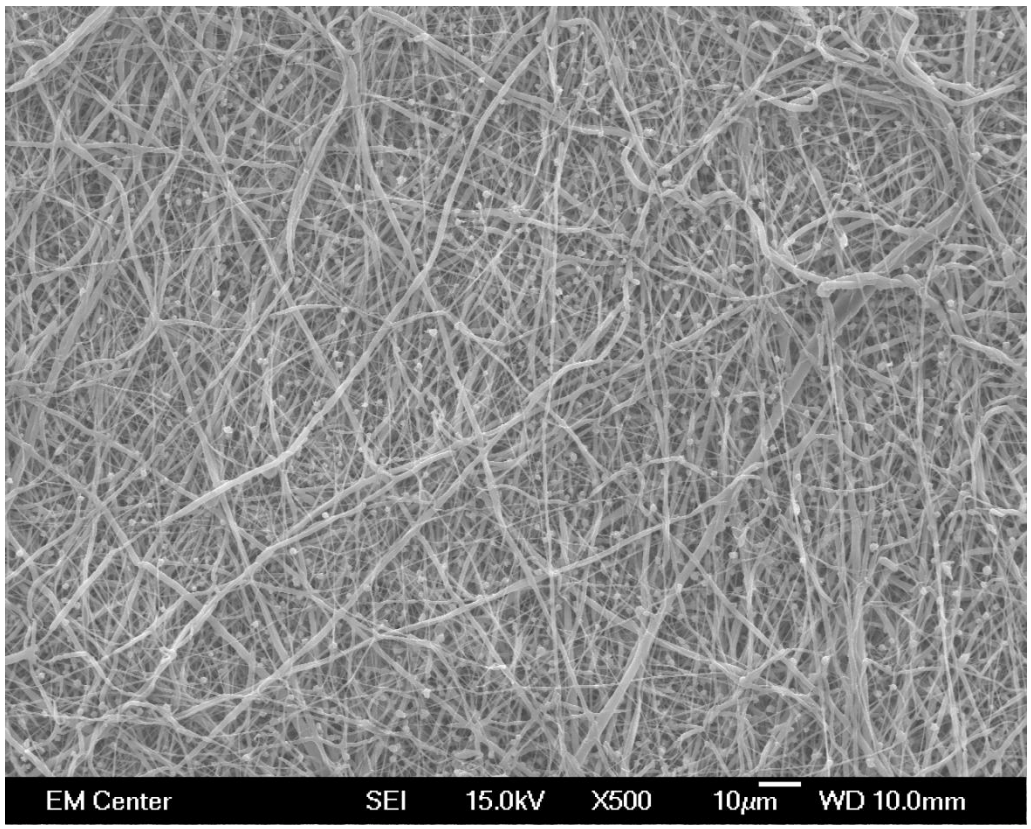

Figure 35 – Stent flow chamber, static plasma exposure, PCL fibers, 500x.

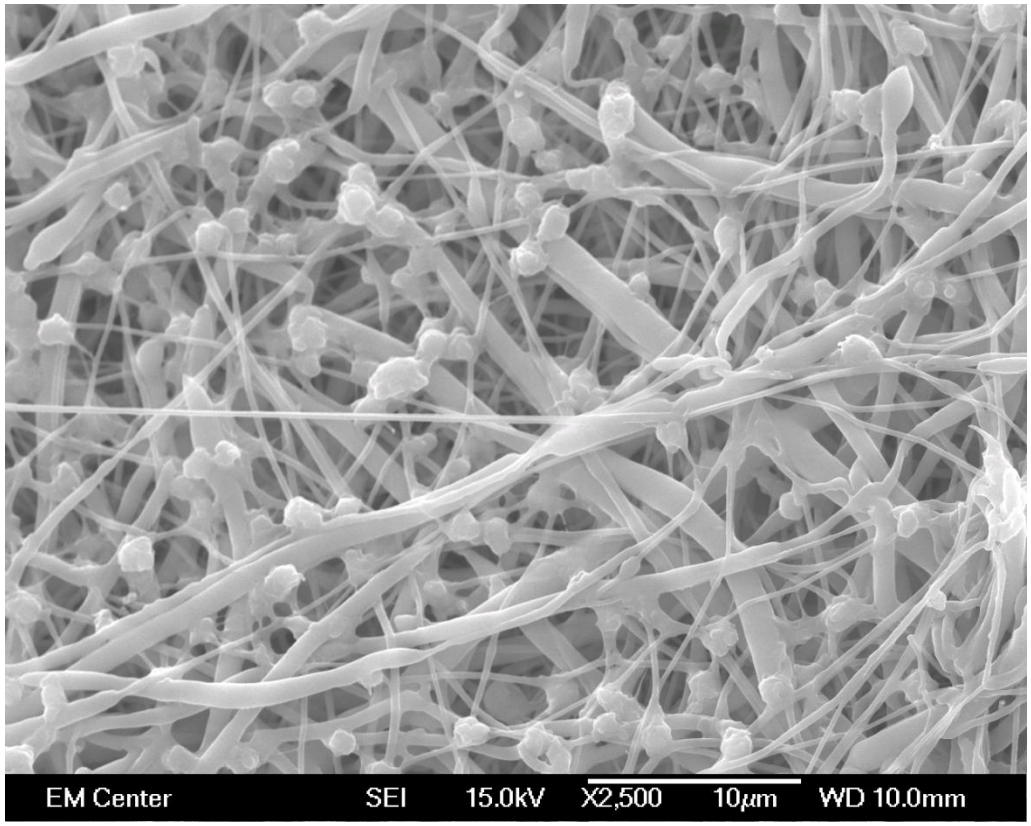

Figure 36 – Stent flow chamber, static plasma exposure, PCL fibers, 2500x.

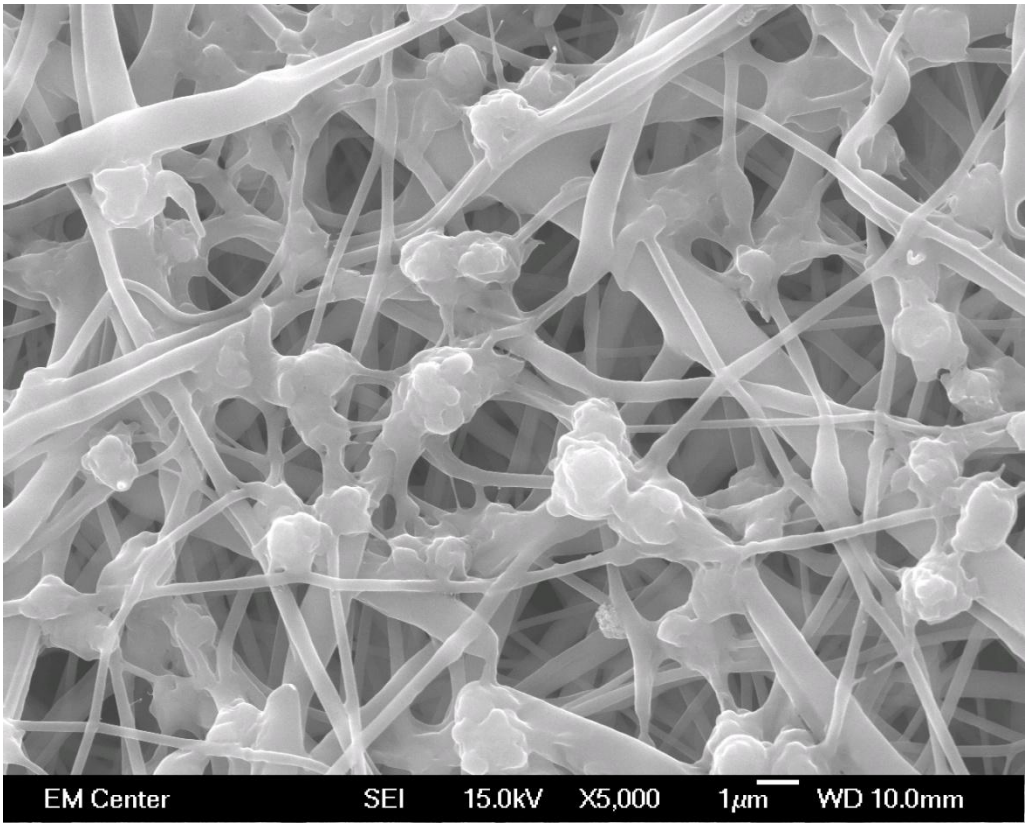

Figure 37 – Stent flow chamber, static plasma exposure, PCL fibers, 5000x.

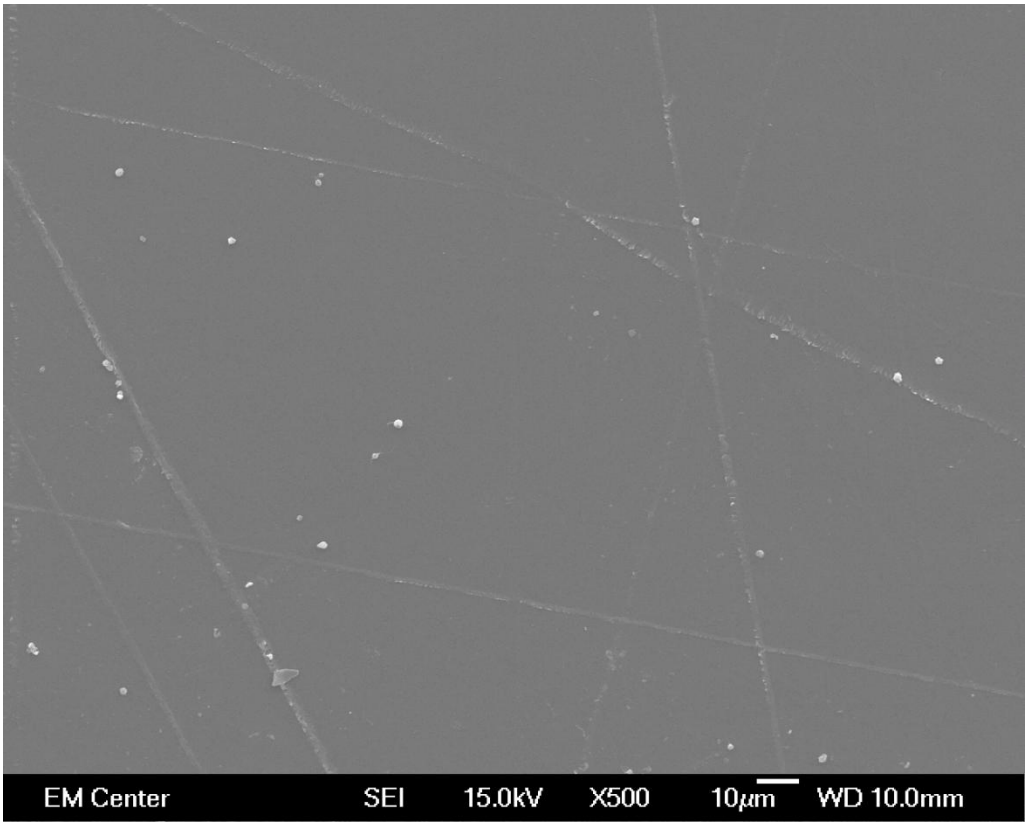

Figure 38 – Stent flow chamber, dynamic plasma exposure, flat PCL, chamber center, 500x.

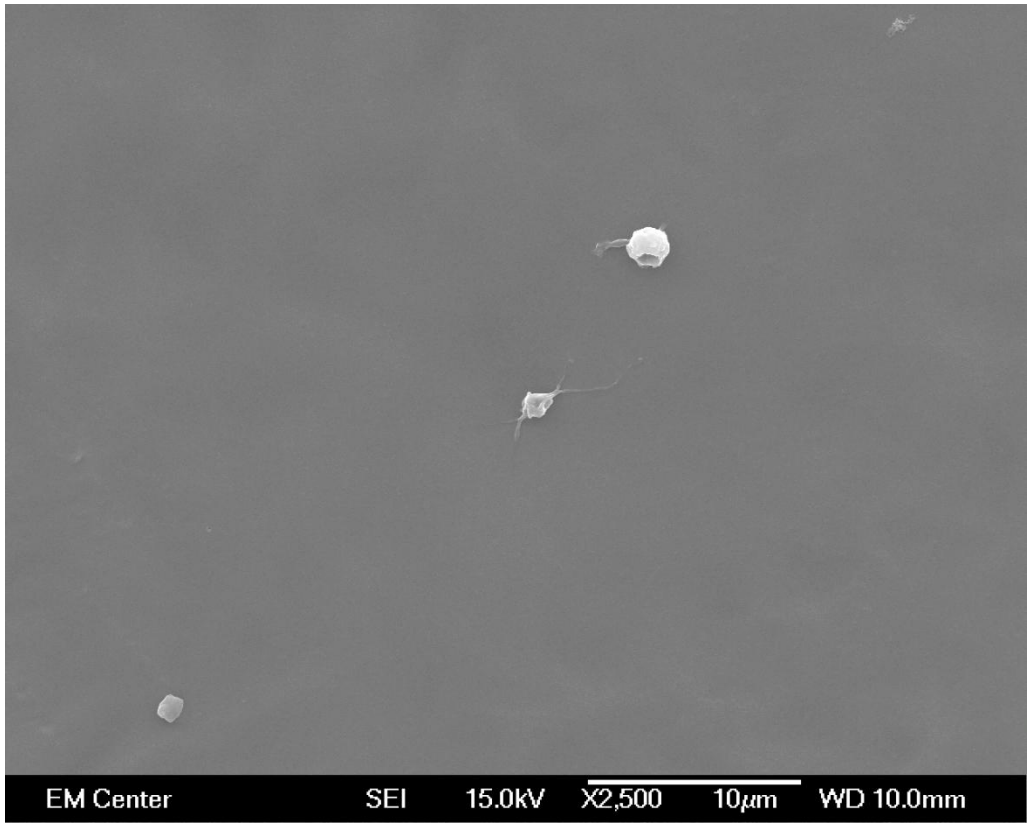

Figure 39 – Stent flow chamber, dynamic plasma exposure, flat PCL, chamber center, 2500x.

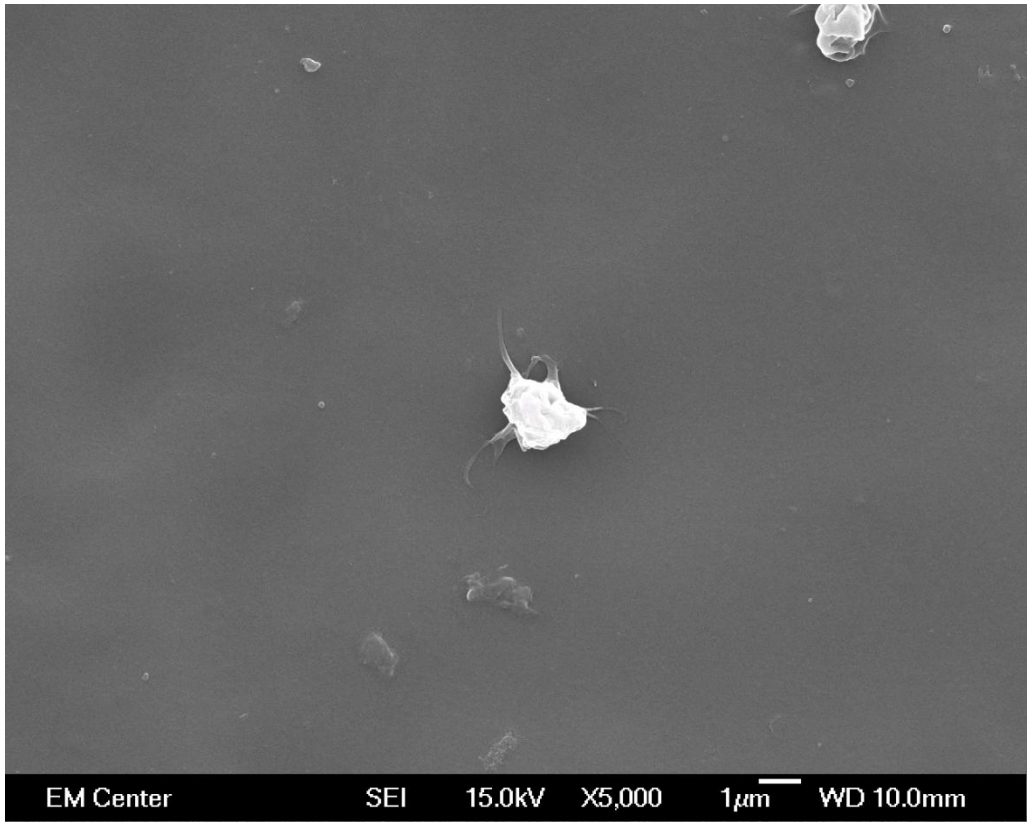

Figure 40 – Stent flow chamber, dynamic plasma exposure, flat PCL, chamber center, 5000x.

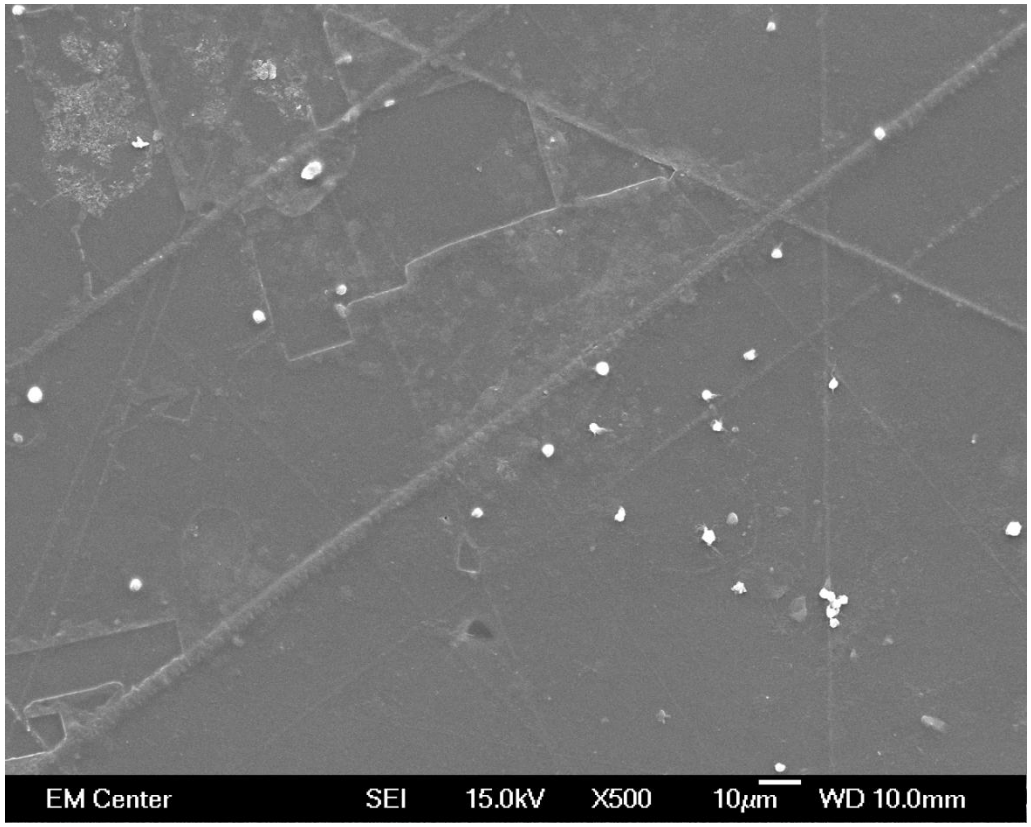

Figure 41 – Stent flow chamber, dynamic plasma exposure, flat PCL, stagnation zone, 500x.

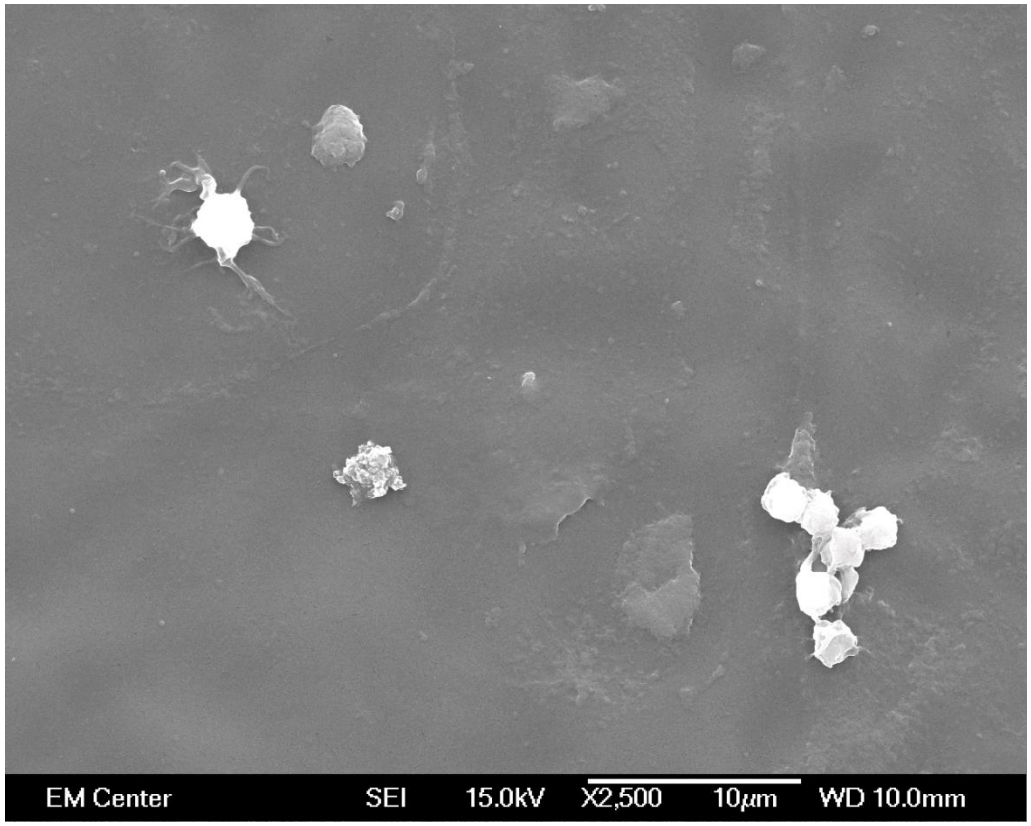

Figure 42 – Stent flow chamber, dynamic plasma exposure, flat PCL, stagnation zone, 2500x.

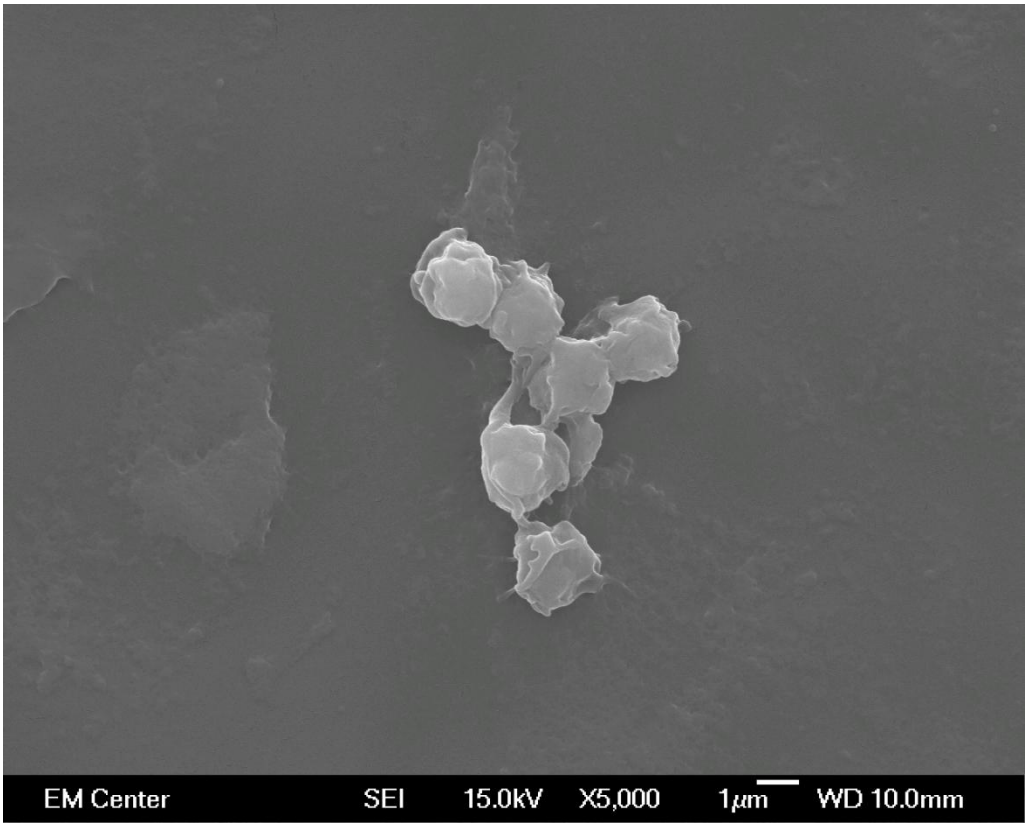

Figure 43 – Stent flow chamber, dynamic plasma exposure, flat PCL, stagnation zone, 5000x.

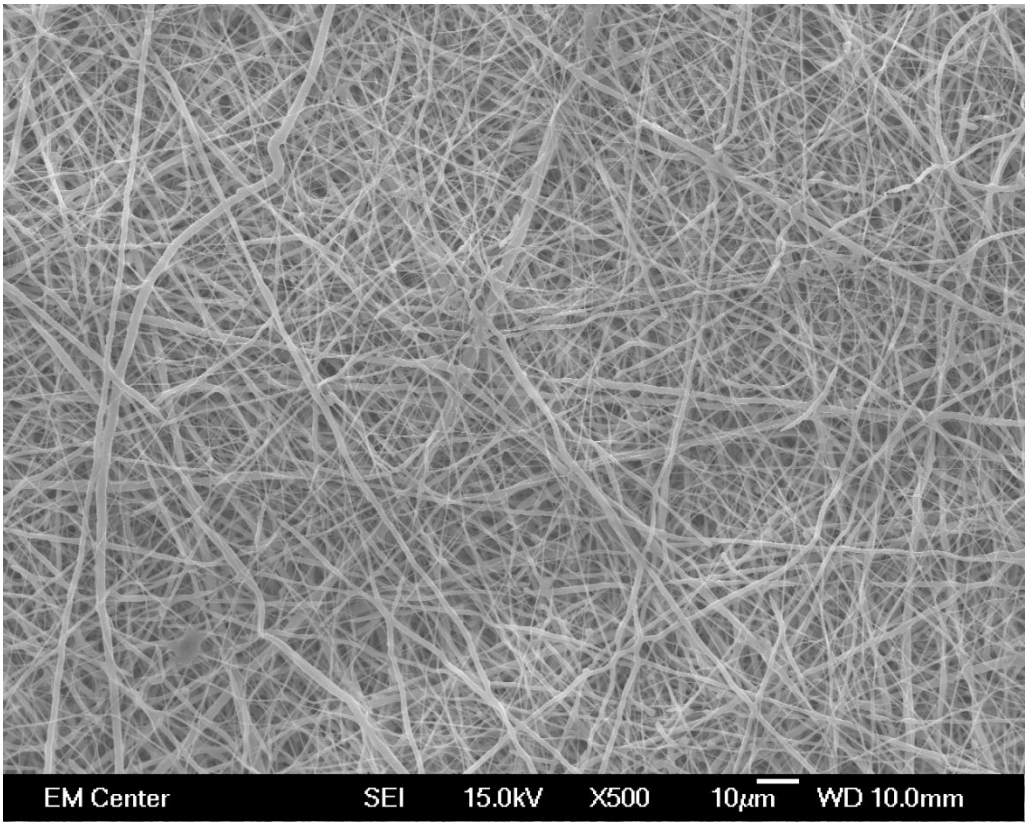

Figure 44 – Stent flow chamber, dynamic plasma exposure, PCL fibers, chamber center, 500x.

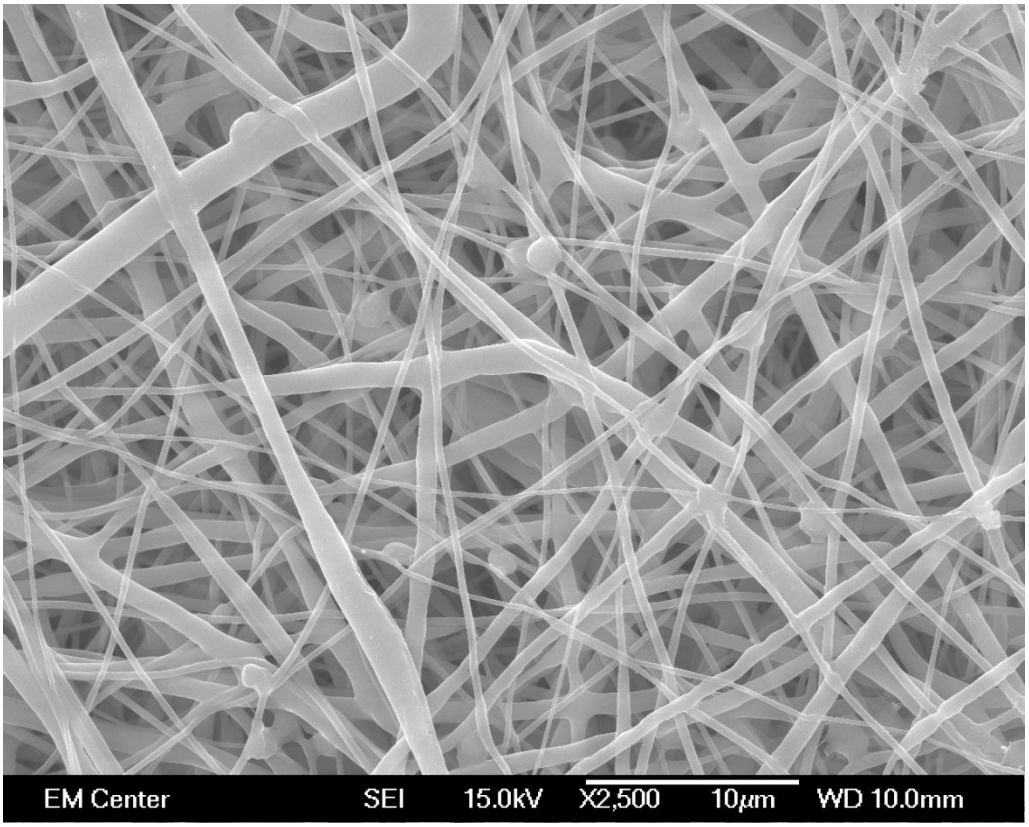

Figure 45 – Stent flow chamber, dynamic plasma exposure, PCL fibers, chamber center, 2500x.

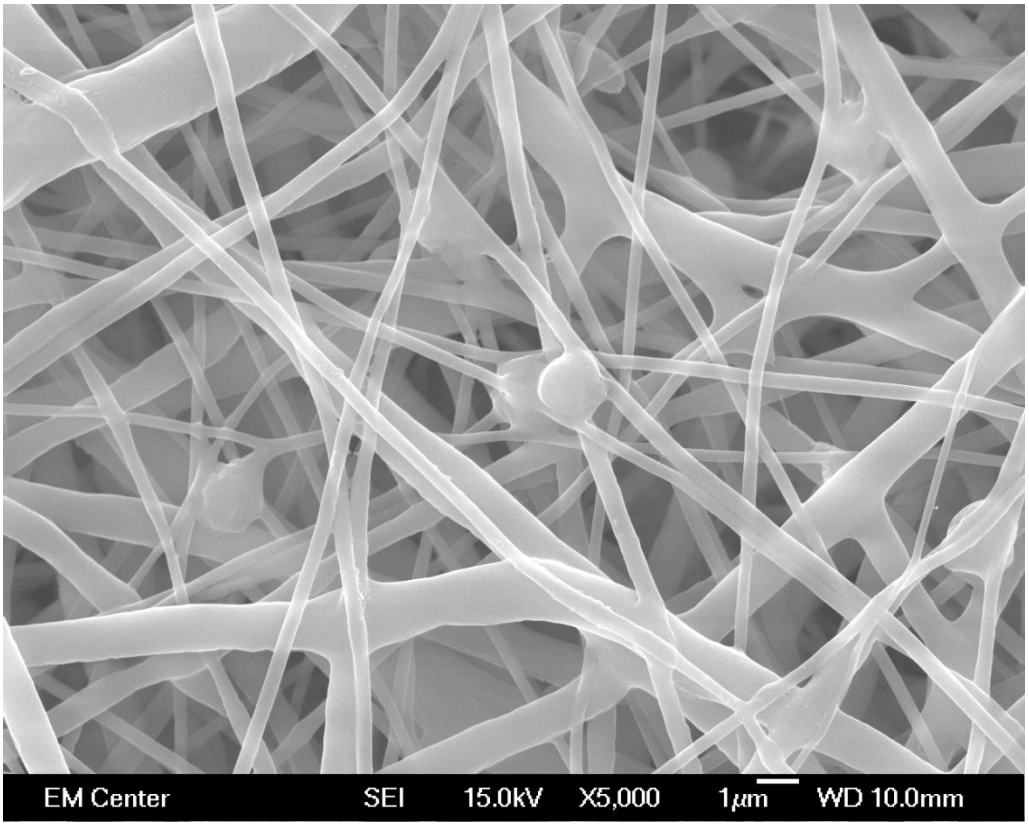

Figure 46 – Stent flow chamber, dynamic plasma exposure, PCL fibers, chamber center, 5000x.

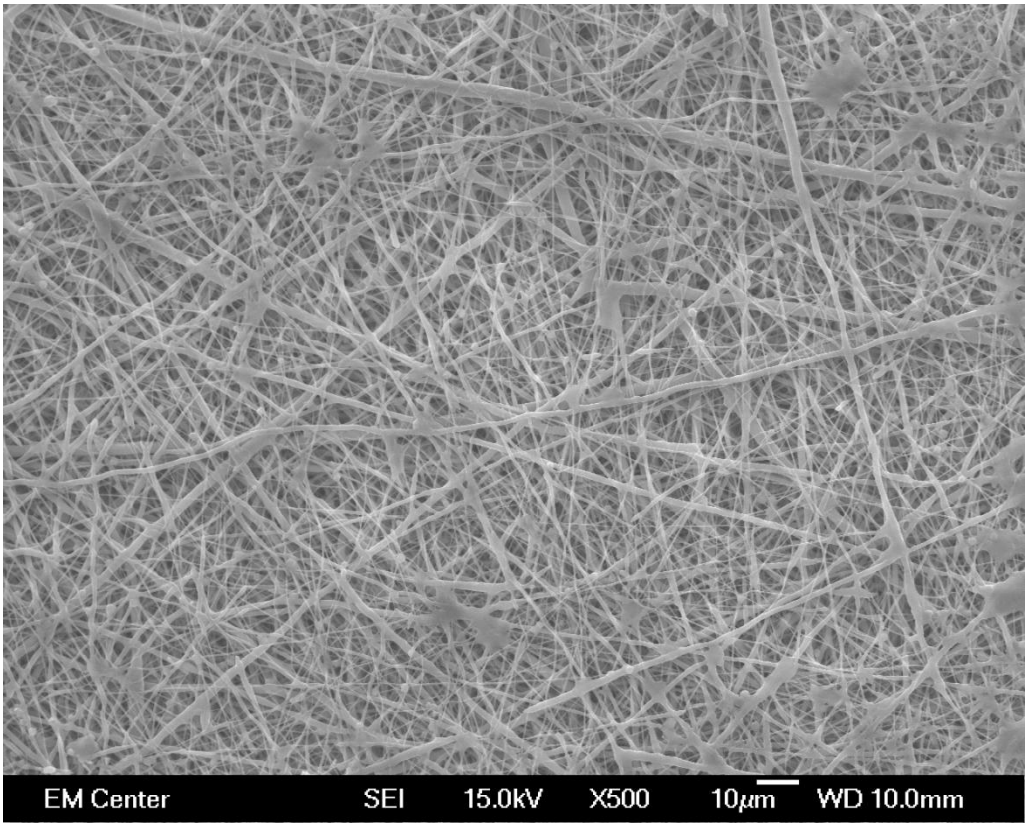

Figure 47 – Stent flow chamber, dynamic plasma exposure, PCL fibers, stagnation zone, 500x.

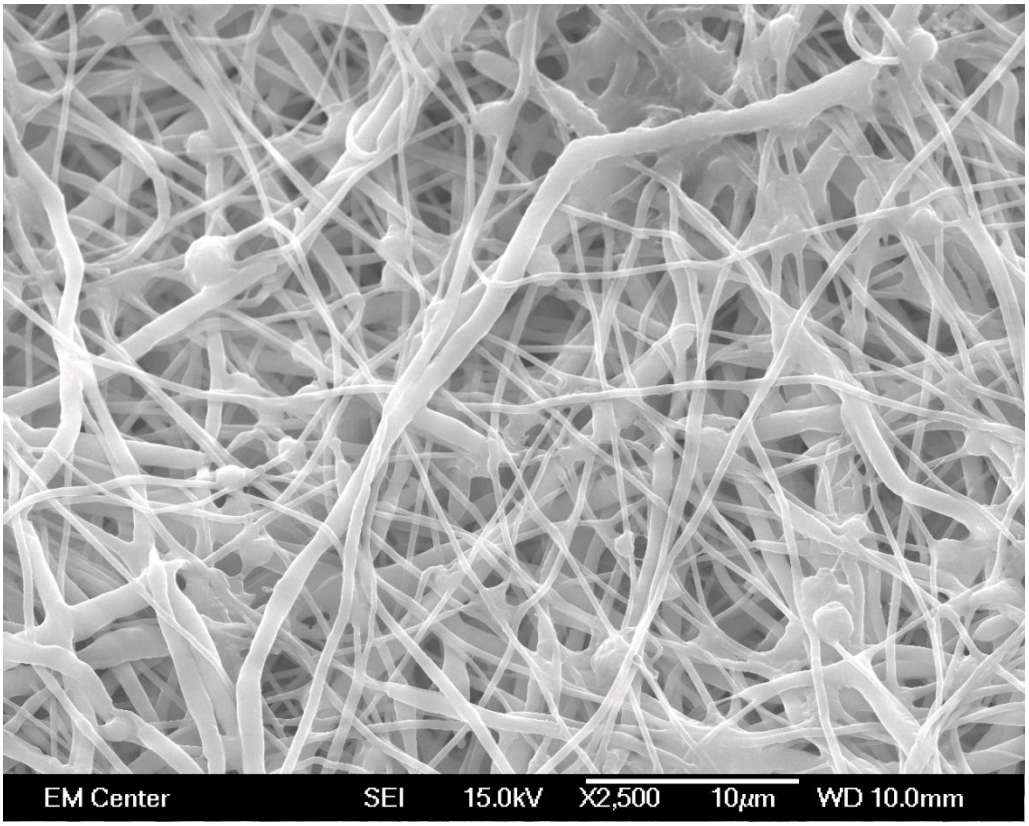

Figure 48 – Stent flow chamber, dynamic plasma exposure, PCL fibers, stagnation zone, 2500x.

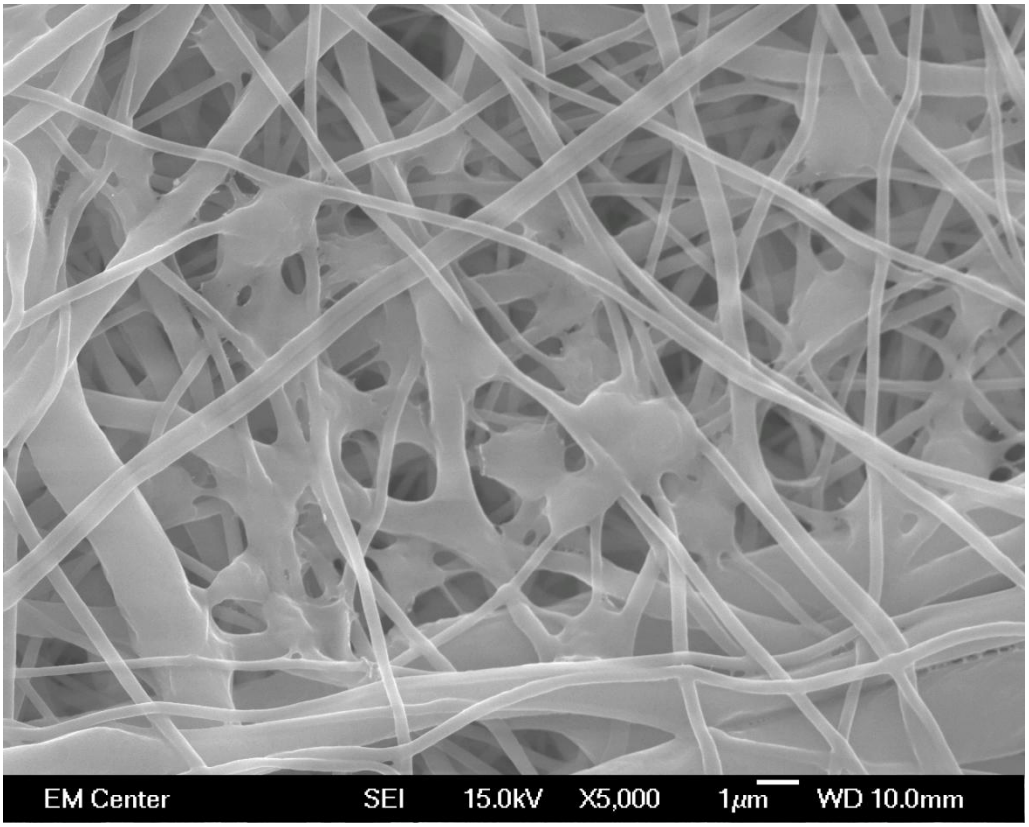

Figure 49 – Stent flow chamber, dynamic plasma exposure, PCL fibers, stagnation zone, 5000x.

Live Cell Flouresence Microscopy

Adhesion of platelets to PCL flat surfaces and electrospun nanofibers was evaluated after 30 minutes of exposure to the PCL samples under static and dynamic flow in both the laminar and stent flow chambers followed by staining adhered platelets with calcein-AM stain. Results from comparison of PCL flat surfaces to electrosupun nanofibers at low magnification reveal significantly higher platelet adhesion to the nanofiber surfaces (Figures 50 vs. 53, 56 vs. 59, 62 vs. 65 and 68 vs. 71). Comparisons are made with similar studies that share all non test variables. Analysis at higher magnifications reveal possible platelet activation and adhesion along the fiber axis in electrospun PCL samples (Figures 55, 61 and 70) while platelets adhered to flat surfaces retain a discoid shape

Results from the analysis of dynamic and static plasma flow reveal reduced platelet adhesion on surfaces tested under dynamic conditions when compared to static studies, at lower

magnification, larger platelet clusters and aggregates, with the exception of figure 68, appear to be more prevalent on the samples exposed to flow (Figures 50 vs. 56, 53 vs. 59, 62 vs. 68 and 65 vs. 71). The same studies observed at higher magnification only supply evidence to support the claim that there are fewer adhered platelets on samples subjected to flow (Figures 51 vs. 57, 54 vs. 60, 63 vs. 69 and 66 vs. 72).

The laminar flow and stent chambers only produce variance in adhesion when the samples were subjected to flow so analysis of the flow chambers were limited to dynamic studies. In addition separation of high velocity flow and stagnation zones were not performed in this test. Comparison of flow in the chambers over flat PCL showed no difference in platelet density or adhesion platelets exposed to flow on this surface remain discoid (Figures 56-58 vs 68-70). In comparison of flow in the chambers over PCL electrospun nanofibers we observed slightly more platelet adhesion on the samples run through the stent chambers while larger activation of platelets appeared present in the laminar flow chamber (Figures 59-61 vs. 71-73).

Figure 50 – Laminar flow chamber, static plasma exposure, flat PCL, 10x.

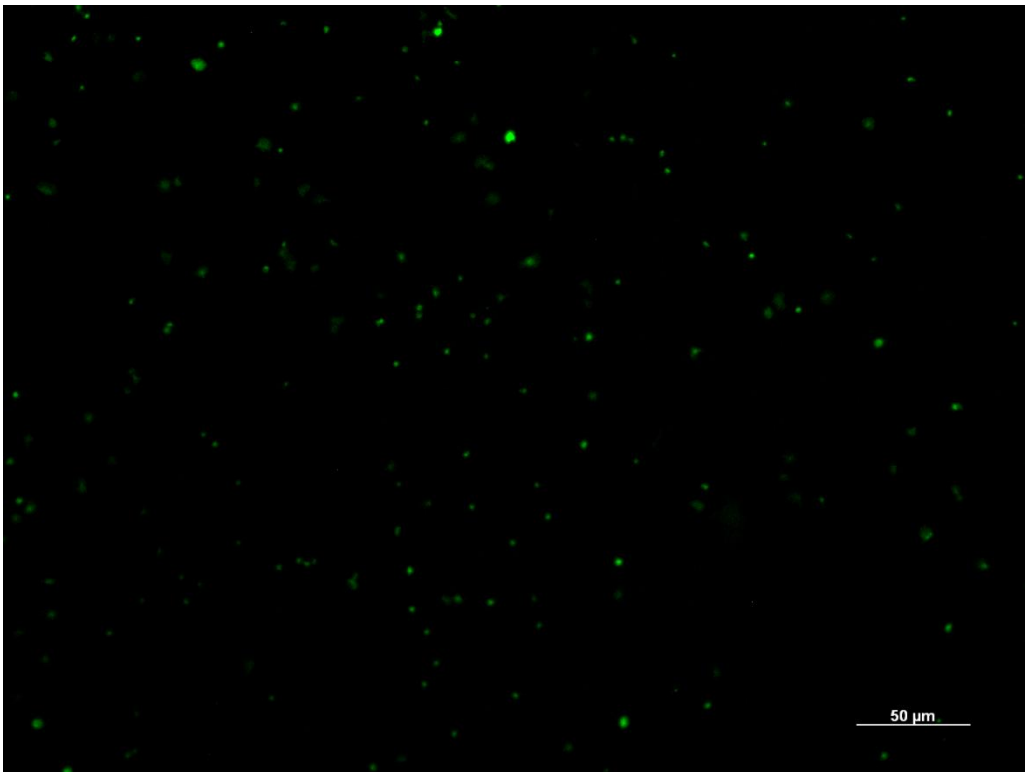

Figure 51 – Laminar flow chamber, static plasma exposure, flat PCL, 20x.

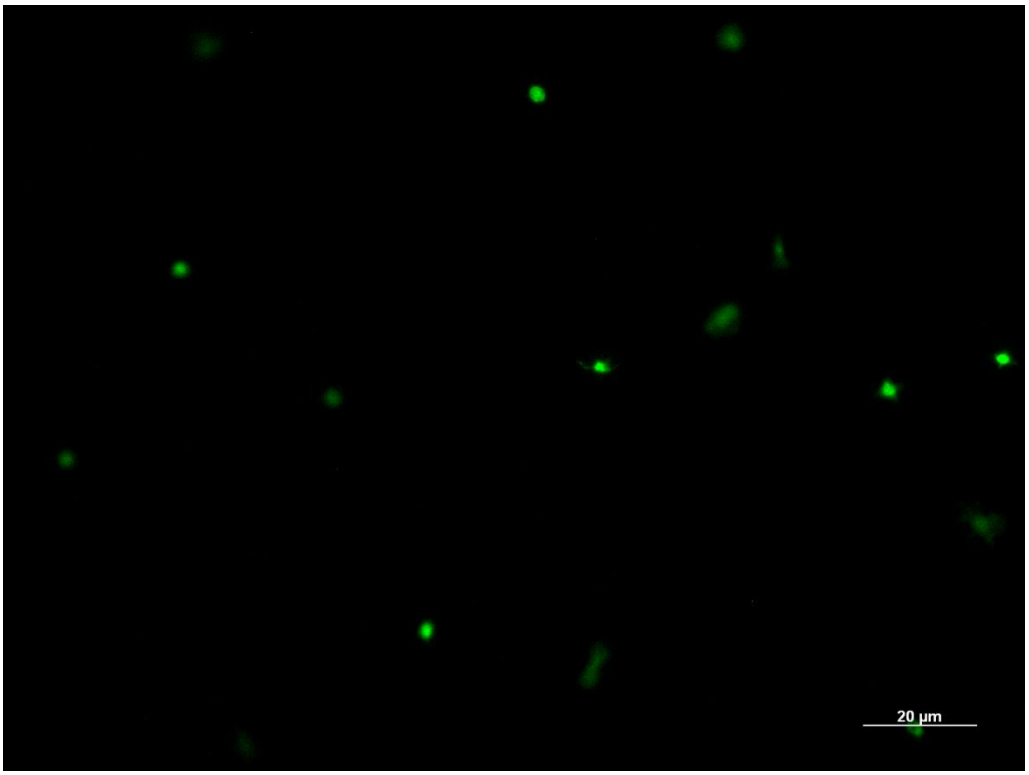

Figure 52 – Laminar flow chamber, static plasma exposure, flat PCL, 50x.

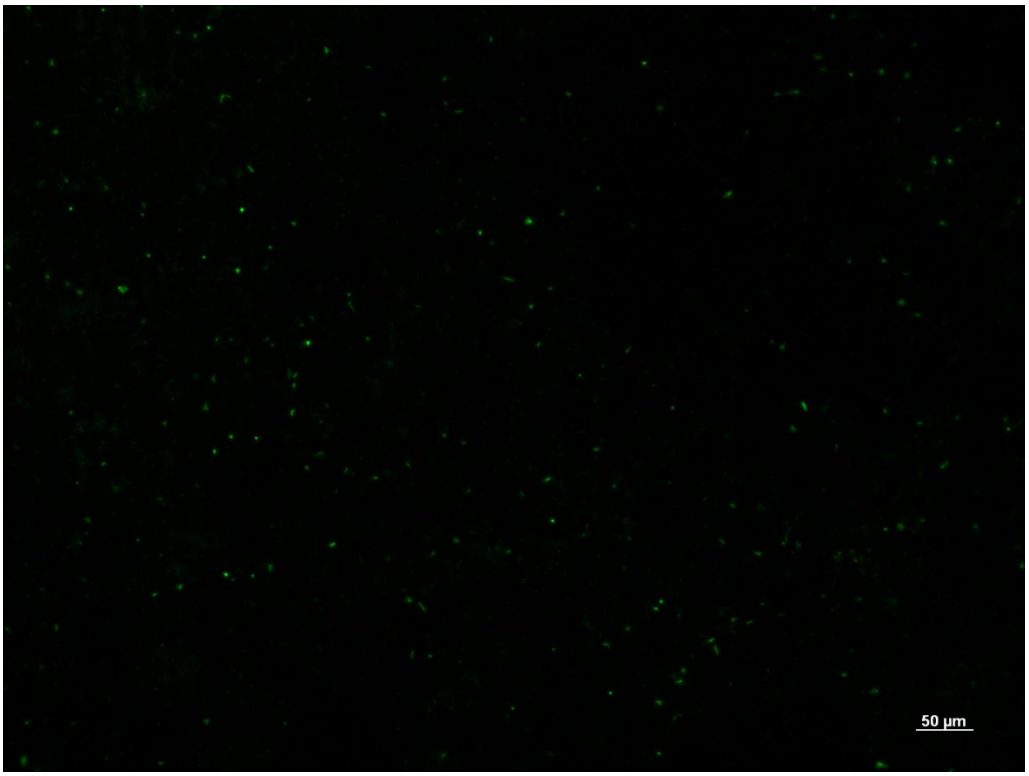

Figure 53 – Laminar flow chamber, static plasma exposure, PCL fibers, 10x.

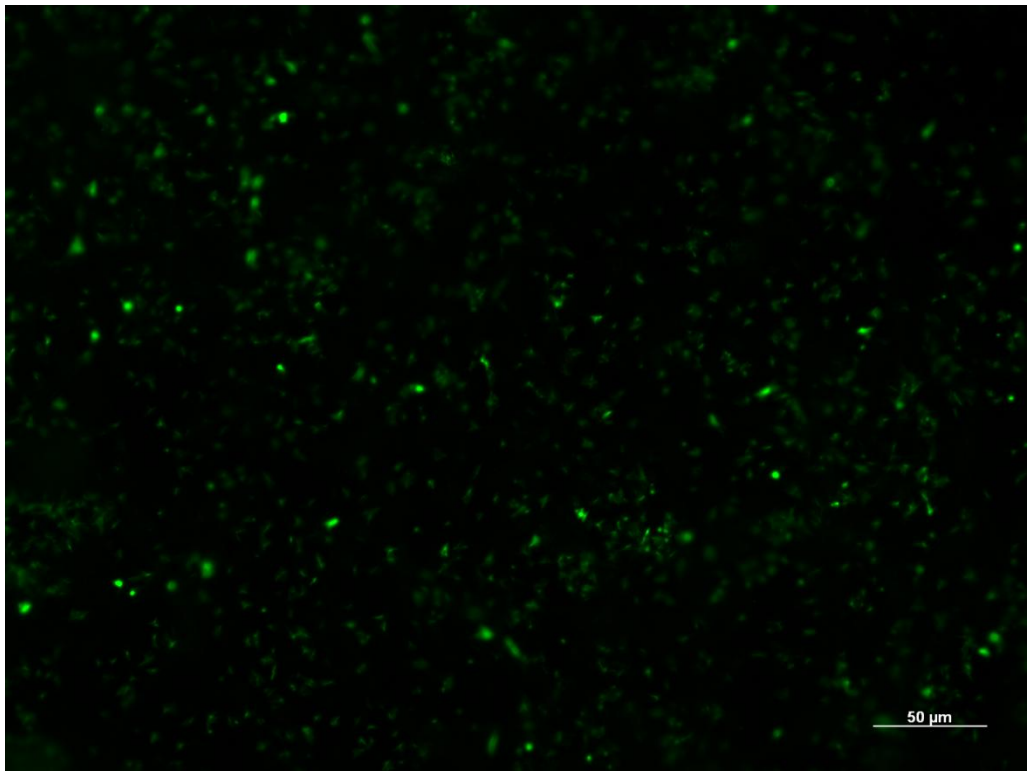

Figure 54 – Laminar flow chamber, static plasma exposure, PCL fibers, 20x.

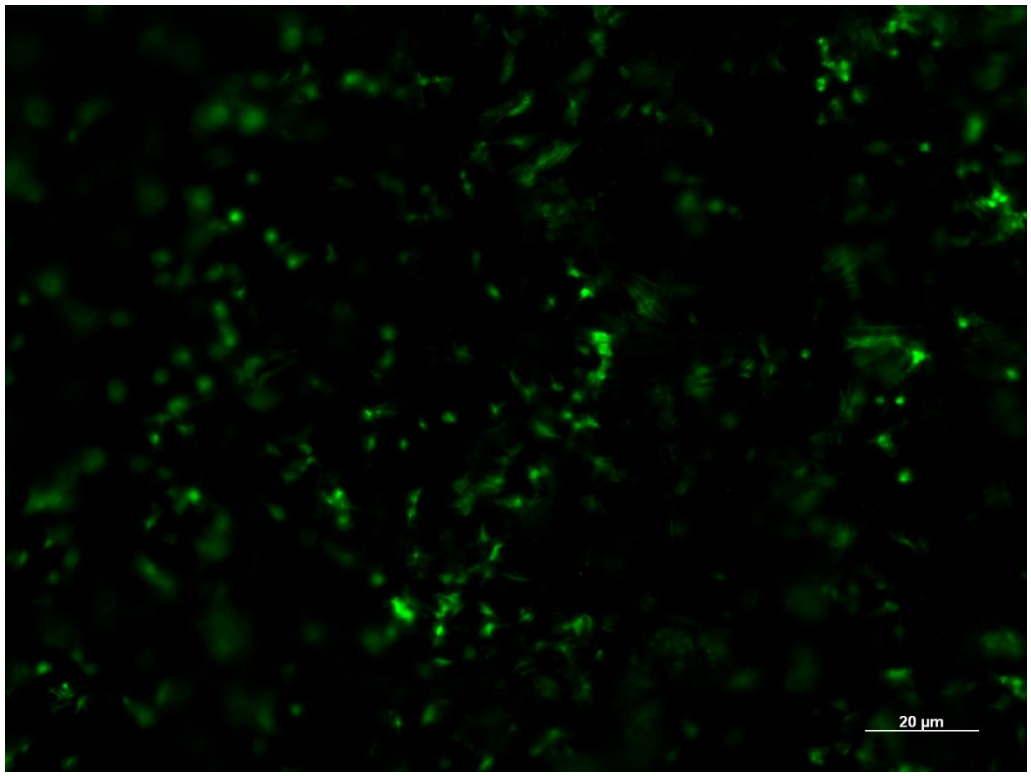

Figure 55 – Laminar flow chamber, static plasma exposure, PCL fibers, 50x.

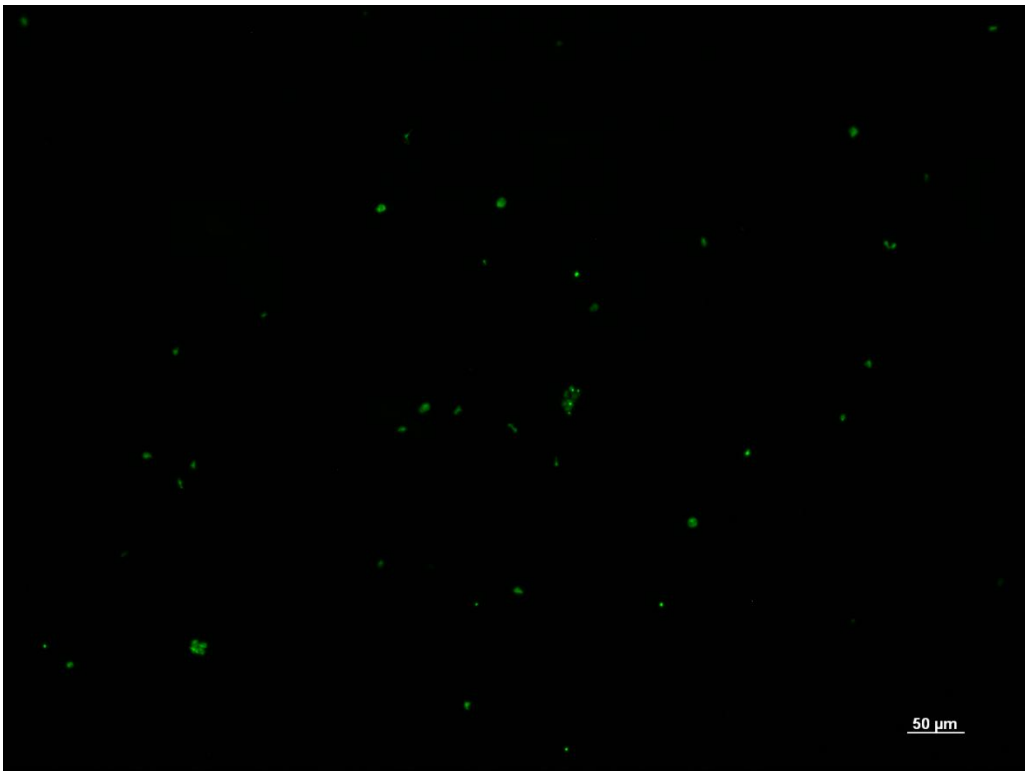

Figure 56 – Laminar flow chamber, dynamic plasma exposure, flat PCL, 10x.

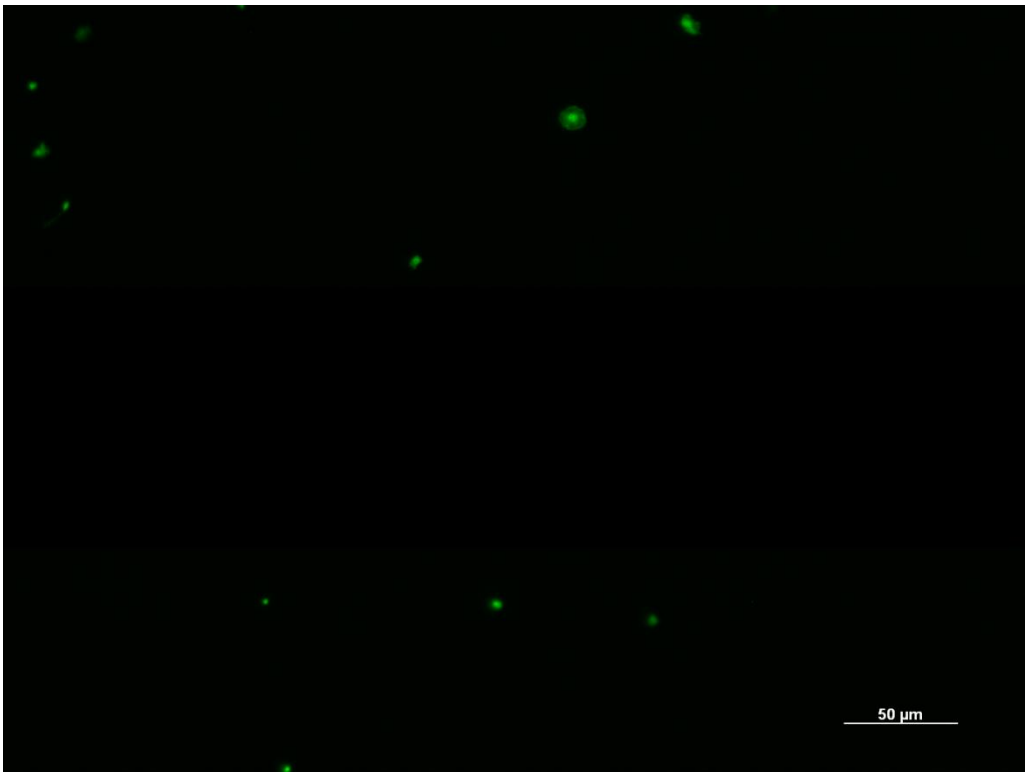

Figure 57 – Laminar flow chamber, dynamic plasma exposure, flat PCL, 20x.

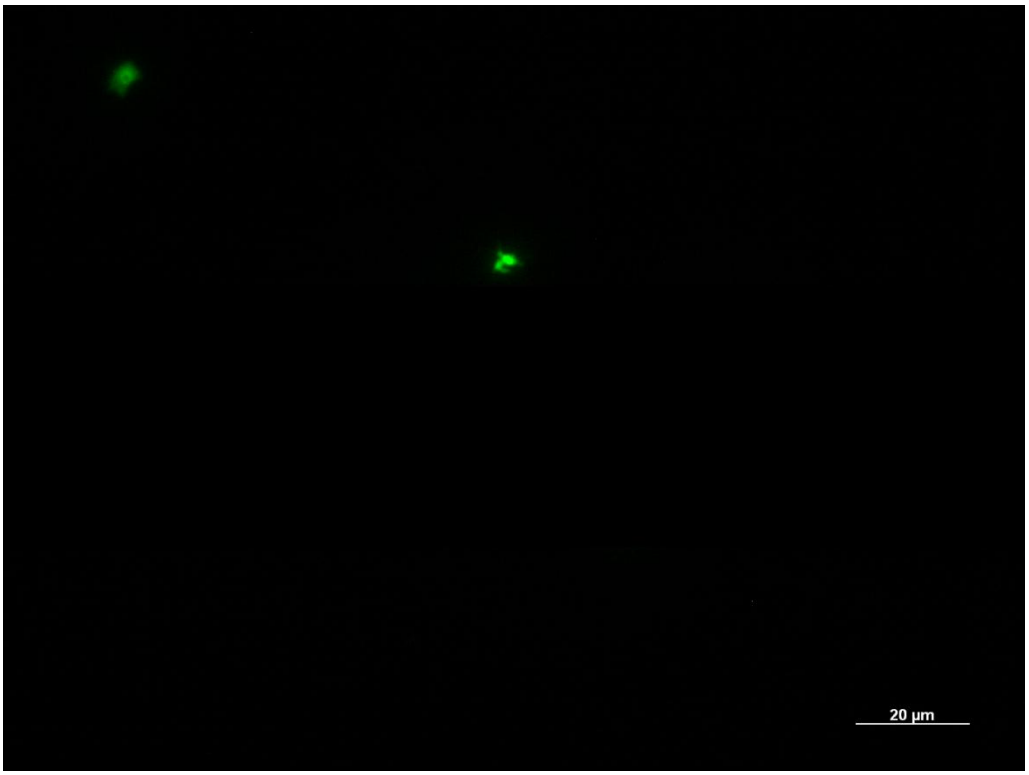

Figure 58 – Laminar flow chamber, dynamic plasma exposure, flat PCL, 50x.

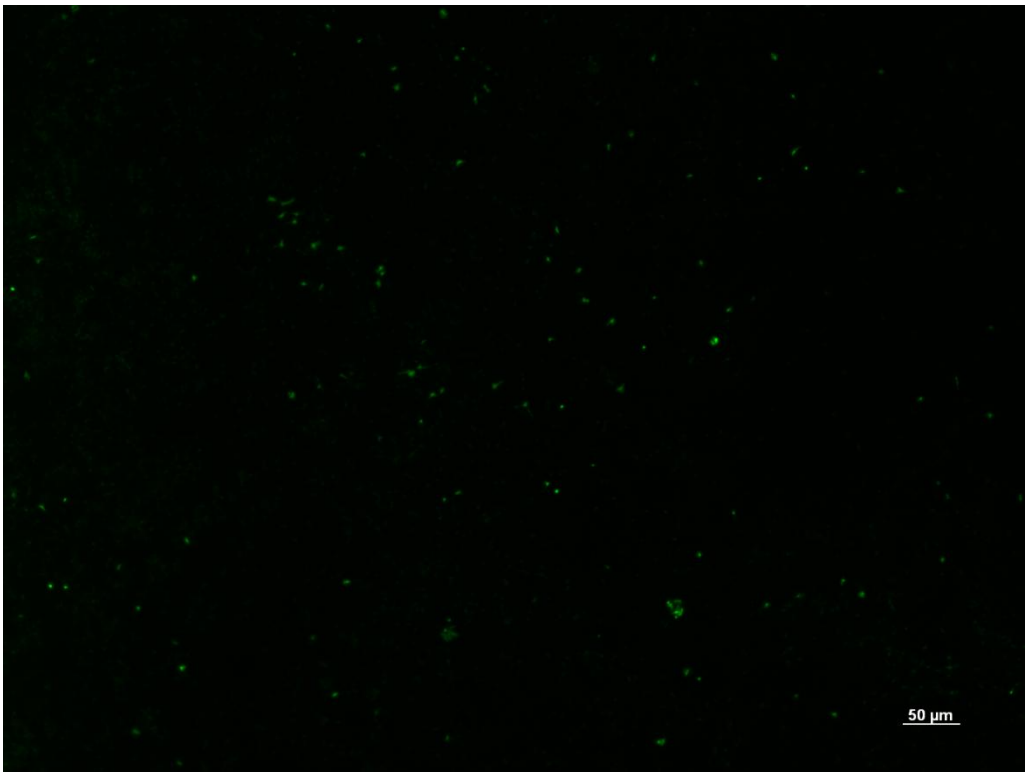

Figure 59 – Laminar flow chamber, dynamic plasma exposure, PCL fibers, 10x.

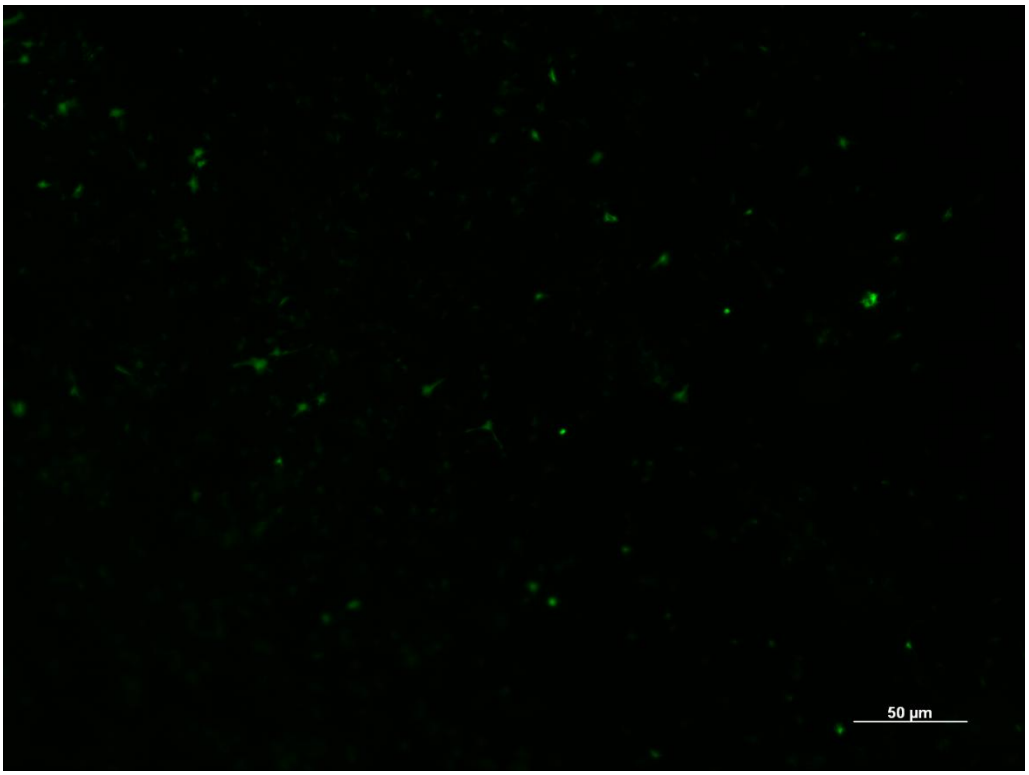

Figure 60 – Laminar flow chamber, dynamic plasma exposure, PCL fibers, 20x.

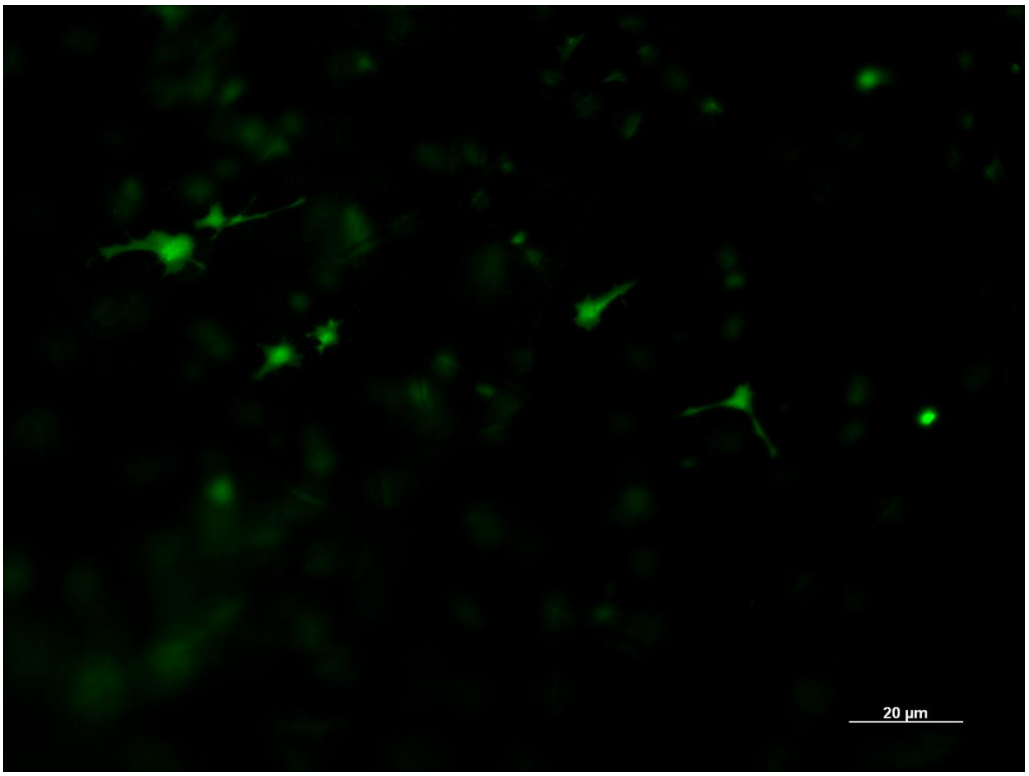

Figure 61 – Laminar flow chamber, dynamic plasma exposure, PCL fibers, 50x.

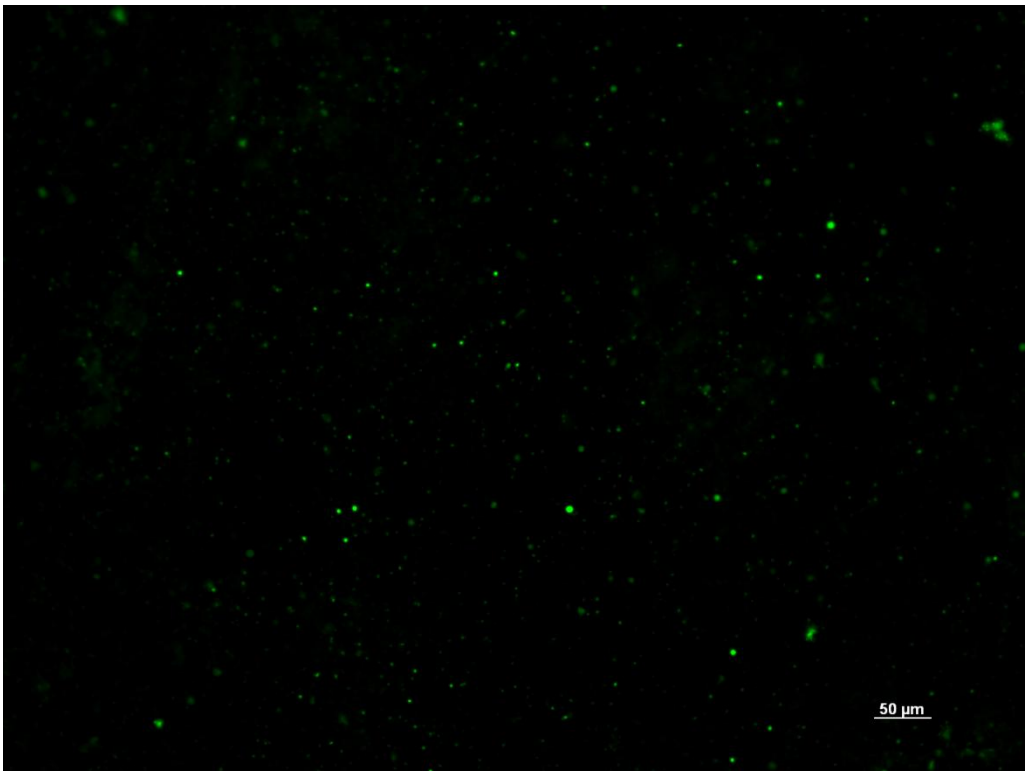

Figure 62– Stent flow chamber, static plasma exposure, flat PCl, 10x.

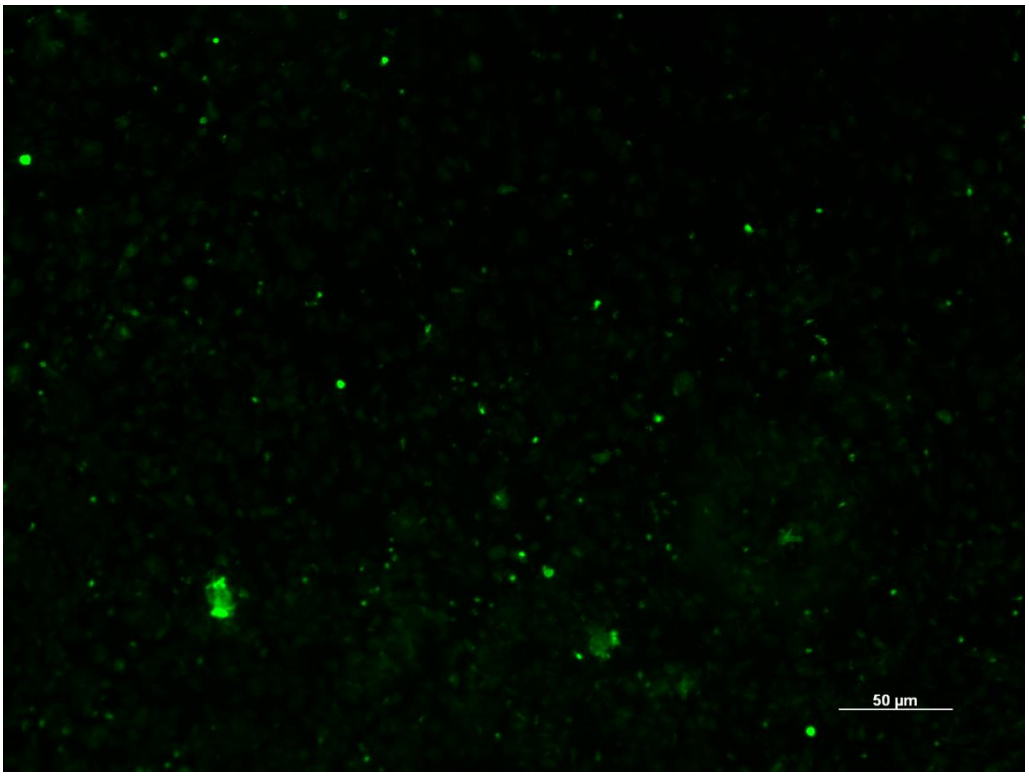

Figure 63– Stent flow chamber, static plasma exposure, flat PCl, 20x.

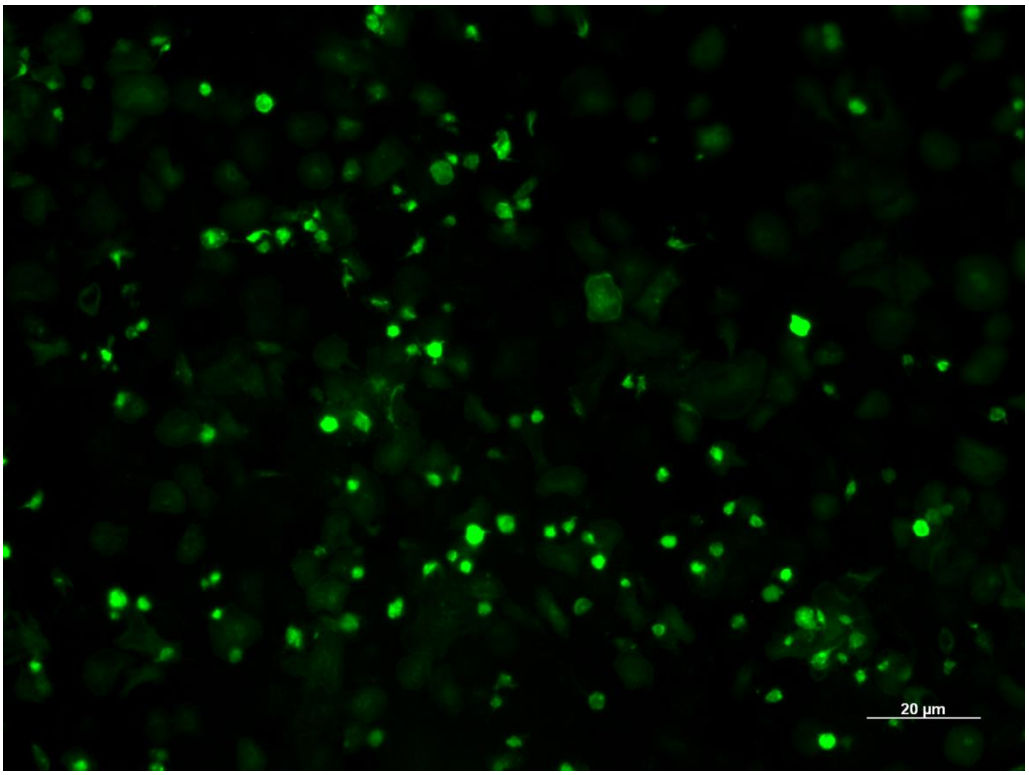

Figure 64– Stent flow chamber, static plasma exposure, flat PCl, 50x.

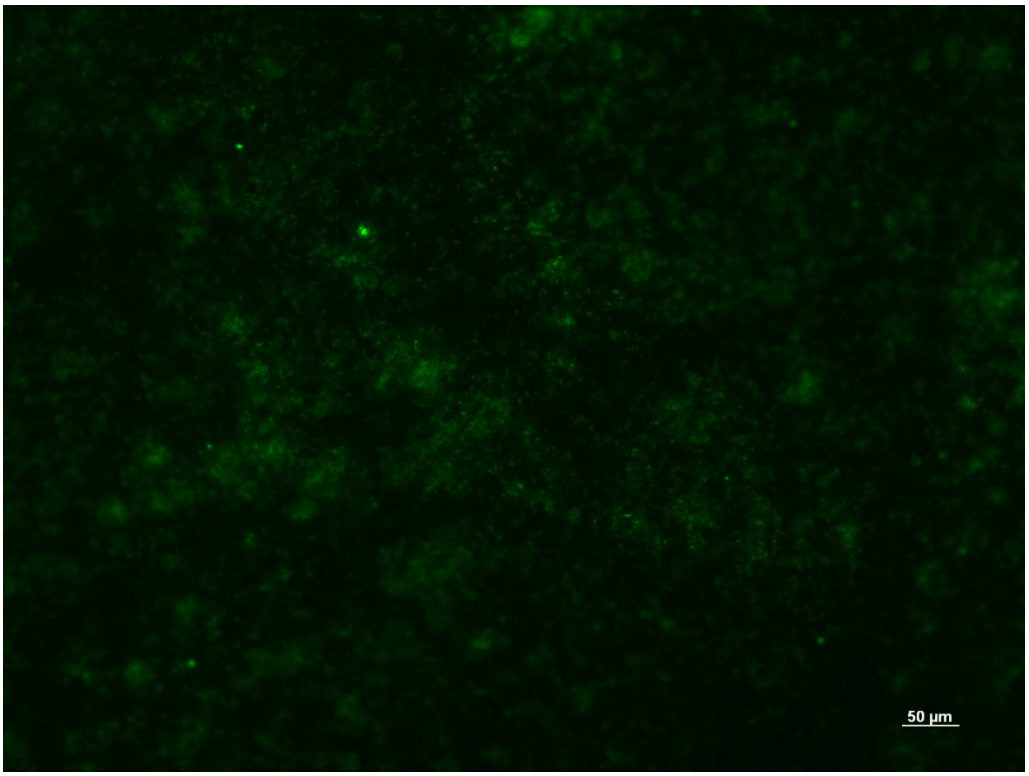

Figure 65 – Stent flow chamber, static plasma exposure, PCL fibers, 10x.

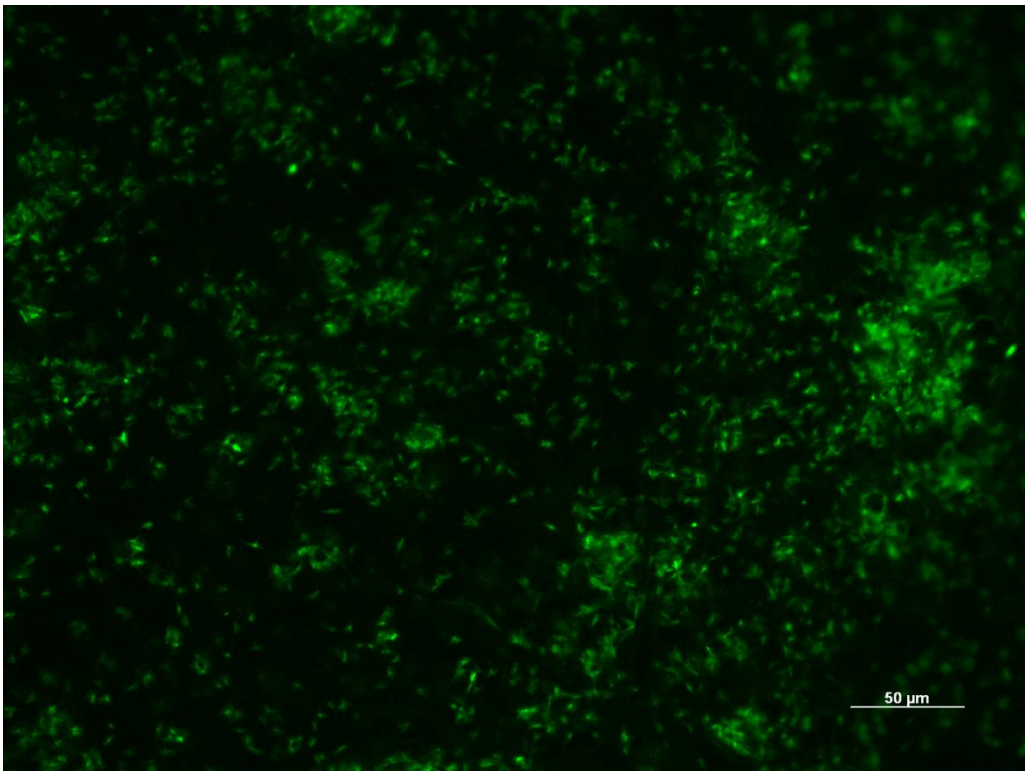

Figure 66 – Stent flow chamber, static plasma exposure, PCL fibers, 20x.

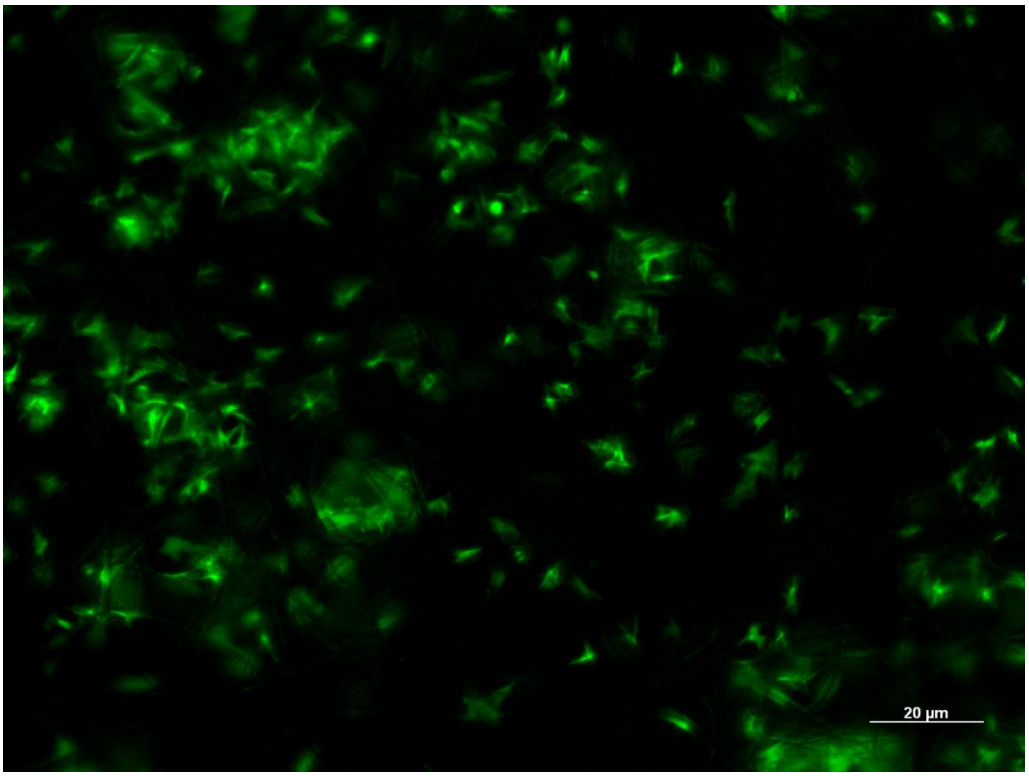

Figure 67 – Stent flow chamber, static plasma exposure, PCL fibers, 50x.

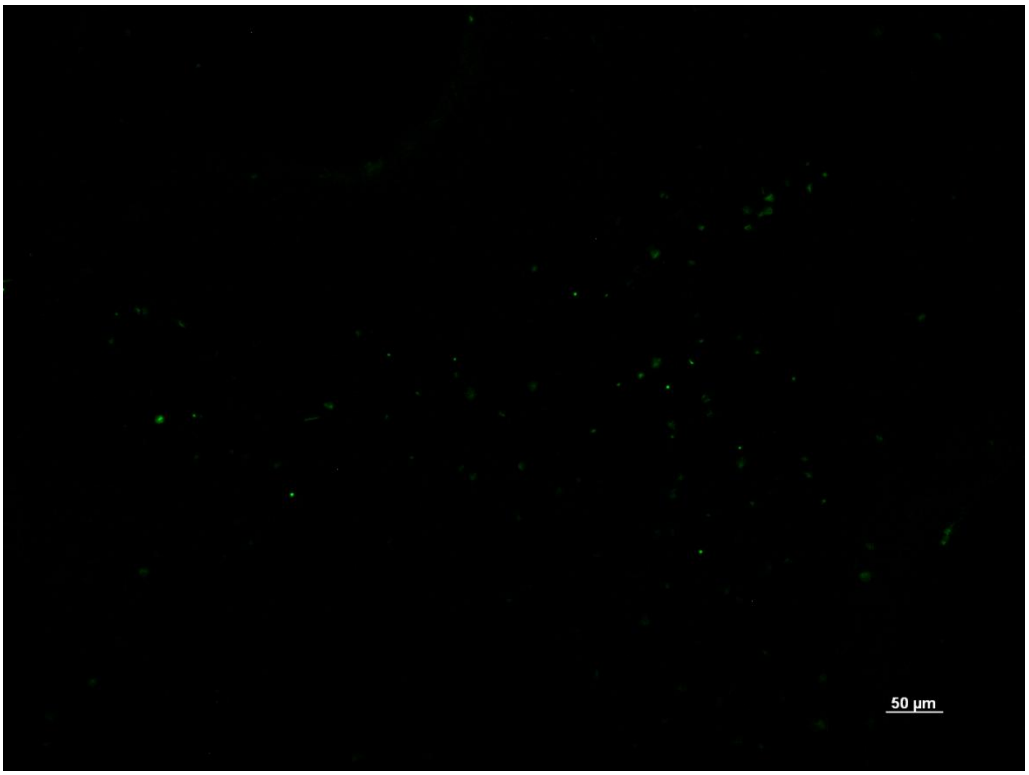

Figure 68 – Stent flow chamber, dynamic plasma exposure, flat PCL, 10x.

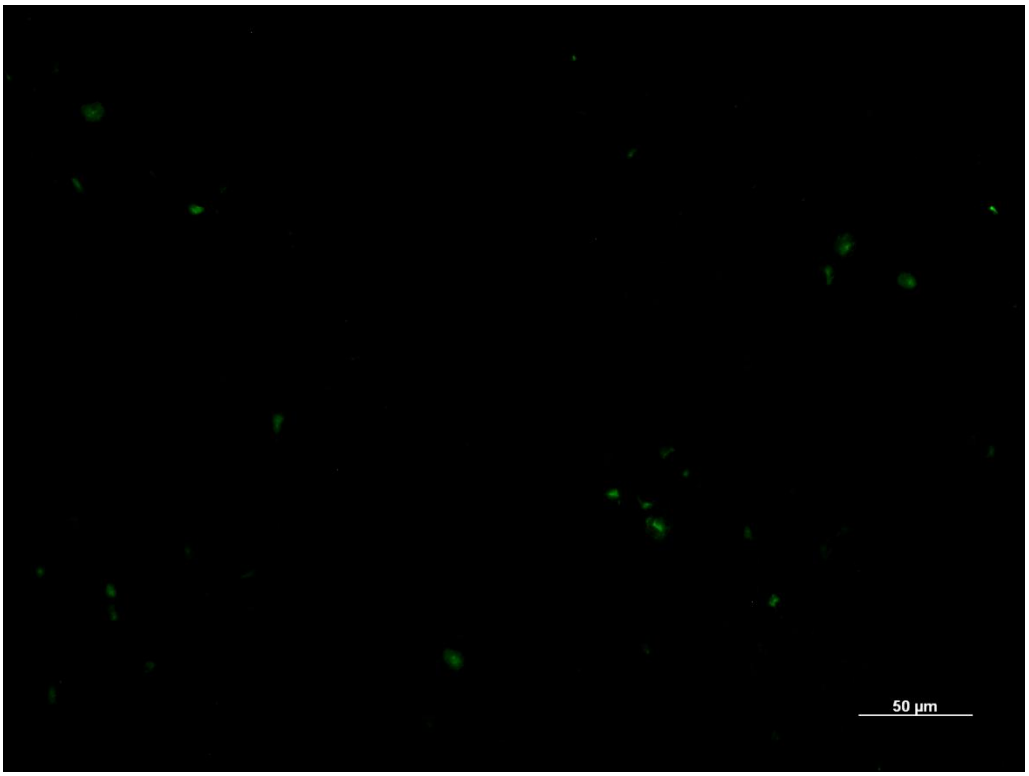

Figure 69 – Stent flow chamber, dynamic plasma exposure, flat PCL, 20x.

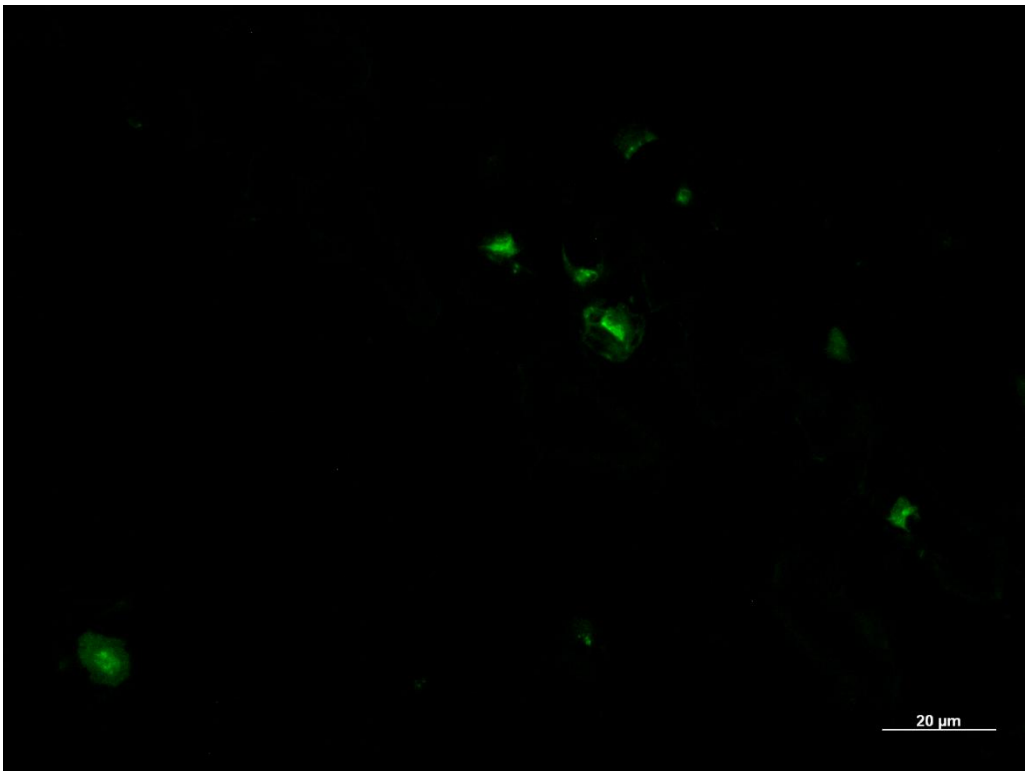

Figure 70 – Stent flow chamber, dynamic plasma exposure, flat PCL, 50x.

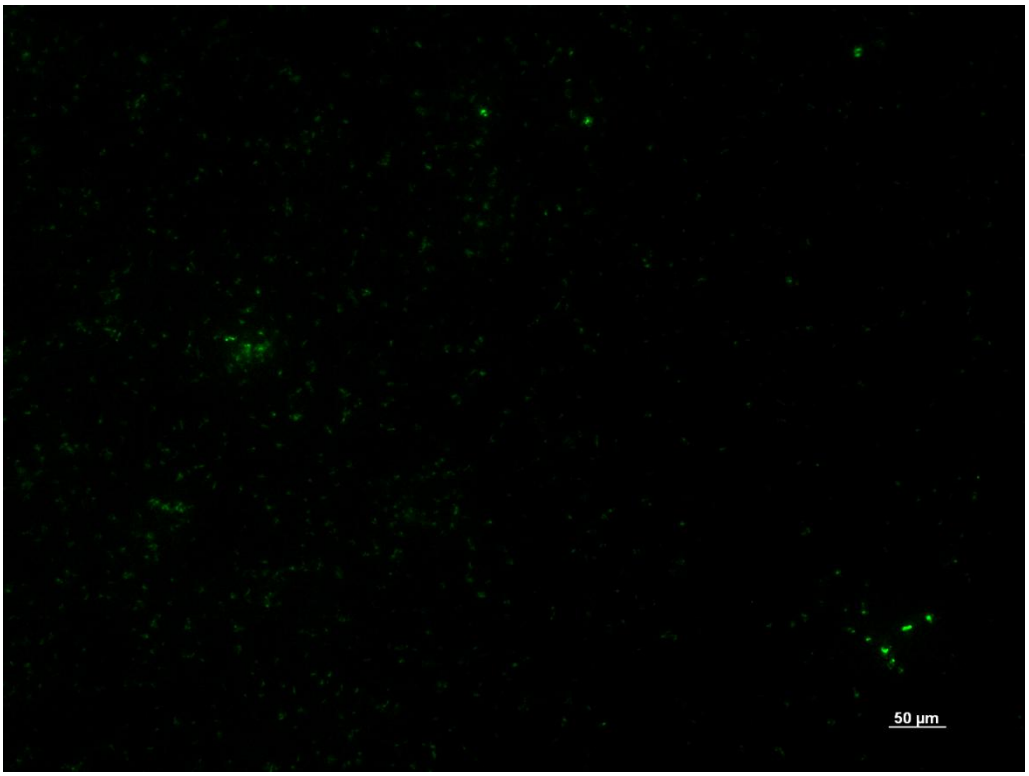

Figure 71 – Stent flow chamber, dynamic plasma exposure, PCL fibers, 10x.

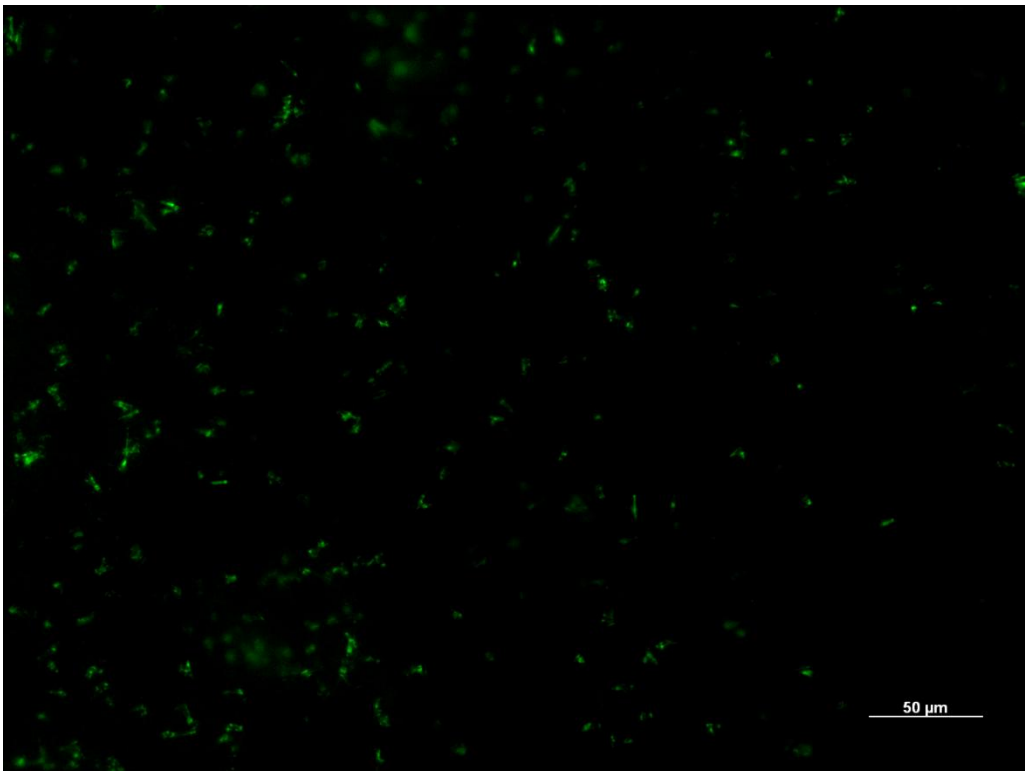

Figure 72 – Stent flow chamber, dynamic plasma exposure, PCL fibers, 20x.

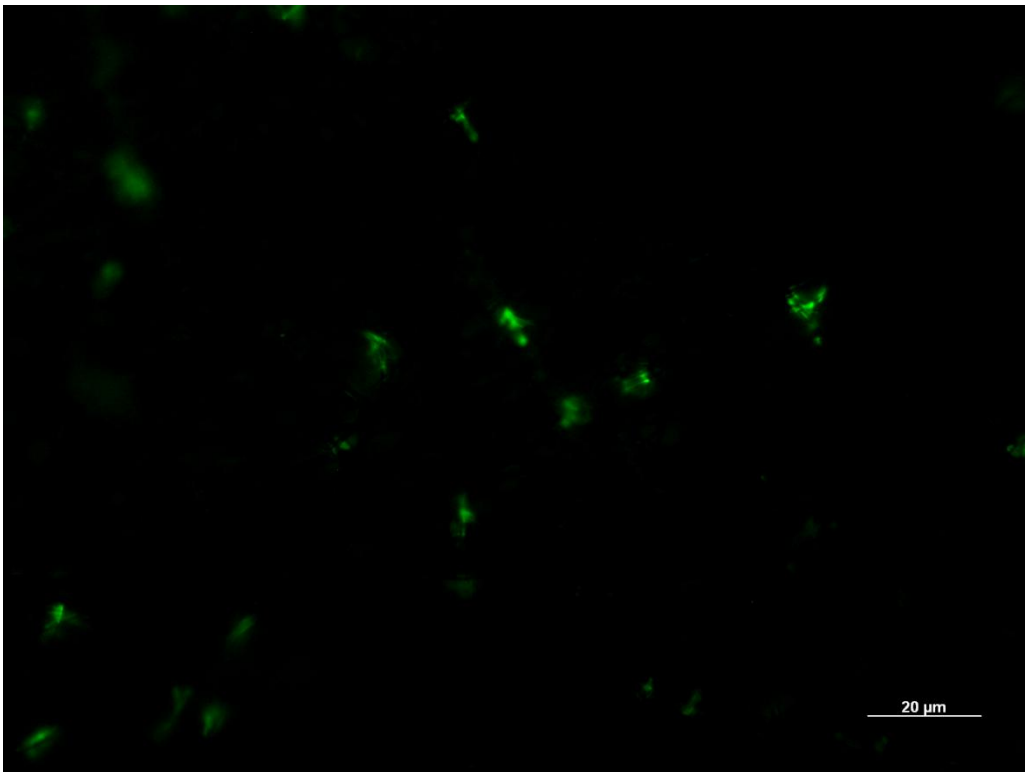

Figure 73 – Stent flow chamber, dynamic plasma exposure, PCL fibers, 50x.

CONCLUSION

The development of porous, biodegradable, three dimensional scaffolds seeded with cells for the development of new tissue has become a trend in the biomedical field. Biomaterial rejection remains a serious issue within the field eliciting the need of increased understanding the material cell interaction to reduce the problem in upcoming technologies. The study of hemocompatiability of tissue engineering scaffolds remains viable as contact with blood and related cells during implantation and foreign body responses is inevitable. Though blood flow and mechanisms of platelet adhesion and thrombis formation under flow conditions *in vivo* are well researched, very few studies of hemocompatibility on biomaterials in general include discussion of the dynamic aspect.

The perfused flow chamber was designed with the objectives of immobilizing a tissue engineered scaffold or biomaterial with application of laminar, homogenous flow across the fixed sample area with the added advantage of changing chamber profile, altering fluid path and live imaging of the flow. The chamber durability was proved with consistent runs at a constant flow of 10ml/min for a study period of 30 minutes and with a single chamber enduring multiple terms of operation. PIV of the fluid within the laminar flow and stent flow chambers provided visual evidence in the creation of homogenous flow in the laminar flow chamber and the formation of co-exisiting linear and cyclical flow within the stent chamber. Calculation of flow velocity from retention time and extrapolation from vector field analysis determined flow in both designs to be laminar at the flow rate described in all conducted studies.

Application of extracted human plasma from whole blood across PCL flat and nanofiber surfaces in both static and dynamic states yielded insight of the importance of surface topology and flow

to cellular adhesion and hemocompatibility. It was observed through SEM and fluorescence imaging that platelets adhered on PCL electrospun surfaces at a much greater density than on flat PCL in both static and dynamic studies. Dynamic studies showed a decrease in the adhesion of platelets to the PCL surfaces with increased activation, application of flow to electrospun nanofibers showed comparable platelet adhesion to flat PCL samples in the absence of flow. Flow velocity as described in the stent flow chamber also impacts the adhesion of platelets to both flat and nanofiber PCL surfaces. High velocity of flow yielded fewer adhered platelets though activation appears to be similar.

In conclusion the flow chamber displayed all physical attributes outlined in the objectives and performance was robust and yielded consistent results with minimal leakage under operating conditions. With validation of the perfused flow chamber as a viable device for the study of platelet adhesion and activation on a biomaterial surface attention can be drawn to further refining the chamber construction methods and operation. While the experimental focus of the chamber was limited to hemocompatibility and platelet adhesion, the chamber dimensions are very flexible and can be adapted for the study of a number of mechanisms utilizing different biomaterial, cell and fluid types in a dynamic setting.

REFERENCES

[1] Hollister, SJ. Porous Scaffold Design for Tissue Engineering. Nature Materials 2005; 4: 518–524.

[2] Ratner, BD., Hench, L. Perspectives on Biomaterials. Current Opinion in Solid State and Materials Science 1999; 4(4):379-380.

[3] Langer, R. Biomaterials: Status, Challenges and Perspectives. AIChE Journal 2000; 46(7): 1286-1289.

[4] Yarlagadda, P.K.D.V., Chandrasekharan, M., Shyan, J.Y.M. Recent advances and current developments in tissue scaffolding. Bio-Medical Materials and Engineering 2005; 15(3): 159-177.

[5] He, W., Yong, T., Teo, W.E., Ma, Z., Ramakrishna, S. Fabrication and Endothelialization of Collagen-Blended Biodegradable Polymer Nanofibers: Potential Vascular Graft for Blood Vessel Tissue Engineering. Tissue Engineering 2005; 11(9/10): 1574-1588.

[6] Hershel, U., Dahmen, C., Kessler, H. RGD modified polymers: Biomaterials for stimulated cell adhesion and beyond. Biomaterials 2003; 24: 4385-4415.

[7] Bacakova, L., Filova, E., Rypacek, F., Svorcik, V., Stary, V. Cell Adhesion on Artificial Materials for Tissue Engineering. Physiol. Res. 2004; 53: S35-S45.

[8] Adelow C, Segura T, Hubbell JA, Frey P. The effect of enzymatically degradable poly(ethylene glycol) hydrogels on smooth muscle cell phenotype. Biomaterials 2008; 29: 314–326.

[9] Hu, J., Sun, X., Ma, H., Xie, C., Chen, Y.E., Ma, P.X. Parous Nanofibrous PLLA scaffolds for vascular tissue engineering. Biomaterials 2010; 31(31): 7971-7979.

[10] Cole MA, Voelcker NH, Thissen H, Griesser HJ. Stimuli-responsive interfaces and systems for the control of protein-surface and cellsurface interactions. Biomaterials 2009;30:1827–1850.

[11] Horii, A., Wang, X., Gelain, F., Zhang, S. Biological designer sellf-assembling peptide nanofiber scaffolds significantly enhance osteoblast proliferation, differentiation and 3-D migration. PLoS One 2007; 2(2): e190.

[12] Yoshimoto, H., Shin, Y.M., Terai, H,. Vacanti, J.P. A biodegradable nanofiber scaffold by electrospinning and its potential for bone tissue engineering. Biomaterials 2003;24(12):2077-82.

[13] Rathbone, S., Furrer, P., Lubben, J., Zinn, M., Cartmell, S. Biocompatibility of polyhydroxyalkanoate as a potential material for ligament and tendon scaffold material. Journal of Biomedical Materials Research Part A 2009; 93A(4): 1391-1403

[14] McBane, J.E., Sharifpoor, S., Cai, K., Labow, R.S., Santerre, J.P. Biodegradation and in vivo biocompatibility of a degradable, polar/hydrophobic/ionic polyurethane for tissue engineering applications. Biomaterials 2011 June.

[15] Gomes, M.E., Reis, R.L., Cunha, A.M., Blitterswijk, C.A., de Bruijn, J.D. Cytocompatibility and response of osteoblastic-like cells to starch-based polymers: effect of several additives and processing conditions. Biomaterials 2001; 22(13): 1911-1917.

[16] Xiang, P., Li, M., Zhang, C.Y., Chen, D.L., Zhou, Z.H. Cytocompatibility of electrospun nanofiber tubular scaffolds for small diameter tissue engineering blood vessels. International Journal of Biological Macromolecules 2011 May.

[17] Wu, J.M., Xu, Y.Y., Li, Z.H., Yuan, X.Y., Wang, P.F., Zhang, X.Z., Liu, Y.Q., Guan, J., Guo, Y., Li, R.X., Zhang, H. Heparin-functionalized collagen matricies with controlled release of basic fibroblast growth factor. Journal of Material Science: Materials in Medicine 2011; 22: 107-114.

[18] Srouji, S., Dror, Ben-David, D., Lotan, R., Livine, E., Avrahami, R. Zussman, E. Growth factor/heparin-immobilized collagen gel system enhances viability of transplanted hepatocytes and induces angiogenesis. Tissue Engineering: Part A 2011; 17(3/4): 269-277.

[19] Ruckh, T.T., Kumar, K., Kipper, M.J., Popat, K.C. Osteogenic differentiation of bone marrow stromal cells on poly(ε-caprolactone) nanofiber scaffolds. Acta Biomaterialia 2010; 6: 2949-2959.

[20] Li, W.J., Cooper, J.A. Jr., Mauck, R.L., Tuan, R.S. Fabrication and characterization of six electrospun poly(alpha-hydroxy ester)-based fibrous scaffolds for tissue engineering applications. Acta Biomaterialia 2006; 2(4): 377-385.

[21] Bass, J.D., Belamie, E., Grosso, D., Boissiere, C., Coradin, T., Sanchez, C. Nanostructuration of titania thin films prepared by self-assembly to affect cell adhesion. Journal of Biomedical Materials Research Part A 2010; 93(1): 96-106.

[22] Anderson, J.M., Rodriguez, A., Chang, D.T. Foreign body reaction to biomaterials. Seminars in Immunology 2008; 20: 86-100.

[23] Gorbet, M.B., Sefton, M.V. Biomaterial-associated thrombosis: roles of coagulation factors, complement, platelets and leukocytes. Biomaterials 2004; 25: 5681-5703.

[24] Amara, U., Rittirsch, D., Flierl, M., Bruckner, U., Klos, A., Gebhard, F., Lambris, J.D., Huber-Lang, M. Interaction Between the Coagulation and Complement System. Advances in Experimental Medicine and Biology 2008; 632: 71-79.

[25] Romney, G., Glick, M. An Updated Concept of Coagulation with Clinical Implications. The Journal of the American Dental Association 2009; 140: 567-574.

[26] Smith, B.S., Yoriya, S., Grissom, L, Grimes, C.A., Popat, K.C. Hemocompatibility of titania nanotube arrays. Journal of Biomedical Materials Research A 2010; 95A(2): 350-360.

[27] Motlagh, D., Yang, J., Lui, K., Webb, A.R., Ameer, G.A. Hemocompatibility evaluation of poly(glycerol-sebacate) in vitro for vascular tissue engineering. Biomaterials 2006; 27: 4315-4324.

[28] Besteiro, M.C., Guiomar, A.J., Goncalves, C.A., Bairos, V.A., de Pinho, M.N., Helena Gil, M. Characterization and in vitro hemocompatibility of bi-soft segment, polycaprolactone-based poly(ester urethane urea) membranes. Journal of Biomedical Materials Research Part A 2009; : 954-964.

[29] Chen, J., Chen, C., Chen, Z., Chen, J., Li, Q., Hung, N. Collagen/heparin coating on titanium surface improves the biocompatibility of titanium applied as a blood contacting biomaterial. Journal of Biomedical Materials Research Part A 2010; 95A(2): 341-349.

[30] Amarnath, L.P., Srinivas, A., Ramamurthi, A. In vitrohemocompatibility testing of UV-modified hyaluronan hydrogels. Biomaterials 2006; 27: 1416-1424.

[31] McDonald, J.C., Whitesides, G.M. Poly(dimethylsiloxane) as a Material for Fabricating Microfluidic Devices. Accounts of Chemical Research 2002; 35(7): 491-499.

[32] Lotters, J.C., Olthuis, W., Veltink, P.H., Bergveld, P. The mechanical properties of the rubber elastic polymer polydimethylsiloxane for sensor applications. Journal of Micromechanics and Microengineering 1997; 7: 145-147.

[33] Demirci, U., Geckil, H. Editorial: Micro and nanofluidics - applications in biotechnology. Biotechnology Journal 2011; 6(2): 131.

[34] Chantiwas, R., Park, S., Soper, S.A., Kim, B.C., Takayama, S., Sunkara, V., Hwang, H., Cho, Y.K. Flexible fabrication and applications of polymer nanochannels and nanoslits. Chemical Society Reviews 2011; 40(7): 3677-3702.

[35] Taylor, A.M., Rhee, S.W., Jeon, N.L. Microfluidic Chambers for Cell Migration and Neuroscience Research. Methods in Molecular Biology 2006; 321: 167-177.
[36] Zhang C., van Noort, D. Cells in Microfluidics. Topics in Current Chemistry 2011 May.
[37] Lovchik, R.D., Bianco, F., Matteoli, M., Delamarche, E. Controlled deposition of cells in sealed microfluidics using flow velocity boundaries. Lab on a Chip 2009; 9: 1395-1402.
[38] Wang, J., Bettinger, C.J., Langer, R.S., Borenstein, J.T. Biodegradable Microfluidic Scaffolds for Tissue Engineering from Amino Alcohol-based Poly(ester amide) Elastomers. Organogenesis 2010; 6(4): 212-216.
[39] Hwang, C.M., Khademhosseini, A., Park, Y., Sun, K., Lee, S.H. Microfluidic chip-based fabrication of PLGA microfiber scaffolds for tissue engineering. Langmuir: the ACS journal of surfaces and colloids 2008; 24(13): 6845-6851.
[40] Cuchiara, M.P., Allen, A.C., Chen, T.M., Miller, J.S., West, J.L. Multilayer microfluidic PEGDA hydrogels. Biomaterials 2010; 31(21): 5491-5497.
[41] Garra, J., Long, T., Currie, J., Schneider, T., White, R., Paranjape, M. Dry etching of polydimethylsiloxane for microfluidic systems. Journal of Vacuum Science and Technology A 2002; 20(3); 975-982.
[42] Luo, Y., Zare, R.N., Perforated membrane method for fabricating three-dimensional polydimethylsiloxane microfluidic devices. Lab on a Chip 2008; 8: 1688-1694.
[43] Jo, B.H., van Lerberghe, L.M., Motsegood, K.M., Beebe, D.J. Three-Dimensional Micro-Channel Fabrication in Polydimethylsiloxane (PDMS) Elastomer. Journal of Microelectromechanical Systems 2000; 9(1): 76-81.
[44] Lima, R., Wada, S., Tanaka, S., Takeda, M., Ishikawa, T., Tsubota, K., Imai, Y., Yamaguchi, T. In vitro blood flow in a rectangular PDMS microchannel: experimental observations using a confocal micro-PIV system. Biomedical Microdevices 2008; 10: 153-167.
[45] Tomaiuolo, G., Barra, M., Preziosi, V. Cassinese, A., Rotoli, B., Guido, S. microfluidics analysis of red blood cell membrane viscoelasticity. Lab on a Chip 2011; 11: 449-454.
[46] Freed, L.E., Vunjak-Novakovic, G., Tissue Engineering Bioreactors. Principles of Tissue Engineering Second Edition. Academic Press (2002).
[47] Martin, I., Wendt, D., Heberer, M. The role of bioreactors in tissue engineering. Trends in Biotechnology 2004; 22(2): 80-86.
[48] Vunjak-Novakovic, G., Obradovic, B., Martin, I.Bursac, P.M., Langer, R., Freed, L.E. Dynamic Cell Seeding of Polymer Scaffolds for Cartilage Tissue Engineering. Biotechnology Progress 1998; 14(2): 193-202.
[49] Zhao, F., Ma, T. Perfusion Bioreactor System for Human Mesenchymal Stem Cell Tissue Engineering: Dynamic Cell Seeding and Construct Development. Biotechnology and Bioengineering 2005; 91(4); 482-493.
[50] Bancroft, G.N., Sikavitsas, V.I., Mikos, A.G. Design of a Flow Perfusion Bioreactor System for Bone Tissue-Engineering Applications. Tissue Engineering 2003; 9(3): 549-554.
[51] Sodian, R., Lemke, T, Fritsche, C., Hoerstrup, S.P., Fu, P., Potapov, E.V., Hausmann, H., Hetzer, R. Tissue-Engineering Bioreactors: A New Combined Cell-Seeding and Perfusion System for Vascular Tissue Engineering. Tissue Engineering 2002; 8(5): 863-870.
[52] Nikolaev, N.I., Obradovic, B., Versteeg, H.K., Lemon, G., Williams, D.J. A validated model of GAG deposition, cell distribution, and growth of tissue engineered cartilage cultured in a rotating bioreactor. Biotechnology and Bioengineering 2010; 105(4): 842-853.
[53] Frank, A.O., Walsh, P.W., Moore, J.E.Jr. Computational Fluid Dynamics and Stent Design. Artificial Organs 2002; 26(7): 614-621.

[54] LaDisa, J.F.Jr., Olson, L.E., Guler, I, Hettrick, D.A., Audi, S.H., Kersten, J.R., Warltier, D.C., Pagel, P.S. Stent design properties and development ratio influence indexes of wall shear stress: a three-dimensional computational fluid dynamics investigation within a normal artery. Journal of Applied Physiology 2004; 97: 424-430.

[55] Berry, J.L., Moore, J.E. Jr., Newman, V.S., Routh, W.D. In vitro flow visualization in stented arterial segments. Journal of Vascular Investigation 1997; 2: 63–68.

[56] O'Brien, J.R. Shear-induced Platelet Aggregation. The Lancet 1990; 335: 711-713.

[57] Kroll, M.H., Hellums, J.D., McIntire, L.V., Schafer, A.I., Moake, J.L. Platelets and Shear Stress. The Journal of The American Society of Hematology 1996; 88(5): 1525-1541.

[58] Maxwell, M.J., Westien, E., Nesbitt, W.S., Giuliano, S., Dopheide, S.M., Jackson, S.P. Identification of a 2-stage platelet aggregation process mediating shear-dependent thrombus formation. Blood 2007; 109(2): 566-576.

[59] Nesbitt, W.S., Westein, E., Tovar-Lopez, F.J., Tolouei, E., Mitchell, A., Hu, J., Carberry, J., Fouras, A., Jackson, S.P. A shear gradient-dependent platelet aggregation mechanism drives thrombus formation. Nature Medicine 2009; 15(6): 655-673.

[60] Jackson, S.P., Nesbitt, W.S., Westien, E. Dynamics of Platelet Thrombus Formation. Journal of Thrombosis and Hemostasis 2009; 7(S1): 17-20.

[61] Haidekker, M.A., Tsai, A.G., Brady, T., Stevens, H.Y., Frangos, J.A., Theodorakis, E. Intaglietta, M. A novel approach to blood plasma viscosity measurement using fluorescent molecular rotors. Heart and Circulatory Physiology 2002; 282(5): 1609-1614.

[62] Cheng, C.P., Parker, D., Taylor, C.A. Quantification of Wall Shear Stress in Large Blood Vessels Using Lagrangian Interpolation Functions with Cine Phase-Contrast Magnetic Resonance Imaging. Anals of Biomedical Engineering 202; 30: 1020-1032.

[63] Baez, J.E., Ramirez-Hernandez, A, Marcos-Fernandez, A. Synthesis, characterization, and degradation of poly(ethylene-*b*-ε-caprolactone) diblock copolymer. Polymers for Advanced Technologies 2010; 21(1): 55-64.

[64] Ashammakhi N, Ndreu A, Piras A, Nikkola L, Sindelar T, Ylikauppila H, et al. Biodegradable nanomats produced by electrospinning: expanding multifunctionality and potential for tissue engineering. J Nanosci Nanotechnol 2006;6:2693.

[65] Pitt, C.G., Gratzl, M.M., Kimmel, G.L., Surles, J., Schindler, A. Aliphatic polyesters II. The degradation of poly (DL-lactide), poly (epsilon-caprolactone), and their copolymers in vivo. Biomaterials 1981; 2: 215.

[66] Woodward, S.C., Brewer, P.S., Moatamed, F., Schindler, A., Pitt, C.G. The intracellular degradation of poly(epsilon-caprolactone). J. Biomed. Mater. Res. 1985; 19: 437.

[67] Darney, P.D., Monroe, S.E., Klaisle, C.M., Alvarado, A. Clinical evaluation of the Capronor contraceptive implant: preliminary report. Am J Obstet. Gynecol. 1989; 160: 1292.

[68] Bezwada, R.S., Jamiolkowski, D.D., Lee, I.Y., Agarwal, V., Persivale, J., Trenka-Benthin S, et al. Monocryl suture, a new ultra-pliable absorbable monofilament suture. Biomaterials 1995; 16: 1141.

[69] Soppimath, K.S., Aminabhavi, T.M., Kulkarni, A.R., Rudzinski, W.E. Biodegradable polymeric nanoparticles as drug delivery devices. Journal of Controlled Release 2001; 70: 1-20.

[70] Yang, J., Park, S.B., Yoon, H.G., Huh, Y.M., Haam, S. Preparation of poly ε-caprolactone nanoparticles containing magnetite for magnetic drug carrier. International Journal of Pharmaceutics 2006; 324: 185-190.

[71] Moutos, F.T., Guilak, F. Preparation of poly ε-caprolactone nanoparticles containing magnetite for magnetic drug carrier. Tissue Engineering Part A 2010; 16(4): 1291-1301.

[72] Wutticharoenmongkol, P., Pavasant, P., Supaphil, P. Osteoblastic Phenotype Expression of MC3T3-E1 Cultured on Electrospun Polycaprolactone Fiber Mats Filled with Hydroxyapatite Nanoparticles. Biomacromolecules 2007; 8(8): 2602-2610.
[73] Wulf, K., Teske, M. Lobler, M., Luderer, F., Schmitz, K.P., Sternberg, K. Surface functionalization of poly(ε-caprolactone) improves its biocompatibility as scaffold material for bioartificial vessel prostheses. Journal of Biomedical Materials Research Part B 2011; 98(1): 89-100.
[74] Maraganore, J.M. The Arterial Thrombotic Process and Emerging Drugs for its Control. Texas Heart Institute Journal 1993; 20(1): 43-47.
[75] Schopka, S., Schmid, F.X., Hirt, S., Birnbaum, D.E., Schmid, C., Lehle, K. Recellularization of biological heart valves with human vascular cells: in vitro hemocompatibility assessment. Journal of Biomedical Materials Research Part B 2009; 88(1): 130-138.
[76] Bolz, A., Schaldach, M. Artificial heart valves: improved blood compatibility by PECVD a-SiC:H coating. Artificial Organs 1990; 14(4): 260-169.
[77] Pinto, T.D.J.A., Ribeiro, A.D.F. The Influence of the Intravenous Catheter Compositiong n it's Hemocompatibility. PDA Journal of Pharmaceutical cience and Technology 1999; 59(1): 27-30.
[78] Mueller, X.M., Augstburger, M., Boone, Y., von, S. Hemocompatibility of a coaxial pump catheter for less invasive heart surgery. Perfusion 2002; 17(1): 3-7.
[79] Fujiwara, N.H., Kallmes, D.F., Li, S.T., Lin, H.B., Hagspiel, K.D. Type I collagen as an endocascular stent graft material for small-diameter vessels: a biocompatibility study. Journal of Vascular and Interventional Radiology 2005; 16(9): 1229-1236.
[80] Frank, A.O., Walsh, P.W., Moore, J.E.Jr. Computational Fluid Dynamics and Stent Design. Artificial Organs 2002; 26(7): 614-621.
[81] Nishida, M., Maruyama, O., Kosaka, R., Yamane, T., Kogure, H., Kawamura, H., Yamamoto, Y., Kuwana, K., Sankai, Y., Tsutsui, T. Hemocompatibility evaluation with experimental and computational fluid dynamic analyses for a monopivot circulatory assist pump. Artificial Organs 2009; 33(4): 378-386.
[82] Seyfert, U.T., Biehl, V., Schenk, J. In vitro hemocompatibility testing of biomaterials according to the ISO 10993-4. Biomolecular Engineering 2002; 19: 91-96.
[83] Broos, K., Feys, H.B., De Meyer, S.F., Vanhoorelbeke, K., Deckmyn, H. Plarelets at work in primary hemostasis. Blood Reviews 2011; 25(4): 155-167.
[84] Tovar-Lopez, F.J., Rosengarten, G., Westein, E., Khoshmanesh, K., Jackson S.P., Mitchell, A., Nesbitt, W.S. A microfluidics device to monitor platelet aggregation dynamics in response to strain rate micro-gradients in flowing blood. Lab on a Chip 2010; 10: 291-302.